

# SMIP07

## SMIP07 SEMINAR ON UTILIZATION OF STRONG-MOTION DATA

Sacramento, California  
September 13, 2007

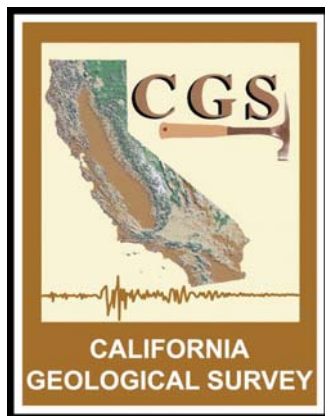
### PROCEEDINGS

Sponsored by

California Strong Motion Instrumentation Program  
California Geological Survey  
California Department of Conservation

Co-Sponsors

California Seismic Safety Commission  
California Office of Emergency Services  
California Department of Transportation  
Office of Statewide Health Planning and Development



The California Strong Motion Instrumentation Program (CSMIP), a program within the California Geological Survey (CGS) of the California Department of Conservation, records the strong shaking of the ground and structures during earthquakes for analysis and utilization by the engineering and seismology communities through a statewide network of strong motion instruments ([www.conservation.ca.gov/CGS/smip](http://www.conservation.ca.gov/CGS/smip)). CSMIP is advised by the Strong Motion Instrumentation Advisory Committee (SMIAC), a committee of the California Seismic Safety Commission. Major program funding is provided by an assessment on construction costs for building permits issued by cities and counties in California, with additional funding from the California Office of Emergency Services, the California Department of Transportation and the Office of Statewide Health Planning and Development.

In July 2001, the California Office of Emergency Services began funding for the California Integrated Seismic Network (CISN), a newly formed consortium of institutions engaged in statewide earthquake monitoring that grew out of TriNet, funded by FEMA, and includes CGS, USGS, Caltech and UC Berkeley. The goals are to record and rapidly communicate ground shaking information in California, and to analyze the data for the improvement of seismic codes and standards ([www.cisn.org](http://www.cisn.org)). CISN produces ShakeMaps of ground shaking, based on shaking recorded by stations in the network, within minutes following an earthquake. The ShakeMap identifies areas of greatest ground shaking for use by OES and other emergency response agencies in the event of a damaging earthquake.

The U.S. National Center for Engineering Strong Motion Data (NCESMD) is operated by the CSMIP Program of the CGS in cooperation with the National Strong-Motion Project (NSMP) and the Advanced National Seismic System (ANSS) of the USGS. The NCESMD builds on the CISN Engineering Data Center and will continue to serve the California region while expanding to serve other ANSS regions. The Data Center provides strong-motion data rapidly after a significant earthquake in the United States. Users also have direct access to data from previous earthquakes and detailed information about the instrumented structures and sites. The National Center is co-hosted by CGS and USGS at [www.strongmotioncenter.org](http://www.strongmotioncenter.org)

## **DISCLAIMER**

Neither the sponsoring nor supporting agencies assume responsibility for the accuracy of the information presented in this report or for the opinions expressed herein. The material presented in this publication should not be used or relied upon for any specific application without competent examination and verification of its accuracy, suitability, and applicability by qualified professionals. Users of information from this publication assume all liability arising from such use.

# SMIP07

## SMIP07 SEMINAR ON UTILIZATION OF STRONG-MOTION DATA

Sacramento, California  
September 13, 2007

### PROCEEDINGS

Edited by

Moh Huang

Sponsored by

California Strong Motion Instrumentation Program  
California Geological Survey  
California Department of Conservation

Co-Sponsors

California Seismic Safety Commission  
California Office of Emergency Services  
California Department of Transportation  
Office of Statewide Health Planning and Development



### PREFACE

The California Strong Motion Instrumentation Program (CSMIP) in the California Geological Survey of the California Department of Conservation established a Data Interpretation Project in 1989. Each year CSMIP Program funds several data interpretation contracts for the analysis and utilization of strong-motion data. The primary objectives of the Data Interpretation Project are to further the understanding of strong ground shaking and the response of structures, and to increase the utilization of strong-motion data in improving post-earthquake response, seismic code provisions and design practices.

As part of the Data Interpretation Project, CSMIP holds annual seminars to transfer recent research findings on strong-motion data to practicing seismic design professionals, earth scientists and post-earthquake response personnel. The purpose of the annual seminar is to provide information that will be useful immediately in seismic design practice and post-earthquake response, and in the longer term, useful in the improvement of seismic design codes and practices. Proceedings and individual papers for each of the previous annual seminars are available in PDF format at <http://www.consrv.ca.gov/CGS/smip/proceedings.htm> The SMIP07 Seminar is the eighteenth in this series of annual seminars.

The SMIP07 Seminar is divided into two plenary sessions in the morning and two concurrent sessions in the afternoon. The plenary sessions in the morning include presentations by investigators of four CSMIP-funded projects and an introduction of the new U.S. National Center for Engineering Strong Motion Data. The afternoon sessions include presentations by six invited speakers on topics related to ground motion attenuation, design ground motion library, tall buildings in California, real-time structural monitoring and new building code provisions. Professor Kazuyoshi Kudo from Japan will present a luncheon address on recent developments in strong motion measurements in Japan and the damaging Niigata area earthquake of 2007.

The Seminar includes presentations by investigators of CMIP-funded projects. These projects are scheduled to be completed by the end of 2007 and the final results will be published in their final reports.

Moh J. Huang, Ph.D., P.E.  
CSMIP Data Interpretation Project Manager

**Members of the  
Strong Motion Instrumentation Advisory Committee**

**Main Committee**

Chris Poland, Chair, Degenkolb Engineers  
Norman Abrahamson, Pacific Gas & Electric Company  
Anil Chopra, UC Berkeley  
Bruce Clark, Seismic Safety Commission, Leighton & Associates  
C. Allin Cornell, Stanford University  
Martin Eskijian, California State Lands Commission  
Wilfred Iwan, California Institute of Technology  
Jerve Jones, Jones & Jones  
Michael Kever, Caltrans  
Maurice Power, Geomatrix Consultants  
Daniel Shapiro, Seismic Safety Commission, SOHA Engineers  
Edward Bortugno (ex-officio), Office of Emergency Services  
Robert Anderson (ex-officio), Seismic Safety Commission

**Ground Response Subcommittee**

Maurice Power, Chair, Geomatrix Consultants  
Abbas Abghari, Caltrans  
Yousef Bozorgnia, PEER  
Brian Chiou, Caltrans  
Marshall Lew, MACTEC Engineering & Consulting  
Geoffrey Martin, Univ. of Southern California  
Ben Tsai, Pacific Gas & Electric Company

**Buildings Subcommittee**

Chris Poland, Chair, Degenkolb Engineers  
Kenneth Honda, URS Corporation  
Donald Jephcott, Structural Engineer  
Jerve Jones, Jones & Jones  
David Leung, City of San Francisco  
Bret Lizundia, Rutherford & Chekene  
Eduardo Miranda, Stanford University  
Farzad Naeim, John A. Martin & Associates  
John Robb, Structural Engineer  
Daniel Shapiro, SOHA Engineers  
Chia-Ming Uang, UC San Diego

**Lifelines Subcommittee**

Martin Eskijian, Chair, California State Lands Commission  
David Gutierrez, DWR Division of Safety of Dams  
Michael Kever, Caltrans  
LeVal Lund, Civil Engineer  
Edward Matsuda, BART  
Stuart Nishenko, Pacific Gas & Electric Company  
Vern Persson, DWR Division of Safety of Dams (retired)

**Data Utilization Subcommittee**

Wilfred Iwan, Chair, California Institute of Technology  
Representatives from each Subcommittee

**TABLE OF CONTENTS**

**Seminar Final Program**.....v

**Analysis of Strong Ground Motions from the June 12, 2005 Anza Earthquake** .....1  
 Robert Graves, Paul Somerville, Nancy Collins, Arben Pitarka and Sidao Ni

**Analysis of Seismic Response of Seven Oaks Dam** .....21  
 Lelio Mejia and Ethan Dawson

**US National Center for Engineering Strong Motion Data (NCESMD)**.....41  
 Hamid Haddadi, Tony Shakal, Woody Savage, Chris Stephen and Moh Huang

**Evaluation of Current Nonlinear Static Procedures for Concrete Buildings Using Recorded Strong-Motion Data** .....57  
 Rakesh Goel and Charles Chadwell

**Predictive Capability of Nonlinear Static Analysis Procedures for Seismic Evaluation of Buildings** .....81  
 Dionisio Bernal and Arash Nasser

**Recent Developments in Strong Motion Measurements in Japan and the Damaging Niigata Area Earthquakes of 2007 (Abstract)**.....103  
 Kazuyoshi Kudo

**Results and Implications of the Next Generation Attenuation (NGA) Ground Motion Project (Abstract)**.....107  
 Norman Abrahamson

**Design Ground Motion Library (DGML) – Tool for Selecting Time History Records for Specific Engineering Applications (Abstract)** .....109  
 Robert Youngs, M. Power, G. Wang, F. Makdisi and C.-C. Chin

**Directivity in NGA Earthquake Ground Motions: Analysis Using Isochrone Theory (Abstract)** .....111  
 Paul Spudich, USGS and Brian Chiou

**Development of Criteria for the Seismic Design and Analysis of Tall Buildings in California (Abstract)** .....113  
 Jack Moehle and Yousef Bozorgnia

**The Intersection of Earthquake Structural Response Monitoring and Structural Health Monitoring (Abstract)** .....115  
 Robert Nigbor

**New Building Code Provisions and their Implications for Design and Construction in California (Abstract)** .....117  
 David Bonneville





**SMIP07 SEMINAR ON  
UTILIZATION OF STRONG-MOTION DATA**

September 13, 2007

Hilton Sacramento Arden West  
2200 Harvard Street, Sacramento, California

**FINAL PROGRAM**

8:00 am **REGISTRATION**

9:15 am **WELCOMING REMARKS**

*Chris Poland*, Chair, Strong Motion Instrumentation Advisory Committee (SMIAC)  
*John Parrish*, State Geologist, California Geological Survey  
*Anthony Shakal*, Manager, Strong Motion Instrumentation Program

9:25 am **INTRODUCTION**

*Moh Huang*, Strong Motion Instrumentation Program

***Plenary Session I***

**Moderator:** *Wilfred Iwan*, Caltech and SMIAC

9:30 am **Analysis of Strong Ground Motions from the June 12, 2005 Anza Earthquake**

*Robert Graves*, *Paul Somerville*, *Nancy Collins*, *Arben Pitarka* and *Sidao Ni*, URS Corporation, Pasadena

10:00 am **Analysis of Seismic Response of Seven Oaks Dam**

*Lelio Mejia* and *Ethan Dawson*, URS Corporation, Oakland

10:30 am **US National Center for Engineering Strong Motion Data (NCESMD)**

*Hamid Haddadi*, *Tony Shakal*, *Woody Savage*, *Chris Stephen* and *Moh Huang*, CGS and USGS

11:00 am Break

***Plenary Session II***

**Moderator:** *Chris Poland*, Degenkolb Engineers and SMIAC

11:15 am **Evaluation of Current Nonlinear Static Procedures for Concrete Buildings Using Recorded Strong-Motion Data**

*Rakesh Goel* and Charles Chadwell, Cal Poly State University, San Luis Obispo

11:45 am **Predictive Capability of Nonlinear Static Analysis Procedures for Seismic Evaluation of Buildings**

*Dionisio Bernal* and *Arash Nasseri*, Northeastern University, Boston

12:15 pm **Luncheon**

Introduction *John Parrish*, State Geologist, California Geological Survey

Speaker: *Kazuyoshi Kudo*, Nihon University and Tokyo Electric Power Services Co.

Title: **Recent Developments in Strong Motion Measurements in Japan and the Damaging Niigata Area Earthquakes of 2007**

*Afternoon Sessions*

**Track 1**

**Moderator:** *Maurice Power*, Geomatrix Consultants and SMIAC

**Track 2**

**Moderator:** *Martin Eskijian*, California State Lands Commission and SMIAC

2:00 pm **Results and Implications of the Next Generation Attenuation (NGA) Ground Motion Project**

*Norman Abrahamson*, PG & E, San Francisco

**Development of Criteria for the Seismic Design and Analysis of Tall Buildings in California**

*Jack Moehle* and *Yousef Bozorgnia*, Pacific Earthquake Engineering Research Center, UC Berkeley

2:30 pm **Design Ground Motion Library (DGML) – Tool for Selecting Time History Records for Specific Engineering Applications**

*Robert Youngs*, *M. Power*, *G. Wang*, *F. Makdisi* and *C.-C. Chin*, Geomatrix Consultants, Oakland

**The Intersection of Earthquake Structural Response Monitoring and Structural Health Monitoring**

*Robert Nigbor*, UC Los Angeles

3:00 pm **Directivity in NGA Earthquake Ground Motions: Analysis using Isochrone Theory**

*Paul Spudich*, USGS and *Brian Chiou*, Caltrans

**New Building Code Provisions and their Implications for Design and Construction in California**

*David Bonneville*, Degenkolb Engineers, San Francisco

3:30 pm **Adjourn**

## ANALYSIS OF STRONG GROUND MOTIONS FROM THE JUNE 12, 2005 ANZA EARTHQUAKE

Robert Graves, Paul Somerville, Nancy Collins, Arben Pitarka and Sidao Ni

URS Corporation  
Pasadena, CA

### Abstract

For shaking periods less than about 1 second, the observed ground motions from the 2005 Anza earthquake are significantly higher (around +1 sigma) than predicted by three recent NGA attenuation relations, with little systematic dependence on distance, Vs30 or Z2.5. This same trend is found comparing these data to motions computed from a broadband simulation technique. For shaking periods greater than about 1 second, both the empirical models and the numerical simulations do well at reproducing the median level of the data. We obtain a significant improvement in the fit to the shorter period motions by increasing the corner frequency in our broadband simulation by a factor of 1.6. These results suggest that the strong short period motions resulted from a rupture process having a relatively high dynamic stress drop.

### Introduction

The Anza earthquake occurred on June 12, 2005 at 08:41:46 PDT. Preliminary analysis placed the event at lon=-116.57 and lat=33.53 with a hypocentral depth of 14.2 km and a magnitude of 5.1 (see <http://earthquake.usgs.gov/eqcenter/shakemaps/sc/shake/14151344>). Several sites in the epicentral region recorded peak ground accelerations (PGA) exceeding 0.2 g, producing areas of instrumental intensity approaching level VI (moderate to strong perceived shaking). The earthquake occurred along the San Jacinto fault zone just south of the Anza “seismic gap” (Figure 1). The occurrence of this earthquake in close proximity to a major active fault, as well as the relatively high ground motions produced during the rupture, has potentially significant implications for seismic hazards in southern California.

In this paper, we analyze the recorded ground motions to investigate the influence of source, path and site effects on the level and pattern of observed strong motions. Our goals are to better understand the processes that control the generation of strong ground motion and to investigate the ability of empirical ground motion models and numerical simulation methods to reproduce the observations. We find that the Anza earthquake produced relatively high short period ground motions independent of propagation distance and site type. This suggests that the earthquake source was the main contributor to the elevated short period motions through a high dynamic stress drop. In the sections that follow, we first discuss the recorded strong motion data and provide comparisons of these data with recently published ground motion attenuation models. Next, we compare the recorded motions with simulated broadband (0-10 Hz) motions

and demonstrate that we are able to improve the modeling of short period motions by a simple increase in the source corner frequency.

### Recorded Ground Motions

A large number of strong ground motion records were obtained during this earthquake. Table 1 lists the organizations and numbers of stations recording the event in the southern California region for which we have obtained waveform data.

**Table 1:** Ground Motion Recordings.

Organization	Instrument Type	Number of Recordings
ANZA Array	broadband	12
CSMIP	strong motion	90
SCSN/TriNet	broadband	178
USGS/NSMP	strong motion	19

A map of free field strong motion recording stations is shown in Figure 2. We obtained the uncorrected strong motion waveform data and then applied baseline and filtering operators to correct these data. The usable bandwidth is 0.2 to 40 Hz. Then we processed the corrected data to extract peak acceleration (PGA) and peak velocity (PGV) values, as well as computing spectral acceleration (SA) values at a variety of periods.

Although most of the near source broadband recordings were clipped, the more distant broadband records, which are not clipped, are useful in constraining the source mechanism. To do this, we use both a moment-tensor (MT) inversion and a cut-and-paste (CAP) inversion (Zhu and Helmberger, 1996). The MT inversion uses long period ( $T > 14$  sec) regional surface waves to determine the best fitting moment tensor solution. The CAP inversion uses both long period ( $T > 10$  sec) regional waveforms as well as shorter period ( $T > 3$  sec) Pnl waveforms to find the best fitting double couple solution. For this earthquake, both methods give very similar results, indicating primarily strike slip faulting along steeply dipping planes. The nodal planes are roughly parallel and conjugate to the San Jacinto fault. Table 2 summarizes these best fitting solutions.

**Table 2:** Inverted Source Mechanisms.

	MT Inversion	CAP Inversion
Strike	303	302
Dip	61	60
Rake	178	177
Depth (km)	14	14
$M_w$	5.12	5.08

### Comparison of Recorded Motions with NGA Models

As a first step in our analysis, we compare the recorded motions against the recently developed NGA ground motion relations of Campbell and Bozorgnia (2007), Chiou and Youngs (2006) and Boore and Atkinson (2007). The earthquake is parameterized as a strike-slip event

with a depth of 14 km and a moment magnitude of 5.1. Figure 3 plots PGA as a function of distance. We determine site  $V_{s30}$  values using the map of Wills et al. (2000). For this comparison, the data are grouped into sites with  $V_{s30} < 450$  m/s and sites with  $V_{s30} > 450$  m/s, and then we use reference  $V_{s30}$  values of 300 m/s and 700 m/s, respectively, in the ground motion models. For both  $V_{s30}$  groups, the PGA values for the Anza earthquake are significantly higher than predicted by the models, clustering around the +1 sigma level across a broad distance range.

Figure 4 compares 1 second SA computed from the recorded waveforms against that predicted by the three NGA relations. The same reference  $V_{s30}$  values are used as in Figure 3. For this longer period level, the ground motion models are much closer to the median level of the ground motions across the entire distance range.

We also compare the data and NGA relations using goodness-of-fit measures for 5% damped spectral acceleration calculated from the broadband time histories (e.g., Abrahamson, et al., 1990). For an individual station, the residual  $r(T_i)$  at each period  $T_i$  is given by  $r(T_i) = \ln[sa_O(T_i)/sa_M(T_i)]$ , where  $sa_O(T_i)$  and  $sa_M(T_i)$  are the observed and model predicted spectral acceleration values, respectively. To calculate the model predictions, we use site specific  $V_{s30}$  and Z2.5 (depth to  $V_s=2.5$  km/s) values for each of the stations. The model bias is obtained by averaging the residuals for all stations and both horizontal components at each period. A model bias of zero indicates the model, on average, matches the observed ground motion level. A negative model bias indicates over-prediction and a positive model bias indicates under-prediction of the observations. The results for the three NGA models are shown in Figure 5. All three models have little systematic bias for periods greater than about 1 second, with a standard error of about 0.5 (natural log units). For periods below about 1 second, the models begin to under-predict the data, with a bias that approaches 0.9 in natural log units (factor of 2.5) at a period of about 0.1 second.

Figures 6, 7, and 8 examine these residuals as a function of closest distance,  $V_{s30}$  and Z2.5, respectively. In order to investigate possible azimuthal variations, in each of these figures we have also divided the stations into four quadrants (northeast, southeast, southwest and northwest) relative to the epicenter location. The stations for each quadrant are indicated by a different color/symbol combination in these figures. Finally, each figure shows results for four ground motion metrics: PGA, SA at 0.3 seconds, SA at 1.0 seconds, and SA at 3.0 seconds. The strongest trend seen in these figures is the significant under-prediction of the data by all of the models at the shorter periods. Aside from the slight trend of increasing residual with increasing distance particularly at 0.3 second SA (Figure 6), we do not see any significant correlation of the residuals with either distance,  $V_{s30}$  or Z2.5.

The results shown in Figures 3 through 8 suggest that the elevated level of short period motions may have resulted from a source effect, rather than path and/or site effects. That is, the source process appears to have had very strong high frequency radiation, due for example, to high dynamic stress drop.

## Broadband Ground Motion Simulations

To further investigate the relative contributions of source, path and site effects on the motions, we utilize numerical ground motion simulations. In our approach, the broadband ground motion simulation procedure is a hybrid technique that computes the short period and long period ranges separately and then combines the two to produce a single time history (Graves and Pitarka, 2004). At periods greater than 1 second, the methodology is deterministic and contains a theoretically rigorous representation of kinematic fault rupture and wave propagation effects in 3D viscoelastic media. For this study we derive the 3D velocity structure from the SCEC CVM (version 4). We set the minimum shear velocity at 620 m/s and use a grid spacing of 125 m in the finite-difference grid. Over 500 million nodes are required to represent the model, and the calculation was performed on the Linux cluster at USC's center for High Performance Computing and Communications.

The short-period ( $T < 1$  sec) simulation methodology computes the response assuming a random phase, an omega-squared source spectrum, and simplified Green's functions. The methodology follows from Boore (1983) with the extension to finite-faults given by Frankel (1995) and Hartzell et al. (1999). The source is represented by one or more subfaults, each of which rupture with a moment proportional to the final slip given by the original source model. The subfault moment values are scaled uniformly so that the total moment matches that of the original source model. The subfault corner frequency ( $f_c$ ) is defined by

$$(1) \quad f_c = s_z s_t \frac{v_r}{\pi d}$$

where  $v_r$  is the rupture speed,  $d$  is the subfault dimension,  $s_z$  scales the corner frequency with depth, and  $s_t$  relates the corner frequency to the rise time of the subfault source. In our methodology, we use a uniform value of  $s_t = 1.6$ . From the surface to a depth of 5 km, the depth scaling factor is set to a constant value,  $s_z = 1.0$ . This value increases linearly with depth to a value of  $s_z = 1.4$  at 10 km. Below 10 km depth,  $s_z$  is constant at 1.4. This parameterization follows from the observation in crustal earthquakes that slip rate is relatively low for shallow ruptures and increases with rupture depth (Kagawa et al., 2004). Because corner frequency scales with slip rate, this formulation replicates the trend of the observations. We note that although this formulation reduces the number of free parameters, it is not unique and probably has tradeoffs with other parameters in the stochastic model. In particular, allowing the subfault stress parameters to vary across the fault would accommodate a similar slip rate scaling. Instead, we fix the stress parameter to a uniform value of 50 in our simulations. Finally, the convolution operator of Frankel (1995) scales the subevent corner frequency to the corner frequency of the target event.

The formulation requires the specification of a 1D layered velocity model in calculating simplified Green's functions and impedance effects. In this study, we use a 1D velocity model that roughly follows the average depth variations in the 3D structure, and we include both direct and Moho-reflected rays, which are attenuated by  $1/R_p$ , where  $R_p$  is the total path length traveled by the particular ray. For each ray we compute a radiation pattern coefficient by averaging over a range of slip mechanisms and take-off angles. Anelasticity is incorporated via a travel time

weighted average of the Q values for each of the material layers and a generic rock site spectral decay operator,  $\kappa = 0.05$ . Finally, gross impedance effects are included using quarter wavelength theory (Boore and Joyner, 1997) to derive amplification functions that are consistent with the specified 1D velocity structure.

To account for site specific geologic conditions in both the short and long period simulations, we apply period dependent, non-linear amplification functions to the simulated time histories. These functions were derived empirically by Borchardt (1994) and have the general form

$$(2) \quad F_x = \left( \frac{v_{site}}{v_{ref}} \right)^{m_x}$$

where  $v_{site}$  denotes the 30 m travel-time averaged shear wave speed (Vs30) at the site of interest,  $v_{ref}$  corresponds to the Vs30 where the ground response is known, and  $m_x$  denotes an empirically determined factor that depends on both period and ground motion level. For each location in the simulation grid, we obtain the site specific Vs30 ( $v_{site}$ ) from the map of Wills et al. (2000) and  $v_{ref}$  is set to the shear wave speed from the 3D velocity model for that location.

For the Anza earthquake, we define a fault plane having a total area of 13 km<sup>2</sup> (3.6 km by 3.6 km), consistent with the scaling relation of Somerville et al (1999). The fault depth is 14 km and the orientation of the plane and sense of slip are given by the CAP inversion results in Table 2 with the moment set at  $5 \times 10^{23}$  dyne-cm. The region covered by the simulation included 79 sites which recorded the Anza earthquake, extending to epicentral distances of about 110 km. Most of the stations not included in this region are southwest of the epicenter in the San Diego area (see Figure 2). For the long period simulation, the source is represented as a point moment-tensor within the finite-difference grid. The deterministic slip function is a triangle having a rise time of 0.2 seconds, which is well below the deterministic bandwidth threshold of 1 second. For the short period simulation, we use 1 subfault to represent the source, which has a resulting corner frequency of 1.3 Hz after application of the Frankel convolution operator. Based on the analysis of the simulation results obtained with the above parameterization (described below), we have also run the short period model using a corner frequency scaled by an additional factor of 1.6, giving  $f_c = 2$  Hz.

Figure 9 compares the model bias and goodness-of-fit results between the simulated and recorded spectral accelerations at 79 sites. The top panel of this figure shows the results from the original simulation and the bottom panel shows the results obtained with the additional scaling of corner frequency. The original simulation ( $f_c = 1.3$  Hz) produces results that are quite similar to the goodness-of-fit results obtained with the empirical ground motion models (Figure 5). That is, at long periods ( $T > 1$  sec), the simulation has little bias and a standard error of about 0.5 (natural log units). At short periods, this simulation significantly under-predicts the observed motions in a manner very similar to the empirical models. However, the refined simulation ( $f_c = 2$  Hz) produces a much better match to the observed motions at the shorter periods.

We provide a detailed examination of these residuals in Figures 10, 11 and 12, which plot the results as a function of closest distance, Vs30, and Z2.5, respectively. As was done in the earlier comparisons with the empirical models, we group the stations by quadrant, although, as was mentioned previously, the simulation grid has relatively few sites in the southwest quadrant (blue circles in the figures). These figures show a very clear and systematic difference in the two simulation results. The scaling of corner frequency in the refined simulation produces a much improved fit to the shorter period observations compared to the original simulation. Comparing these results with the results from the empirical ground motion models (Figures 6, 7 and 8), we see that the behavior of the original simulation is quite similar to the empirical models. Again, aside from the slight trend of increasing residual with increasing distance particularly at 0.3 second SA (Figure 10), we do not see any significant correlation of the simulation residuals with either distance, Vs30 or Z2.5.

One of the benefits of the numerical simulation approach is that it produces full three component time histories for each site. Figure 13 compares recorded and simulated ( $f_c = 2$  Hz) ground velocity waveforms at 18 selected sites. For this comparison, we have bandpass filtered both the data and synthetics in the period range  $1 < T < 5$  seconds, in order to concentrate on the more deterministic features of the waveforms. The distance range of the sites shown in Figure 13 spans from 18 to 119 km. For the stations nearest the epicenter, both the recorded and simulated motions are relatively brief. As the distance range increases, the recorded motions begin to show more complexity and significantly longer durations of shaking. In general, the waveforms and amplitudes of the main S-wave pulses are matched reasonably well by the simulations. The match of the synthetics to the data clearly exhibits significant variability among these sites, with some sites being matched quite well (e.g., 13162), and other sites not matched nearly as well (e.g., 12092). We attribute these differences primarily to limitations of the current 3D velocity model used in the simulations.

### Discussion and Conclusions

The comparisons presented in the preceding sections suggest that the 2005 Anza earthquake had a source process that radiated relatively strong short period energy. The success of the numerical modeling using the scaled-up corner frequency further suggests that the increase in short period radiation is related to the dynamics of rupture. One potential mechanism to produce this effect is a relatively high slip velocity possibly in conjunction with a fast rupture across a concentrated high slip patch on the fault. Either of these can produce a relatively high dynamic stress drop during rupture, which will result in elevated levels of shorter period radiation. Unfortunately, the current resolution of our numerical modeling doesn't allow discrimination between these effects. Further study aimed at mapping out the finer scale details of the rupture process are needed to address these questions. These studies might include examination of pre- and post-event seismicity to characterize the spatial and temporal evolution of these ruptures with the aim of constraining the mainshock rupture area. Additionally, analysis of short period directivity effects may also provide constraints on the nature and orientation of rupture (Tan and Helmberger, 2007).

On a broader scale, the features of this earthquake are certainly indicative of the state of stress along this section of the San Jacinto fault zone, with possible implications for seismic



hazard mitigation. The Anza region has several conjugate structures intersecting the San Jacinto fault zone (Tom Rockwell, personal communication). The apparent high dynamic stress drop of the 2005 event is suggestive of rupture on a less well developed conjugate structure. If the 2005 event (and previous events such as 2001) occurred along one of these conjugate structures, then it may suggest that the through-going fault structure (San Jacinto fault) is moving closer to failure. Rockwell has documented numerous  $M \sim 7$  paleo-earthquakes at a site about 10 km northwest of the 2005 event (Hog Lake, just across the seismic gap). Clearly, the main fault trace is active and capable of generating significant earthquakes. Further study of the Anza earthquake may provide valuable insight into the seismogenic process of the San Jacinto fault zone.

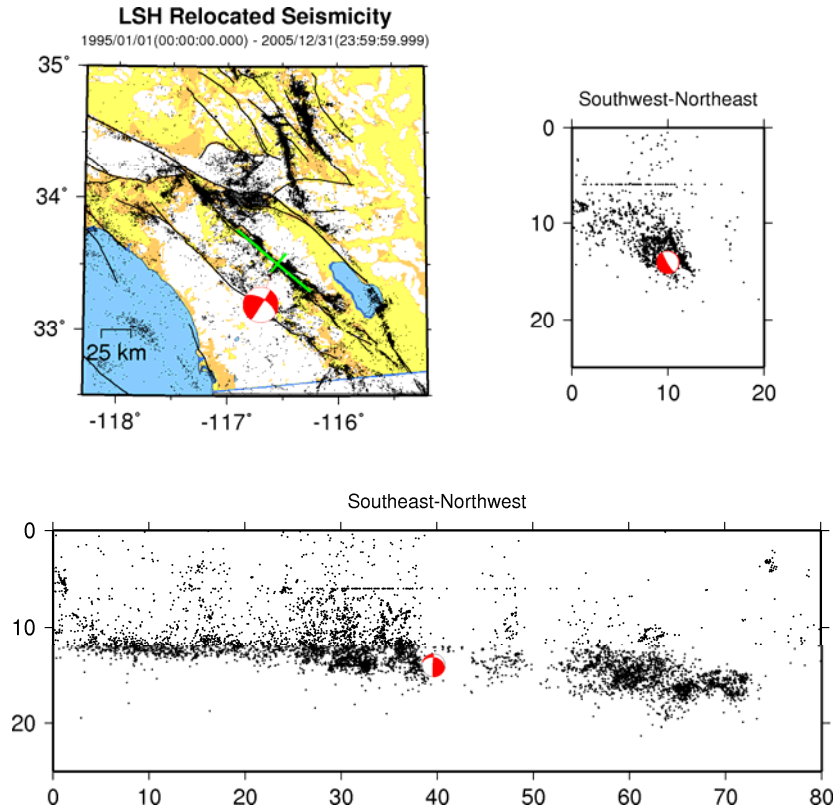
### Acknowledgements

Strong ground motion recordings from the US Geological Survey and the Strong Motion Instrumentation Program (SMIP) of the California Geological Survey provided the bulk of the data used in this study. The large scale 3D numerical calculations were carried out on the Linux cluster at USC's center for High Performance Computing and Communications under a grant to the Southern California Earthquake Center. Funding for this work was provided by the Data Interpretation Project of the California Strong Motion Instrumentation Program.

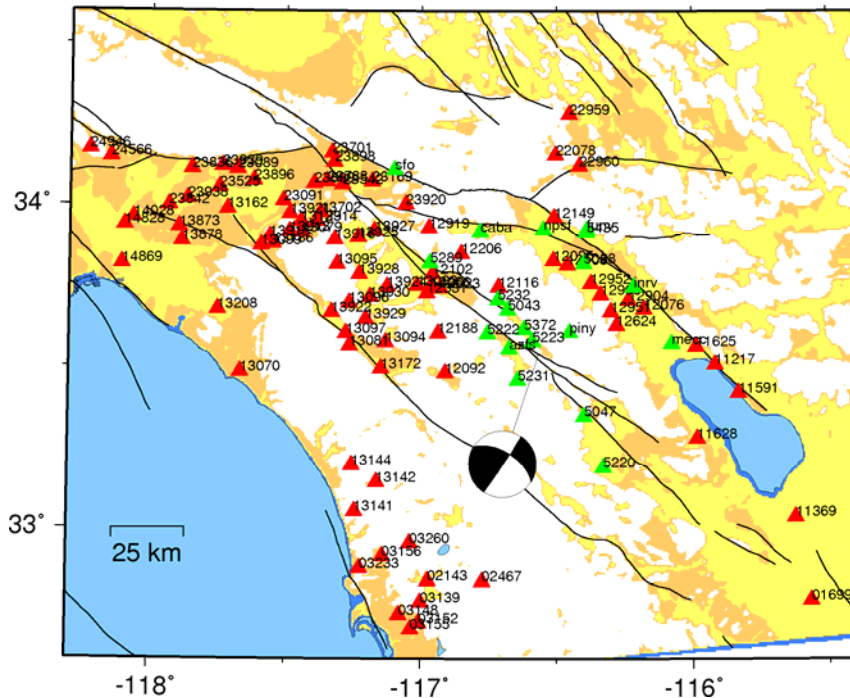
### References

- Abrahamson, N. A., P. G. Somerville, and C. A. Cornell (1990). Uncertainty in numerical strong motion predictions, *Proc. 4th U.S. National Conf. on Earthquake Engineering*, **1**, 407-416.
- Boore, D. M. (1983). Stochastic simulation of high-frequency ground motions based on seismological models of the radiated spectra. *Bull. Seism. Soc. Am.*, **73**, 1865–1894.
- Boore, D. M. and W. B. Joyner (1997). Site amplifications for generic rock sites. *Bull. Seism. Soc. Am.*, **87**, 327–341.
- Boore, D. and G. Atkinson (2007). Boore-Atkinson NGA ground motion relations for the geometric mean horizontal component of peak and spectral ground motion parameters, *Technical Report 2007/01, Pacific Earthquake Engineering Research Center*, University of California, Berkeley, CA.
- Borcherdt, R. D. (1994). Estimates of site-dependent response spectra for design (methodology and justification). *EQ Spectra*, **10**, 617–653.
- Campbell, K.W. and Y. Bozorgnia (2007). Campbell-Bozorgnia NGA ground motion relations for the geometric mean horizontal component of peak and spectral ground motion parameters, *Technical Report 2007/02, Pacific Earthquake Engineering Research Center*, University of California, Berkeley, CA.

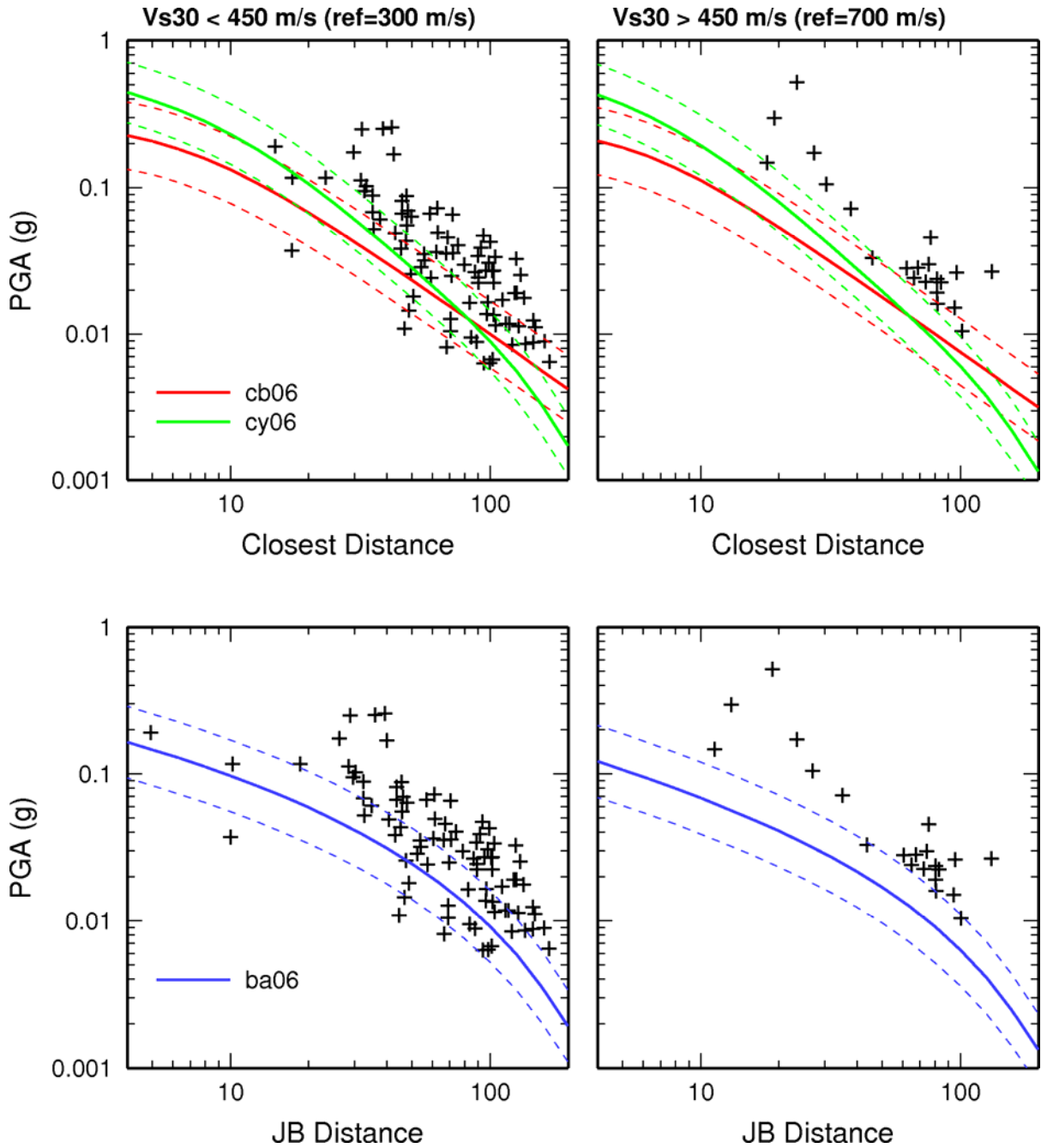
- Chiou, B. S. J. and R. R. Youngs (2006). Chiou and Youngs PEER-NGA empirical ground motion model for the average horizontal component of peak acceleration and pseudo-spectral acceleration for spectral periods of 0.01 to 10 seconds, *Interim Report for USGS Review, Pacific Earthquake Engineering Research Center*, University of California, Berkeley, CA.
- Frankel, A. (1995). Simulating strong motions of large earthquakes using recordings of small earthquakes: the Loma Prieta mainshock as a test case. *Bull. Seism. Soc. Am.*, **85**, 1144–1160.
- Graves, R. W. and A. Pitarka (2004). Broadband time history simulation using a hybrid approach, *Proc. 13th World Conference on Earthquake Engineering*, Vancouver, Canada. paper no. 1098.
- Hartzell, S., S. Harmsen, A. Frankel, and S. Larsen (1999). Calculation of broadband time histories of ground motion: Comparison of methods and validation using strong-ground motion from the 1994 Northridge earthquake, *Bull. Seism. Soc. Am.*, **89**, 1484–1504.
- Kagawa, T., K. Irikura, and P. G. Somerville (2004). Differences in ground motion and fault rupture process between the surface and buried rupture earthquakes, *Earth, Planets, and Space*, **56**, 3–14.
- Lin, G., P. M. Shearer, and E. Hauksson (2007). Applying a 3D velocity model, waveform cross-correlation, and cluster analysis to locate southern California seismicity from 1981 to 2005, *submitted to J. Geophys. Res.*
- Somerville, P. G., K. Irikura, R. Graves, S. Sawada, D. Wald, N. Abrahamson, Y. Iwasaki, T. Kagawa, N. Smith, and A. Kowada (1999). Characterizing crustal earthquake slip models for the prediction of strong ground motion, *Seism. Res. Lett.*, **70**(1), 199–222.
- Tan, Y., and D. Helmberger (2007). Rupture directivity of the 2003 Big Bear aftershocks, *submitted to Bull. Seism. Soc. Am.*
- Wills C, M. Petersen, W. Bryant, M. Reichle, G. Saucedo, S. Tan, G. Taylor and J. Treiman (2000). A site conditions map for California based on geology and shear wave velocity. *Bull. Seism. Soc. Am.*, **90**(6B): S187-S208.
- Zhu, L. and D. Helmberger (1996). Advancement in source estimation techniques using broadband regional seismograms, *Bull. Seism. Soc. Am.*, **86**, 1634-1641.



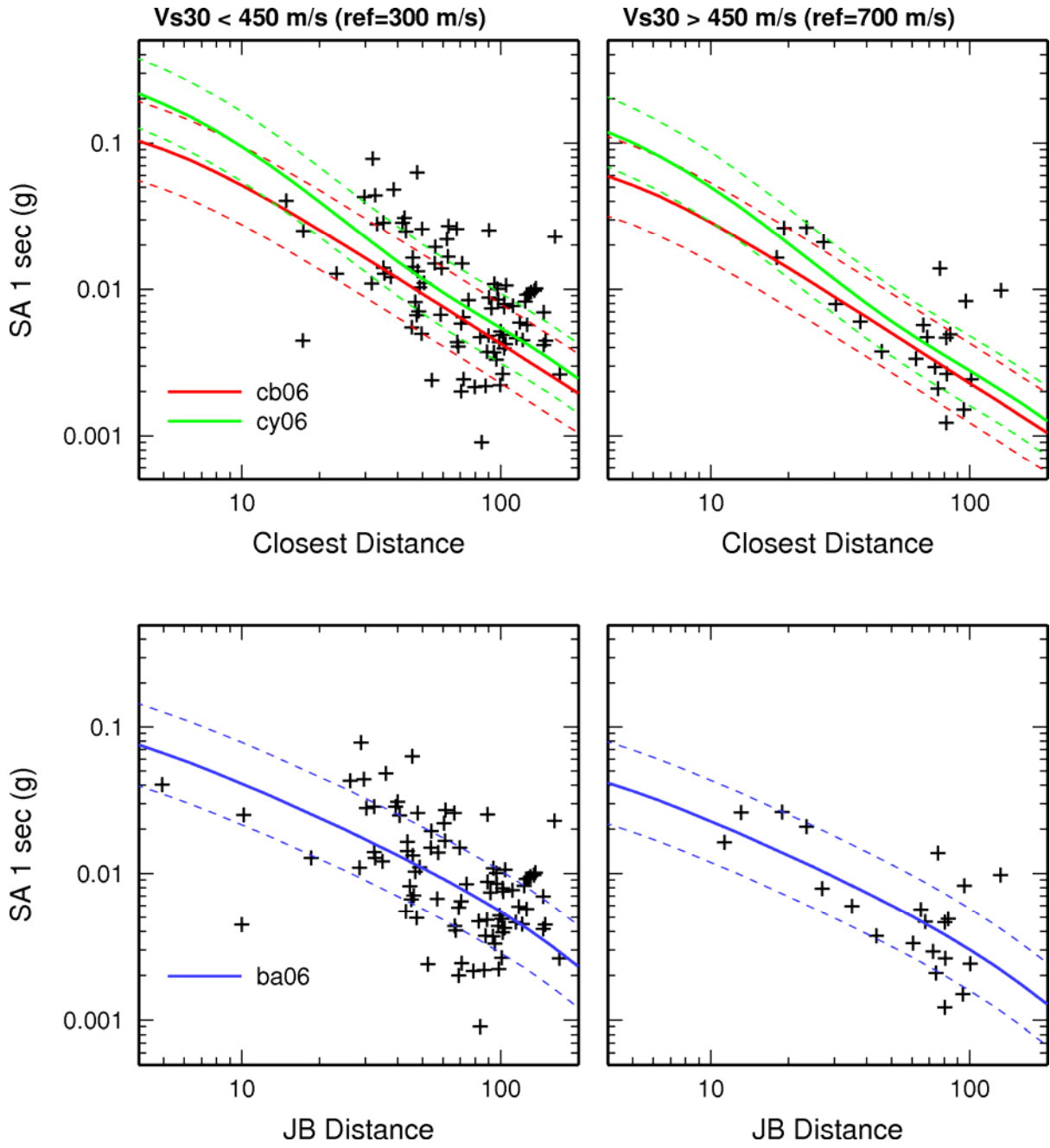
**Figure 1:** Relocated seismicity of southern California from 1995 through 2005 (Lin et al., 2007). The 2005 Anza event is indicated by “beach ball” mechanism. The event occurred at the southern edge of the Anza seismic gap at a depth of about 14 km. The mechanism is primarily strike slip, although the exact fault plane is ambiguous.



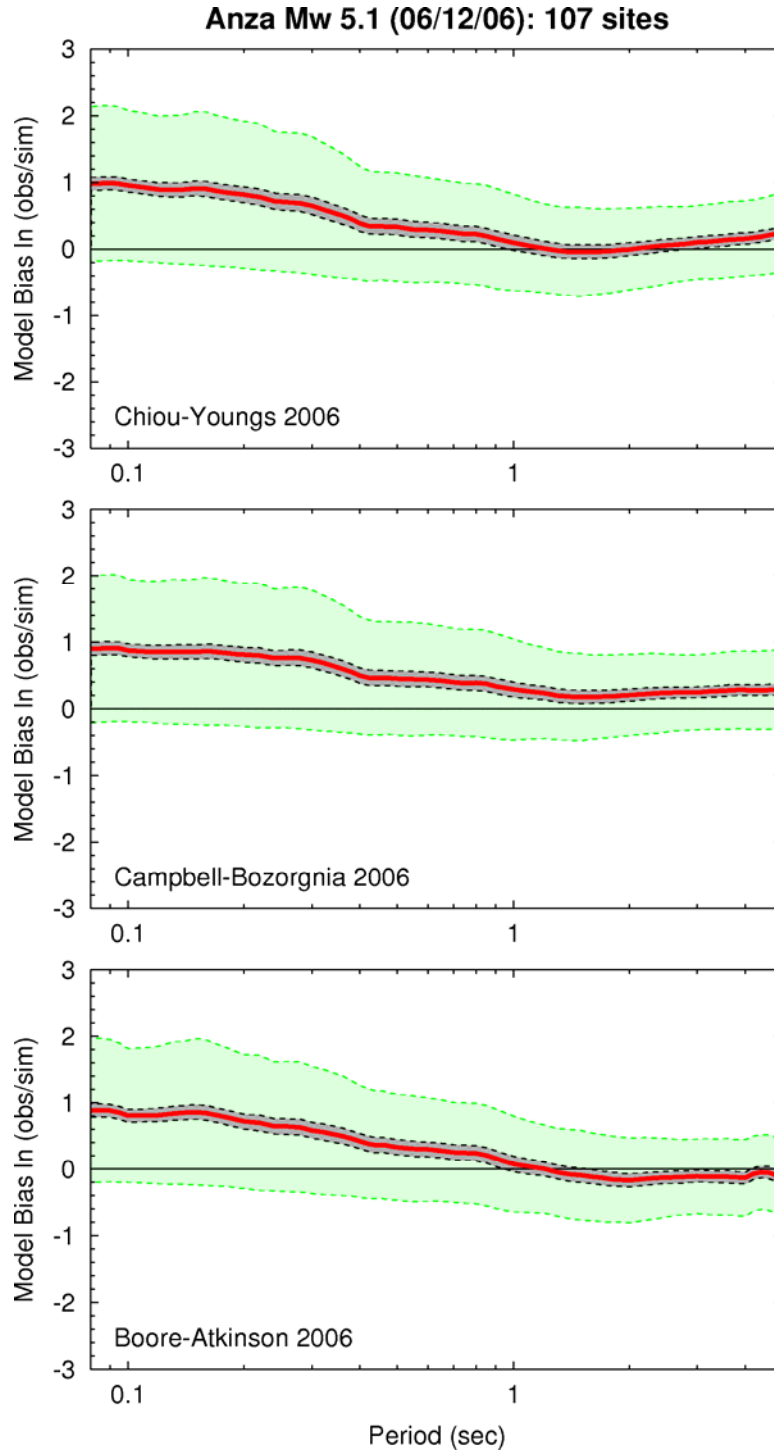
**Figure 2:** Map showing strong motion recording sites for the 2005 Anza earthquake. Green triangles are stations operated by the USGS and red triangles are CGS stations.



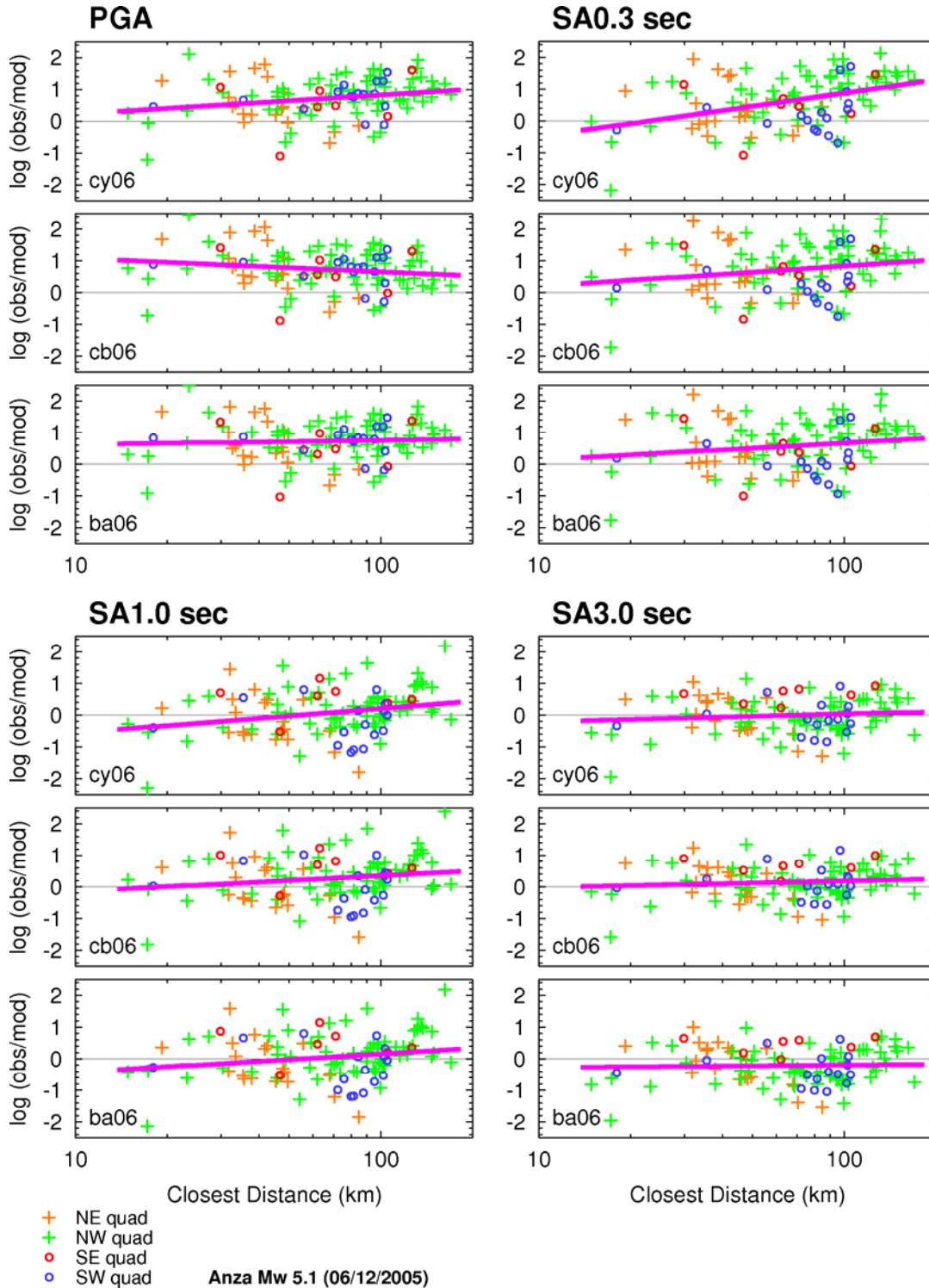
**Figure 3:** Attenuation of peak ground acceleration (PGA) as a function of distance for the Anza earthquake. Closest distance is used in the top panels and Joyner-Boore distance is used in the bottom panels. Median (solid lines) and  $\pm 1$  sigma (dashed lines) attenuation curves from three recent NGA ground motion models are shown as well (cb06 is Campbell and Bozorgnia, 2006; cy06 is Chiou and Youngs, 2006; ba06 is Boore and Atkinson, 2006). The left panels show data from sites having  $V_{s30}$  less than 450 m/s and the right panels show data for site with  $V_{s30}$  greater than 450 m/s. Reference  $V_{s30}$  values used in the empirical models are 300 m/s and 700 m/s for the left and right panels, respectively.



**Figure 4:** Same as Figure 3 except ground motion parameter is spectral acceleration (SA) at 1 second period.



**Figure 5:** Model bias and goodness-of-fit for the three NGA ground motions models for the Anza earthquake data. Ground motions from total of 107 stations are used for this analysis. The heavy red line is the overall model bias, the green shading represents  $\pm 1$  sigma, and the grey shading is the 90% confidence of the mean. All three models produce quite similar results, with a significant under-prediction of the data for periods less than about 1 second.



**Figure 6:** Residuals between observed ground motion values and the three NGA model predictions plotted as a function of closest distance to rupture. Each set of three panels shows results for a different ground motion metric: PGA in upper left, SA at 0.3 seconds in upper right, SA at 1.0 second in lower left, and SA at 3.0 seconds in lower right. Site locations are grouped into four quadrants relative to the epicenter, as denoted by the different colored symbols. The heavy line on each panel is a least square fit to the residuals. There is a clear trend of increasing under-prediction with decreasing period for all models.

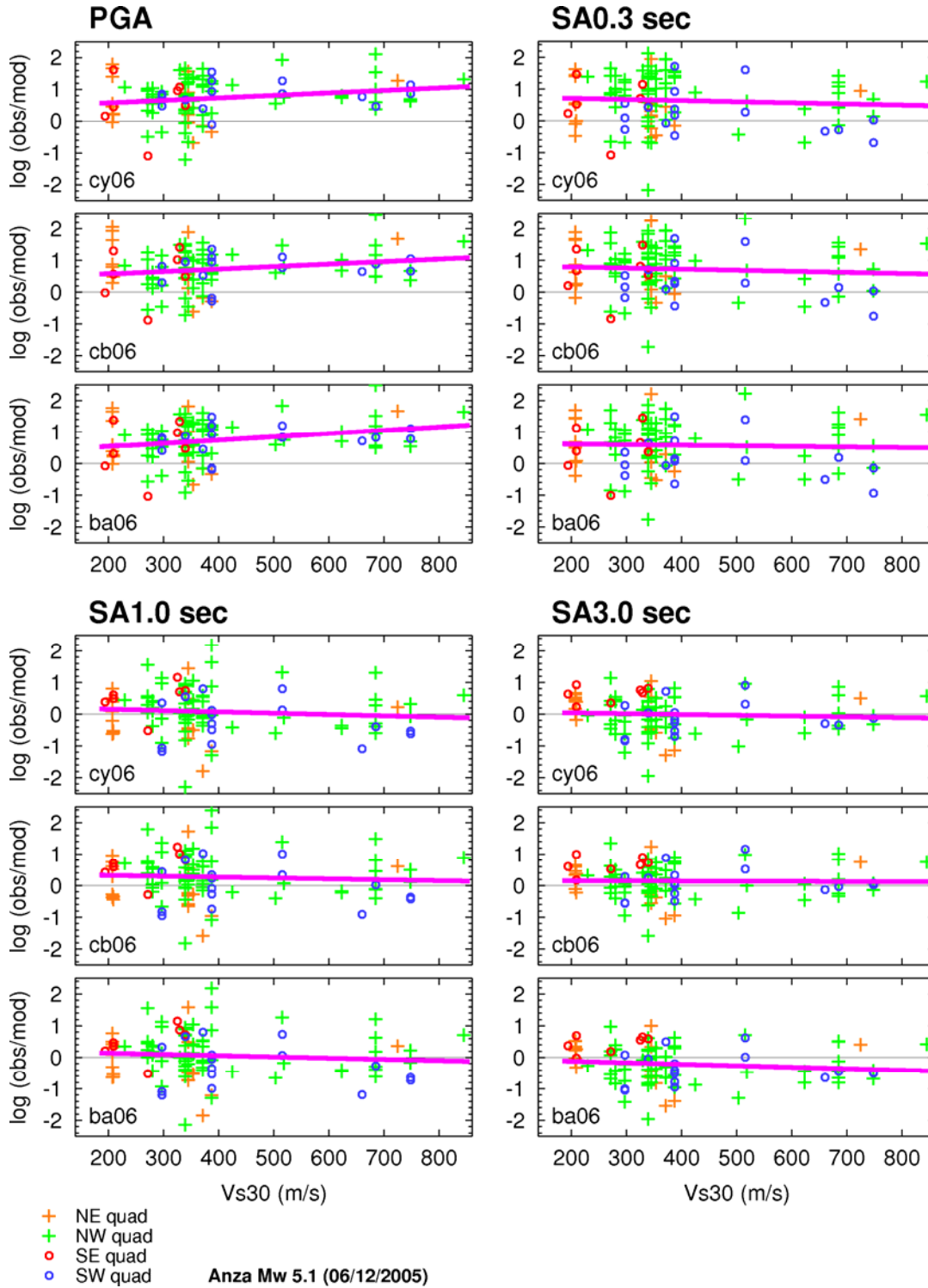


Figure 7: Same as Figure 6 except residuals are plotted as a function of Vs30 value.



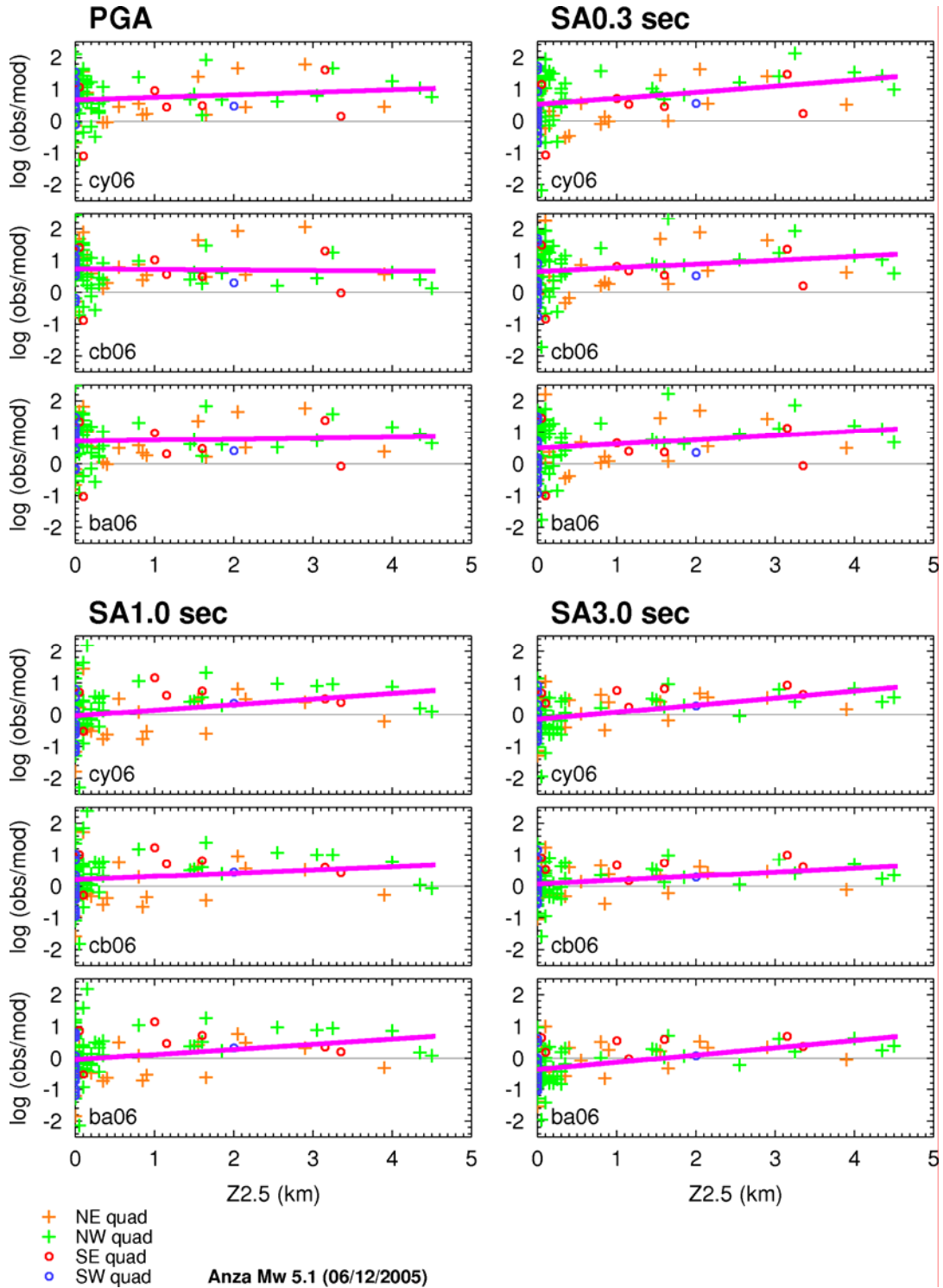
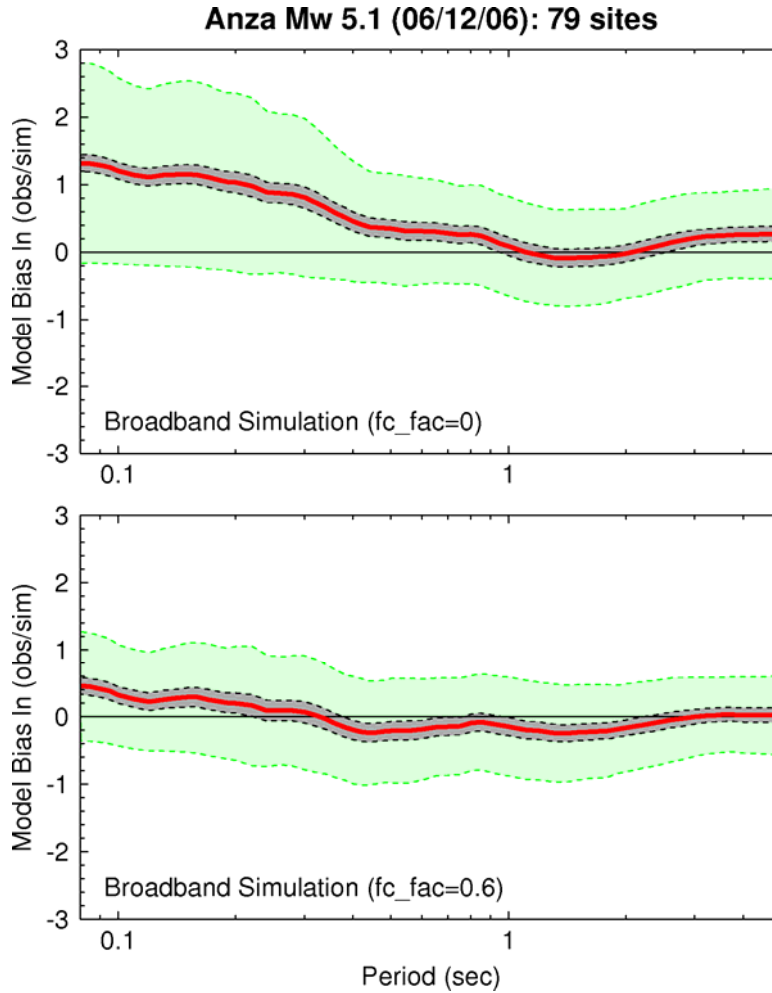
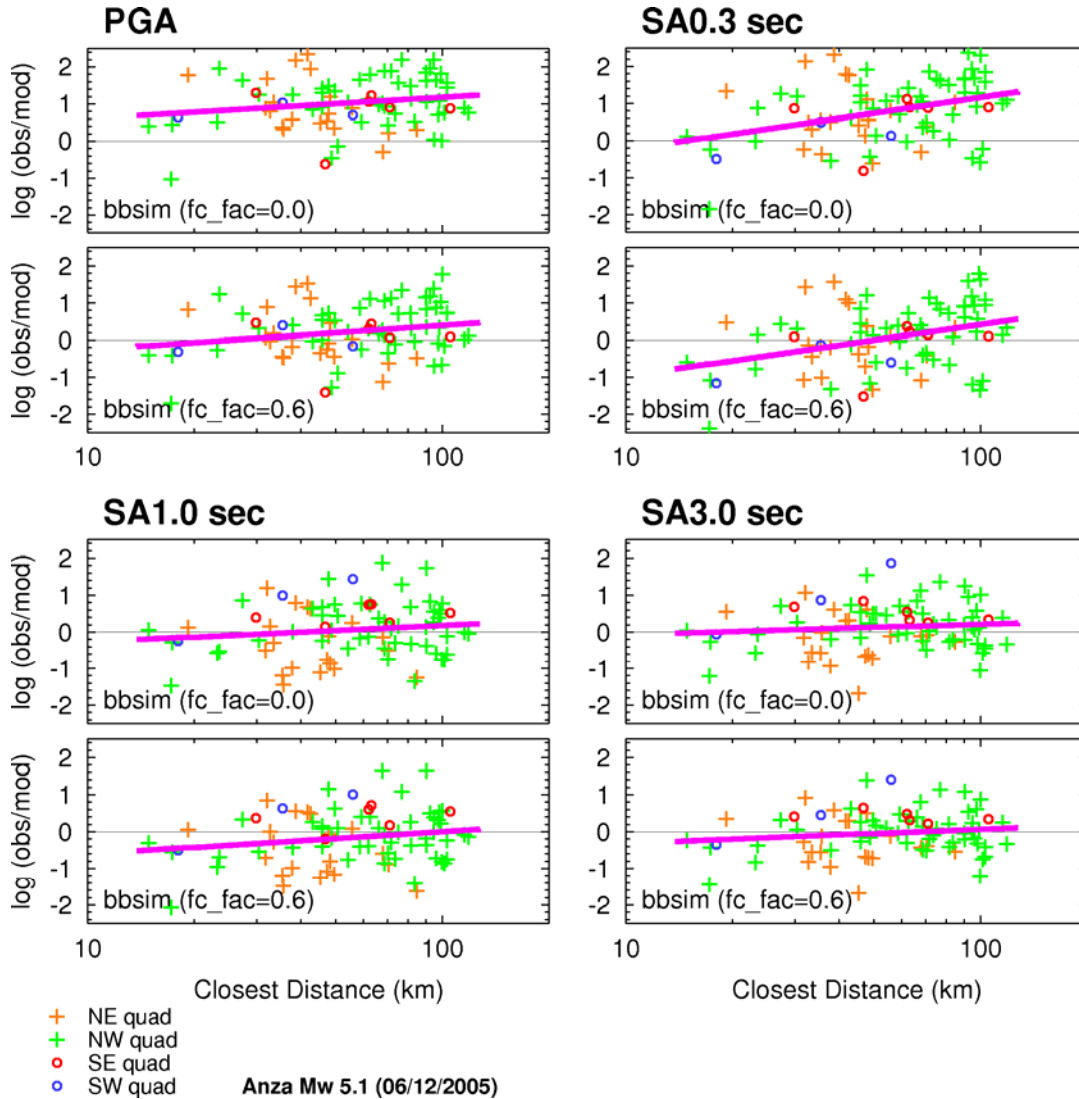


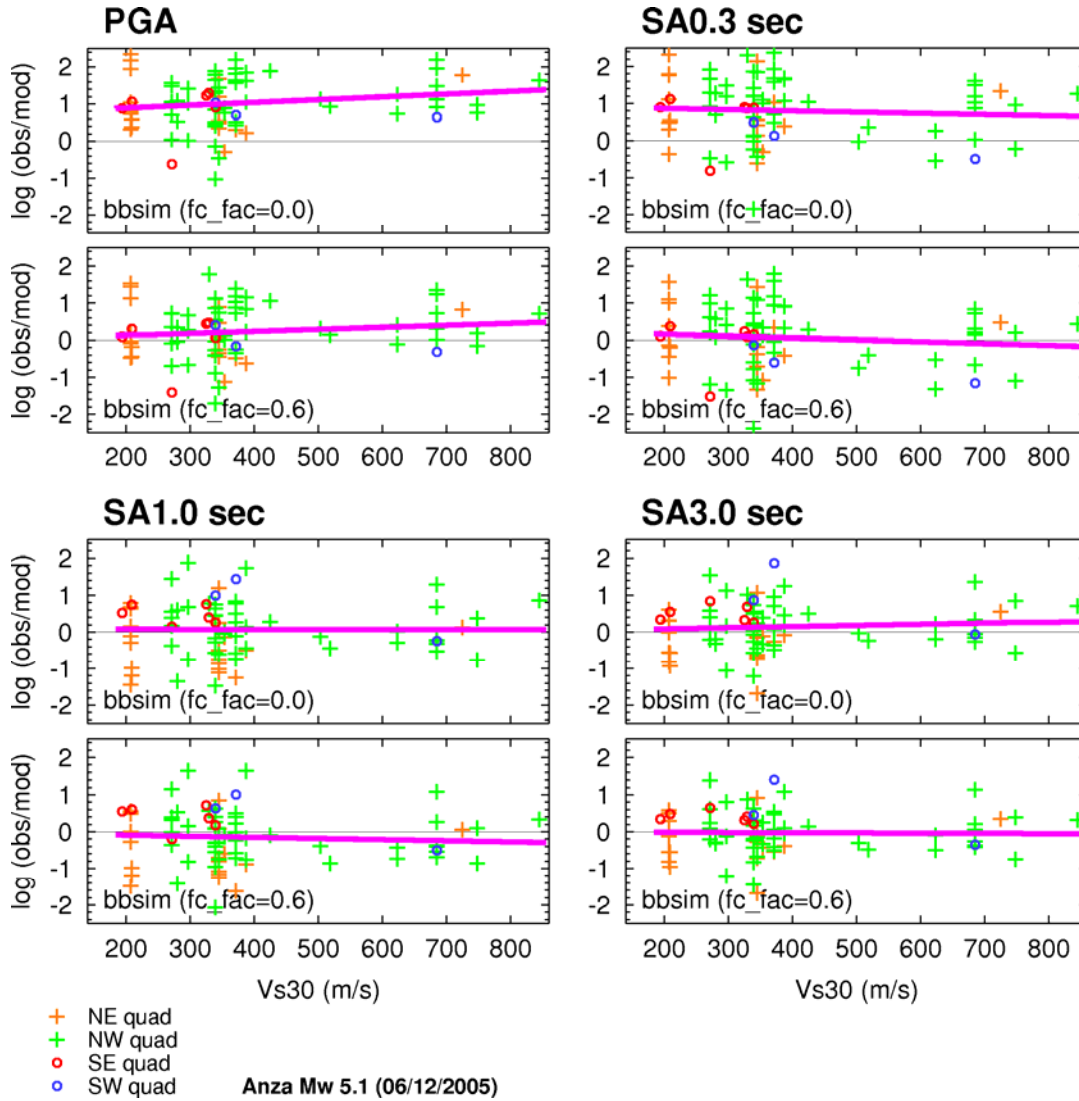
Figure 8: Same as Figure 6 except residuals are plotted as a function of depth to  $V_s=2.5$  km/s isosurface ( $Z_{2.5}$ ).



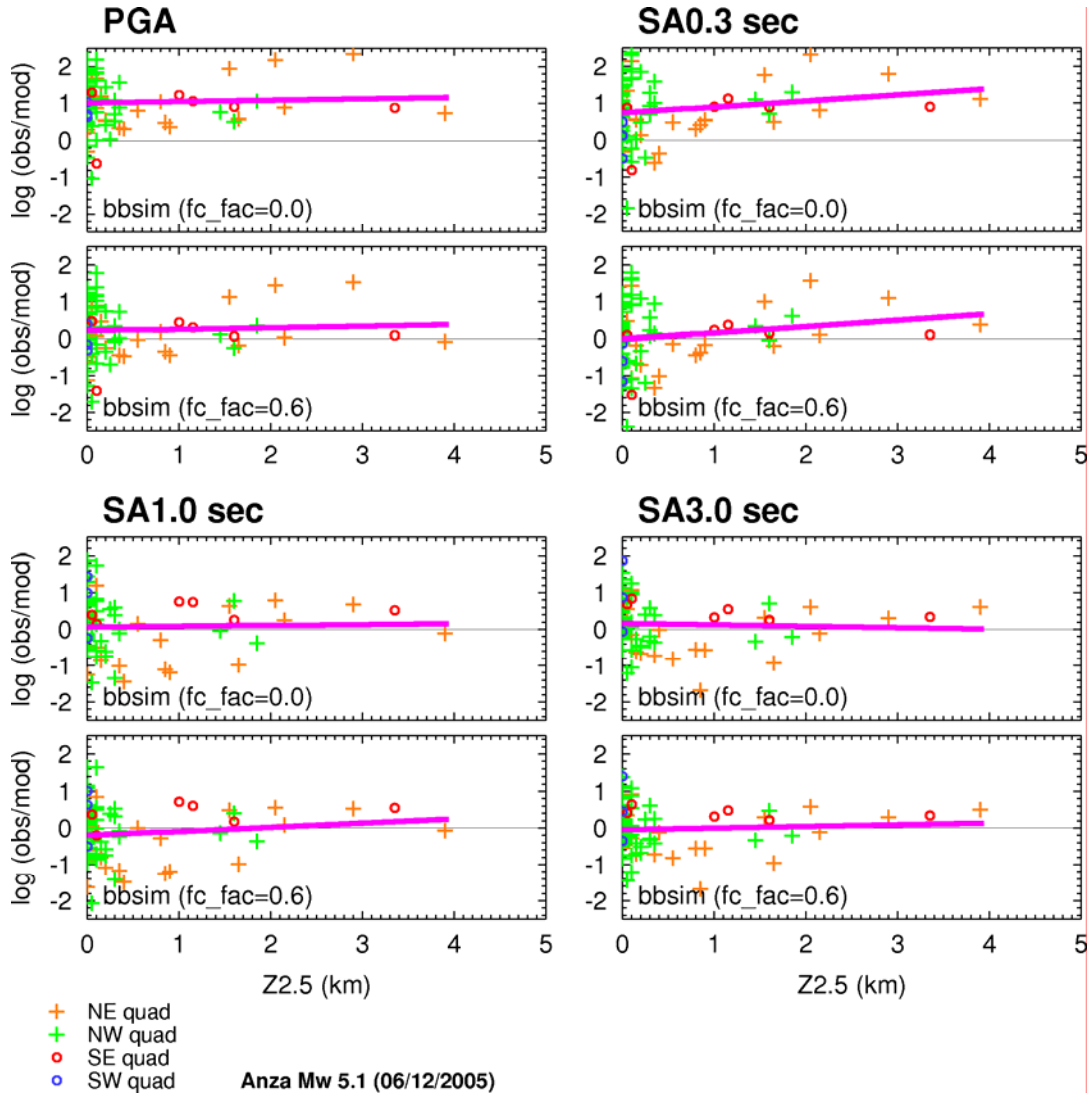
**Figure 9:** Model bias and goodness-of-fit for the numerical ground motion simulations for the Anza earthquake data. Ground motions from total of 79 stations are used for this analysis. The heavy red line is the overall model bias, the green shading represents  $\pm 1$  sigma, and the grey shading is the 90% confidence of the mean. The top panel shows results using a generic source description and is quite similar to the empirical models, with a significant under-prediction of the data for periods less than about 1 second. The bottom panel shows results for a simulation using a 60% increase in the source corner frequency, which produces a much better match to the observations.



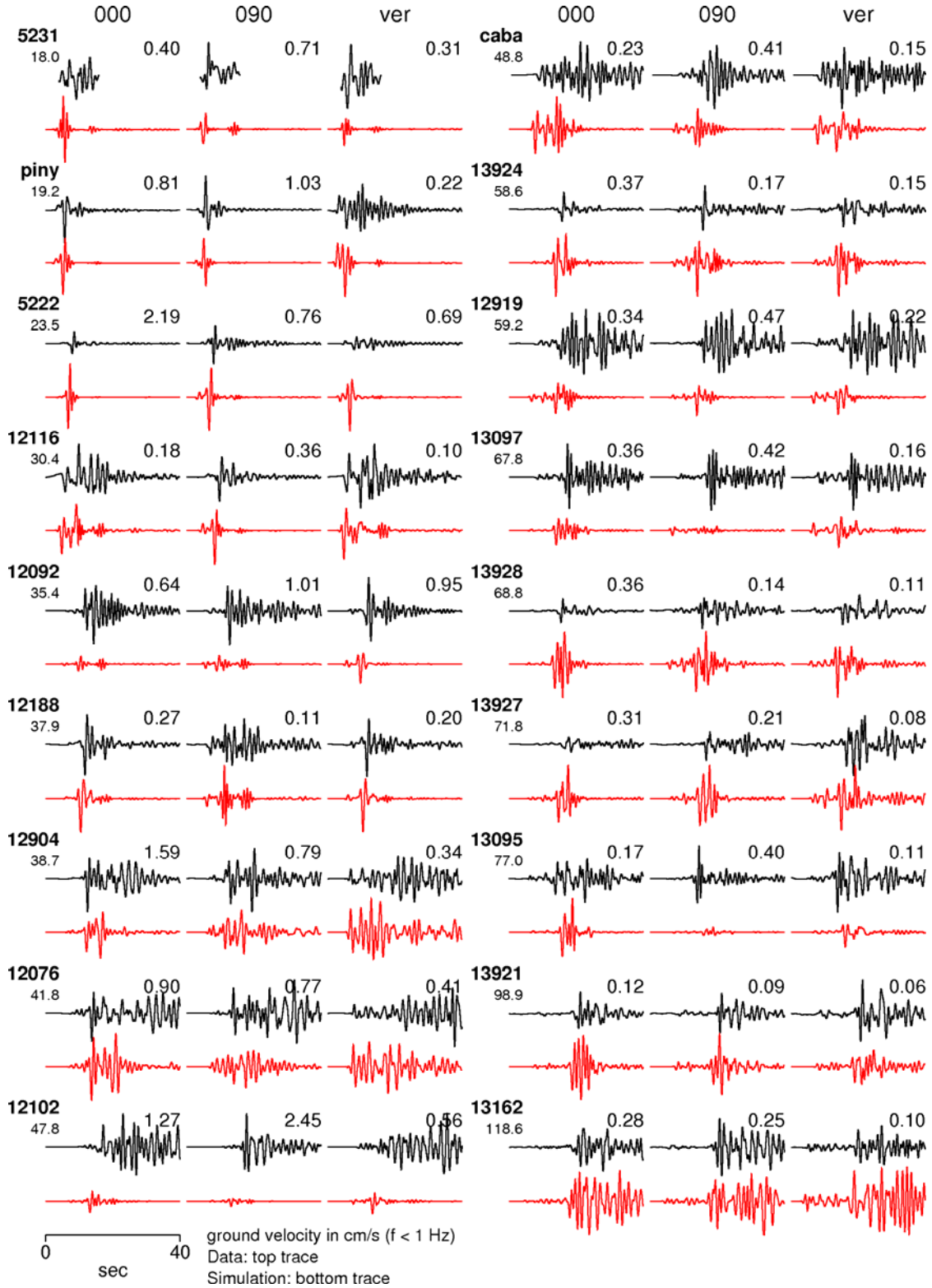
**Figure 10:** Residuals between observed ground motion values and the two broadband ground motion simulations plotted as a function of closest distance to rupture. The top panel in each group shows results using a generic source corner frequency and the bottom panel shows results for a simulation using a 60% increase in the source corner frequency. Each set of two panels shows results for a different ground motion metric: PGA in upper left, SA at 0.3 seconds in upper right, SA at 1.0 second in lower left, and SA at 3.0 seconds in lower right. Site locations are grouped into four quadrants relative to the epicenter, as denoted by the different colored symbols. The heavy line on each panel is a least square fit to the residuals. The first simulation shows a clear trend of increasing under-prediction with decreasing period, similar to the empirical models, whereas the second simulation produces a significantly better fit to the data.



**Figure 11:** Same as Figure 10 except residuals are plotted as a function of Vs30 value.



**Figure 12:** Same as Figure 10 except residuals are plotted as a function of depth to  $V_s=2.5$  km/s isosurface (Z2.5).



**Figure 13:** Comparison of recorded (black) and simulated (red) three component ground velocity waveforms at 18 selected sites. Both recorded and simulated motions have been bandpass filtered between 0.2 and 1.0 Hz. Site names and closest distance are listed to the left of each set of traces. Each data/synthetic pair is scaled to the same peak amplitude value which is shown above the traces (in cm/s).

## ANALYSIS OF SEISMIC RESPONSE OF SEVEN OAKS DAM

Lelio H. Mejia and Ethan M. Dawson

URS Corporation  
Oakland, California

### Abstract

Procedures for the three-dimensional (3-D) dynamic analysis of earth dams have been available for over 25 years. However, additional case histories are needed to assess whether such procedures are capable of simulating the seismic response of dams in narrow canyons, and to further evaluate the effects of 3-D behavior on the response of such dams. This paper describes a study aimed at identifying the vibration characteristics of Seven Oaks Dam during the 2005 Yucaipa and 2001 Big Bear Lake earthquakes, and at evaluating the applicability of 3-D and two-dimensional numerical procedures to simulate the recorded response of the dam.

### Introduction

The seismic stability evaluation of earth and rockfill dams typically requires an analysis of their dynamic response to earthquake shaking. Such analysis is commonly performed using finite element procedures. Although procedures for the three-dimensional (3-D) dynamic response analysis of earth dams in narrow canyons have been available for over 25 years, they are seldom used in practice for design purposes. This is mainly because: a) the effects of 3-D behavior on the seismic stability of such dams are generally believed to be beneficial, and b) the modeling and computational effort associated with 3-D analysis is significantly greater than that associated with two-dimensional (2-D) analysis.

Previous studies have shown that 3-D behavior can have a pronounced effect on the seismic response of earth dams with crest length to height ratios less than about 6 (e.g. Boulanger et al., 1995, Dakoulas, 1993, Mejia and Seed, 1983). Three-dimensional behavior of such dams can result in significantly larger accelerations at the dam crest than might otherwise be expected based on 2-D analysis procedures. Thus, for such types of dams, 3-D analysis procedures may be required to adequately evaluate their acceleration response and potential for seismic deformations.

Additional case histories of dams in narrow canyons are needed to: a) assess the effects of 3-D behavior on the seismic response of those types of dams and the extent to which available methods of 3-D analysis adequately simulate their response, and b) develop guidance for the use of 3-D analysis methods in engineering practice. One such case history is the recorded seismic response of Seven Oaks Dam during the June 16, 2005 Yucaipa and the February 10, 2001 Big Bear Lake earthquakes.

This paper describes a study aimed at identifying the modes of vibration of Seven Oaks Dam during the aforementioned earthquakes and evaluating the applicability of 3-D and 2-D numerical models to simulate the recorded dynamic response of the dam. Because the dam has a curved axis and sits in a canyon of limited width, it may be expected to exhibit 3-D behavior under earthquake shaking. Thus, given that the dam site is well instrumented with strong motion accelerographs, this case history offers an excellent opportunity to evaluate the effects of 3-D vibration modes on the seismic response of a large dam in a relatively narrow canyon, and the ability of available 3-D and 2-D numerical techniques to simulate the key aspects of the dam's recorded response.

## **Description of Seven Oaks Dam**

### **General**

Seven Oaks Dam is a zoned rockfill embankment located on the Santa Ana River about 10 km northeast of the city of Redlands in San Bernardino County, California. The dam was completed in 1999 by the U.S. Army Corps of Engineers (USACE) primarily to provide downstream flood protection to Orange County and other areas of the Santa Ana River Basin. The site is located about 2 km from the San Andreas Fault, and the dam was designed to withstand a maximum credible earthquake of magnitude 8+ on that fault (USACE, 1992; Makdisi et. al, 1996).

The dam has a structural height of about 640 feet, a crest length of 2,760 feet, and a volume of 38 million cubic yards. As shown in Figure 1, the embankment is curved upstream and its width is approximately equal to its length. The outlet works are located on the left abutment and consist of an intake tower, an 18-foot-diameter tunnel, an outlet channel, and a plunge pool. A vertical shaft provides air supply and access to a gate chamber located just downstream of the tunnel midpoint (Figure 1). The spillway is a 500-foot-wide channel cut through a rock ridge east of the left abutment, with a crest elevation 30 feet below that of the dam crest.

### **Embankment and Foundation Materials**

Figure 2 shows the maximum section of the dam, which is located near the midpoint of the crest. The embankment consists of a moderately inclined upstream sloping core flanked upstream by a filter, and alluvial transition and shell zones. On the downstream side, the core is supported by a rockfill transition zone, a chimney drain, and a rockfill shell. A blanket drain extends from the base of the chimney drain beneath the downstream rockfill shell. Along the stream bed, the upstream and downstream shells are founded on very dense alluvium in turn underlain by bedrock. The core is directly founded on bedrock in a trench excavated through the alluvium.

The dam materials were placed to modern compaction standards and may be considered as generally very dense. The core consists of clayey and silty sands with over 25% fines of low to medium plasticity. The filter and drains are sands and gravels processed from alluvial materials. The alluvial transition consists of processed minus 12-inch cobbles, gravels, and



sands and the alluvial shell of minus 18- to 30-inch cobbles and boulders. The rock transition and rockfill materials are sand to minus 9-inch and 15-inch boulders, respectively, processed from the spillway and other rock excavations.

Because the alluvial transition and shell materials are expected to exhibit similar dynamic behavior, those two zones, together with the upstream filter, were combined into a single zone (designated herein as alluvial fill) for purposes of dynamic analysis. Likewise, the rockfill transition, downstream filter and drain, and rockfill shell were combined into a single zone (designated as rockfill).

### Material Properties

For dynamic response analysis of the dam, the key material properties are the dynamic shear modulus at small strain,  $G_{\max}$ , the unit weight of the materials,  $\gamma$ , Poisson's ratio,  $\nu$ , and the relationships between normalized shear modulus,  $G/G_{\max}$ , and damping ratio with shear strain. The maximum shear modulus may be obtained from the shear wave velocity of the materials,  $V_s$ , by the following expression:  $G_{\max} = V_s^2 \gamma / g$ , where  $g$  is the gravitational constant. For granular soils, the maximum shear modulus may be expressed as a function of the mean effective stress,  $\sigma_m'$ , as follows:  $G_{\max} = K_{2\max} (\sigma_m')^{1/2}$ , where  $K_{2\max}$  is a constant,  $\sigma_m'$  is in psf and  $G_{\max}$  is in ksf.

Extensive field and laboratory tests were carried out prior to construction to characterize the embankment and foundation materials (USACE, 1992). The laboratory tests included cyclic triaxial and resonant column tests of the core materials and of scaled-down gradations of the transition materials. Field tests included multiple seismic refraction surveys in the foundation alluvium and rock, and in compaction test fills. Crosshole and downhole surveys were also used to measure the shear and compression wave velocities of compacted alluvial and rockfill materials in the test fills, and of the underlying foundation alluvium. However, no measurements of the shear and compression wave velocities of the dam materials in place are available.

Table 1 summarizes the key material properties selected for initial dynamic analysis of the dam from examination of the available data. The values of  $K_{2\max}$  for the alluvial fill, the rockfill, and the foundation alluvium were obtained from the crosshole velocity measurements in the test fills. The  $K_{2\max}$  value obtained by the USACE (1992) from the dynamic laboratory tests on the core materials was adopted for the core. The rock shear wave velocities were synthesized from the seismic refraction data.

Limited information is available on the modulus reduction and damping relationships of coarse alluvial fill and rockfill. Previous studies of the seismic response of rockfill dams have made the assumption that such relationships may be approximated by available relationships for cohesionless soils. Boulanger et al. (1995) and Mejia et al. (1991) showed that use of the relationships proposed by Seed et al. (1986) for gravels provided a reasonable approximation to the recorded response of two rockfill dams. Rollins et al. (1998) compiled modulus reduction and damping data for sandy gravels and gravelly sands, which fell over the range defined by the relationships by Seed et al. (1986) for gravels and those proposed for sands by Seed and Idriss (1970). Hardin and Kalinski (2005) presented modulus reduction data for gravels and gravelly sands, which appear to be well represented by the Seed et al. gravel relationship. They also

showed that the relationship between normalized modulus,  $G/G_{\max}$ , and shear strain normalized by the ratio  $(\sigma'_m/P_a)^{1/2}$ , where  $P_a$  is atmospheric pressure, is independent of effective stress.

On the above basis, the Seed et al. (1986) gravel relationships were used for the alluvial fill and rockfill materials in the dam, and the Seed and Idriss (1970) sand relationships were used for the core. To account for the dependency of such relationships on effective stress, the upper bound modulus reduction relationships, and the corresponding damping relationships, were used for zones in the dam with mean effective stresses higher than 10 tsf, as outlined in Table 1.

### **Instrumentation**

The dam site is instrumented with six 3-component strong motion accelerometers. In addition, two accelerometers are located in the river valley about 0.5 km downstream of the dam toe, at a site that may be considered representative of the free field. Other instrumentation at the dam site and on the structures includes survey monuments, inclinometers, piezometers, and flow monitoring devices.

Figure 1 shows the approximate locations of the accelerometer instruments. The center crest instruments are located near the midpoint of the crest, on the maximum dam section. The crest downhole instrument is located at a depth of 152 feet directly below the surface instrument, within the rockfill transition zone (Figure 2). The right crest instrument is located about midway between the center instrument and the right abutment. The right abutment instrument is located on rock at the crest elevation, whereas the gate chamber instrument is located at a depth of 516 feet below the crest elevation, within the left abutment. The intake tower instrument is located at the top of the structure 314 feet below the spillway crest elevation, and was damaged by submergence in 2001.

The soil conditions at the site of the downstream accelerometers consist of 37 feet of dense river alluvium underlain by about 17 feet of weathered rock, and fresh bedrock below. One instrument is located on the ground surface within a small one-story utility building, and the other at a depth of 54 feet in rock.

The accelerometers at the dam crest, right abutment, and tunnel chamber are linked to keep common timing. Similarly, the two downstream accelerometers are linked in between. However, the downstream instruments are not synchronized with the instruments at the dam site.

### **Reservoir Levels**

The reservoir fluctuates considerably between seasons and was almost empty at the time of the Yucaipa and Big Bear Lake earthquakes. During the Yucaipa earthquake, the reservoir level was approximately 470 feet below the dam crest elevation. Water levels in the downstream alluvium fluctuate as well. The ground water level at the time of the earthquakes was estimated to be 20 feet below the ground surface at the location of the downstream accelerometers.

## Recorded Seismic Response

### Earthquakes

The accelerometers at the site recorded the June 16, 2005 Yucaipa, the June 12, 2005 Anza, and the February 10, 2001 Big Bear Lake earthquakes. The 2005 Yucaipa earthquake was a moment magnitude ( $M_w$ ) 4.9 event located about 10 km southeast of the dam, near the Banning strand of the San Andreas Fault. Analysis of teleseismic data indicates that the earthquake was a thrust event with a focal depth of 11.8 km, most likely on a fault plane striking approximately N67°E and dipping 62° southeast (<http://www.cisn.org>).

The 2001 Big Bear Lake earthquake had a magnitude  $M_w$  5.1 and was located about 25 km northeast of the dam, whereas the 2005 Anza earthquake had a magnitude  $M_w$  5.2 and was located about 80 km southeast of the dam. This latter event produced very small ground motions at the dam site and is not discussed further herein.

### Ground Motions

The peak accelerations recorded from the Yucaipa and Big Bear Lake earthquakes are summarized in Table 2 (<http://nsmp.wr.usgs.gov>). The Yucaipa earthquake produced peak horizontal accelerations of about 0.2 and 0.3 g at the crest center and downstream surface instruments, respectively. The peak accelerations recorded on rock at the tunnel chamber and downstream downhole instruments were about 0.05 and 0.08 g, respectively. The peak accelerations recorded during the Big Bear Lake earthquake were considerably smaller. Because of space limitations, only the ground motions recorded at the dam site during the Yucaipa earthquake are further reviewed herein.

The time histories for the three components of acceleration recorded at the crest center and at the downstream downhole instruments are shown in Figure 3. The time histories at the crest instrument (Figure 3(a)) are indicative of the dam's seismic response whereas the time histories at the downstream downhole instrument (Figure 3(b)) are roughly representative of the free-field rock motions near the site. The time histories show that the duration of strong acceleration shaking was about 3 seconds at the crest and about 2 seconds in rock downstream. The amplitude of acceleration during strong shaking is similar for the two horizontal components at the crest, and that is also the case for the accelerations in rock downstream.

Figure 4 shows the 360° component of the acceleration time histories recorded at the crest center, right abutment, tunnel chamber, and downstream locations. That component of ground motion is nearly transverse (within a 10° angle) to the dam centerline at the location of the center crest instrument, and thus, is approximately parallel to the upstream-downstream alignment of the dam maximum section. As shown in Figure 4, there is large amplification in acceleration amplitude between the motions recorded at the crest surface and those recorded at the crest downhole instrument. Likewise, there is large amplification between the motions recorded at the downstream surface and those at the downhole instrument below. The amplification between the motions recorded at the tunnel chamber and those at the right abutment is also large. A similar degree of amplification was observed for the 90°-component accelerations.

Figure 5 shows plots of horizontal particle acceleration, velocity, and displacement for the center crest surface and downhole instruments. Analogous plots for the downstream surface and downhole instruments are shown in Figure 6. It may be seen that the downstream motions at the surface and at the downhole instrument in rock have a predominant NW-SE orientation. This orientation is consistent with the mechanism of the earthquake source and its location relative to the dam site. On the other hand, the plots of particle velocity and displacement at the center crest location have a predominant orientation slightly E-W of N-S (Figure 5). Such orientation is transverse to the dam crest at the location of the instruments and coincides with the upstream-downstream direction of the dam maximum section. The change in orientation of the ground motions between the downstream and the dam crest instruments clearly reflects vibration at the dam crest center in an upstream-downstream direction.

### Vibration Characteristics

Various techniques were employed to identify the vibration characteristics of the dam. In addition to inspecting the recorded time histories, the recorded motions were examined in terms of Fourier spectral amplitudes and ratios. In addition, cross spectra were used to identify resonant frequencies of the dam, using the system identification techniques described by Bendat and Piersol (1980). All of the above techniques yielded generally consistent estimates for the first few natural frequencies of vibration of the dam. Selected spectral ratios are discussed herein.

It should be noted that the concept of modes of vibration and natural frequencies is strictly not applicable to an unbounded non-linear system such as the dam and its foundation. Nonetheless, the term ‘natural frequencies’ is used to denote those frequencies at which the dam motions show significant amplification with respect to selected reference motions, and in particular the downstream bedrock motions.

The Fourier spectral ratios between the crest surface and crest downhole acceleration records, and between the crest surface and the downstream downhole records are shown in Figure 7. The ratios were obtained by first smoothing the Fourier spectral amplitudes with a running 1-Hz-aperture triangular weighting function. The ratio for the 360° component between the crest surface and the downstream downhole motions suggests that the fundamental frequency of upstream-downstream vibration of the dam was about 1.2 Hz.

The two ratios for the 360°-component motions in Figure 7 show a peak at a frequency of about 3.6 Hz, possibly corresponding to a higher mode of upstream-downstream vibration. The ratios for the 90°-component motions show peaks at about 1.5 Hz and 3.5 Hz. The peak at 1.5 Hz likely represents a mode of cross-canyon vibration, whereas the peak at 3.5 Hz possibly indicates coupling with the upstream-downstream mode. A vertical mode of vibration seems apparent on the ratio for the vertical-component motions at about 2 Hz. Analogous analyses for the Big Bear Lake earthquake identified approximately the same modes of vibration of the dam (Mejia and Dawson, 2007).

## Dynamic Response Analysis

### Analysis Models

The seismic response of the dam during the Yucaipa and Big Bear Lake earthquakes was analyzed with 3-D and 2-D finite difference techniques using the computer program FLAC (Itasca, 2005). The analyses were used to evaluate the ability of such techniques to simulate the recorded response of the dam, and to develop a better understanding of its vibration modes.

Because the intensity of shaking at the site was relatively low, it seems unlikely that the earthquakes would have induced intense non-linear stress-strain behavior in the dense embankment materials. Accordingly, the use of equivalent-linear procedures to approximate the non-linear behavior of the embankment materials during the earthquakes was deemed suitable. Nonetheless, fully non-linear analyses were also performed using the 'hysteretic' stress-strain model available with the program FLAC (Itasca, 2005). The equivalent-linear analyses are described herein.

Because the dam is located in a relatively narrow canyon and has a curved axis, a 3-D analysis model is appropriate to understand and simulate its dynamic response. Figure 8 shows the 3-D finite element mesh of the dam and its foundation in perspective (Figure 8(a)) and in cross-section (Figure 8(b)). The mesh has about 90,000 elements and 95,000 nodes. It includes the bedrock foundation and abutments to allow for asynchronous motion on the dam foundation, and to properly represent potential interaction between the dam and its abutments.

As shown in Figure 8(a), considerable care was taken to replicate the geometry of the dam and the topography of the surrounding nearby ground. To simulate the unbounded extent of the foundation and abutments, the model is equipped with free-field boundaries on the sides and with a compliant base at the bottom. As shown in Figure 8(b), the embankment model consists of the core, upstream alluvial fill, and downstream rockfill zones. Those materials and the foundation alluvium were assumed to be saturated below the estimated location of the phreatic surface at the time of the earthquakes.

The 2-D analyses were performed with a plane strain model corresponding to a section of the 3-D model cut at the location of the dam maximum section. The 2-D model also includes the bedrock foundation and is equipped with free-field side boundaries and a compliant base.

### Model Vibration Characteristics

Before using the 3-D and 2-D models to analyze the recorded response of the dam, the vibration modes of the models were examined using harmonic base excitation. Those analyses were conducted using the maximum shear moduli,  $G_{\max}$ , of the embankment materials, and assuming elastic behavior with low material damping.

The models were shaken in the N-S direction with base motions corresponding to single-frequency, constant-velocity-amplitude outcrop motions. Multiple analyses were performed by varying the frequency of the input motion over a range spanning the first few modes of vibration

of the models. The variation with frequency of the ratio between the crest center motion and the input outcrop motion (i.e. the crest amplification function) was used to identify the fundamental vibration frequencies of the models. In addition, the displacement patterns at the fundamental frequencies were calculated to examine the corresponding mode shapes.

The fundamental mode of the 3-D elastic model was found to have a frequency of about 1.37 Hz with a crest amplification ratio of about 13. A second mode of upstream-downstream vibration was identified with a frequency of about 1.75 Hz. The 2-D elastic model was found to have a first mode frequency of about 1.25 Hz with an amplification ratio of about 8, and a second mode frequency of about 2.1 Hz.

### **Analysis for Recorded Motions**

The 3-D and 2-D models were used to analyze the response of the dam during the Yucaipa and Big Bear Lake earthquakes. In addition to performing 3-D and 2-D analyses for the initial estimates of the input parameters, multiple 3-D analyses were performed to evaluate the sensitivity of the results to various assumptions, and the effects of uncertainties in the input parameters on uncertainty in the calculated dam response.

Mejia and Dawson (2006) showed that the motion on a free-field outcrop of the materials at the base of the 3-D and 2-D models of the dam is an appropriate input motion for dynamic analysis of such systems with FLAC. Because the location of the downstream accelerographs may be considered representative of the free field near the dam, those instrument records were used to derive the rock outcrop motions for input into the dam analyses. The rock outcrop motions were calculated from a one-dimensional wave propagation analysis of the seismic response of the downstream instrument site. A model of the site was developed using the known site stratigraphy and was shaken with the recorded downhole motions.

Good agreement was obtained between the calculated and recorded motions at the ground surface indicating that the selected model provides a reasonable representation of the seismic response at the downstream instrument site, and is a sensible tool for estimating the free-field outcrop rock motions. The calculated outcrop motions are very close to the recorded downhole bedrock motions, as might be expected given the limited thickness of overburden above the bedrock accelerograph.

### ***Three-dimensional Analysis***

All three components of the calculated outcrop rock motion were input simultaneously in the 3-D dynamic response analyses. In addition, analyses were also performed for the individual horizontal components of the input motions to further evaluate the amount of coupling between components of the dam motions. The timing of the input motions was adjusted to account for the difference in elevation between the base of the model and the downstream bedrock instrument, and the lack of common timing between the dam site and downstream instruments.

The analyses for the estimated dam material and foundation properties and input ground motions during the Yucaipa and Big Bear Lake earthquakes, termed the baseline case, are

presented herein. Multiple parametric analyses were performed to assess the main sources of uncertainty in the calculated dam response, and to evaluate the sensitivity of the analysis results to the input assumptions. In addition, analyses were performed using the material properties adopted in the dynamic analyses for design of the dam (USACE, 1992; Makdisi et al., 1996).

The results of the analyses for the Yucaipa earthquake are illustrated in Figures 9 to 13. As shown in Figures 9 and 10, the calculated and recorded 360°-component acceleration, velocity, and displacement time histories at the crest center and crest downhole locations, respectively, are in reasonable agreement. A similar degree of agreement was observed for the other horizontal component and less so for the vertical component. Figures 11 and 12 show analogous comparisons for the tunnel chamber and right abutment locations. Whereas the calculated and recorded time histories at the tunnel chamber agree reasonably well, the calculated and recorded histories at the right abutment are significantly different. Furthermore, there is a clear time lag between the calculated and recorded time histories. Those differences suggest significant discrepancies between the incident wave field, and/or possibly the bedrock wave propagation velocities, and the corresponding model assumptions.

Figure 13 compares the calculated and recorded spectral ratios between the 360°-component crest surface and crest downhole accelerations and between the crest surface and downstream downhole accelerations. The calculated and recorded ratios between the crest surface and downstream motions are in reasonable agreement, whereas those between the crest surface and downhole motions differ somewhat. A higher degree of agreement was observed in the ratios for the 90° component and the vertical component.

The results of the analyses for the Big Bear Lake earthquake are illustrated in Figures 14 to 16. Figures 14 and 15 show the calculated and recorded 360°-component acceleration, velocity, and displacement time histories at the crest center and crest downhole locations, respectively. It may be seen that the calculated and recorded velocities and displacements are in fair agreement whereas agreement between accelerations is limited. Figure 16 compares the calculated and recorded spectral ratios between the crest surface and crest downhole motions, and between the crest surface and downstream downhole motions. There is reasonable agreement between the calculated and recorded crest surface/crest downhole ratios, whereas the crest surface/downstream downhole ratios differ significantly.

### ***Two-dimensional Analysis***

Analyses were performed using the 2-D FLAC model of the dam maximum section for comparison with the results of the 3-D analyses. The analyses were performed using the same equivalent-linear methodology and material properties as those used in the 3-D analyses. The input motions were also the same as in the 3-D analyses, except that only the 360° and vertical components were used.

The results of the 2-D analysis for the Yucaipa earthquake are shown in Figures 17, 18 and 13. Figure 17 compares the 360°-component time histories calculated at the crest surface from the 2-D and 3-D analyses with the recorded time histories. Figure 18 shows an analogous comparison for the time histories calculated at the crest downhole instrument. It may be seen

that the motions calculated from the 2-D analysis are similar to those calculated from the 3-D analysis. This is also the case for the calculated spectral ratio between the crest surface and crest downhole motions, and less so for the ratio between the crest surface and downstream downhole motions, as shown in Figure 13.

### Discussion

The results of the analyses indicate that available 3-D analysis procedures are capable of simulating the recorded response of the dam during the Yucaipa and Big Bear Lake earthquakes reasonably well. Although reasonable agreement was obtained between the calculated and recorded time histories at the crest and corresponding spectral ratios, the results suggest that considerable uncertainties are associated with the assumed analysis inputs. The main sources of uncertainty appear to lie in the nature of the seismic wave field at the site and the properties of the embankment materials. Significant uncertainty also seems associated with the properties of the dam foundation. Parametric analyses suggest, however, that the calculated horizontal dam response is not highly sensitive to reasonable assumptions for the shear wave velocity of the foundation rock.

The observed difference in the fundamental frequency of vibration during the Yucaipa earthquake indicates that the overall stiffness of the dam is slightly lower than that in the 3-D model. On the other hand, the difference in amplification frequencies between the crest surface and crest downhole motions indicate that the stiffness of the upper 150 feet of the dam is somewhat higher than in the model. Such differences are likely associated with the assumptions for the  $K_{2\max}$  values and modulus reduction relationships of the embankment materials, and possibly the assumption for the values of Poisson's ratio. The uncertainties in  $K_{2\max}$  values would be considerably reduced through measurements of the shear and compression wave velocities of the embankment materials in place.

The results of the analyses indicate that the materials likely exhibited significant nonlinear behavior in spite of the moderate intensity of shaking during the Yucaipa earthquake. The analyses results suggest that shear strains throughout the dam exceeded  $10^{-3}\%$  and approached  $10^{-2}\%$  near the crest, and highlight the importance of the embankment modulus reduction and damping relationships in simulating the dam response.

The good agreement between the crest time histories and spectral ratios calculated with the 3-D and 2-D analyses models suggest that 3-D behavior may not have played as significant a role as anticipated in the upstream-downstream seismic response of the dam maximum section. This may be due to the fact that the canyon has a trapezoidal shape and the average dam height above the base of the canyon is about 550 feet, which yields a crest length to height ratio of about 5, near the threshold value for significant 3-D effects.

### Summary and Conclusions

The recorded response of Seven Oaks Dam during the 2005 Yucaipa and the 2001 Big Bear Lake earthquakes was analyzed to identify the dam's key response characteristics. The seismic response of the dam during the earthquakes was analyzed with 3-D and 2-D finite



difference procedures using detailed geometric models of the dam and its foundation. The dynamic material properties were estimated based on field and laboratory data obtained prior to construction. Multiple analyses were also performed to evaluate the sensitivity of the results to various model assumptions and the effects of uncertainties in the input parameters on the calculated dam response.

The results of the analyses indicate that available 3-D analysis procedures are capable of simulating the recorded response of the dam during the Yucaipa and Big Bear Lake earthquakes reasonably well. However, the results suggest that considerable uncertainties are associated with the assumed analysis inputs. The main sources of uncertainty appear to lie in the assumed seismic wave field at the site, and the properties of the embankment materials. The uncertainties in the shear moduli of the embankment materials at small strains would be considerably reduced through in-situ measurements of the shear and compression wave velocities of the embankment materials.

The results of the analyses indicate that the embankment materials likely exhibited significant nonlinear behavior during the Yucaipa earthquake. Thus, the modulus reduction and damping relationships for the embankment materials are key parameters required to adequately simulate the dam response during the earthquake.

Good agreement was obtained in the calculated crest acceleration response of the dam maximum section with 3-D and 2-D analysis procedures. Thus, the analyses results suggest that 3-D behavior may not have played a major role in the recorded upstream-downstream response at the dam crest center.

### **Acknowledgements**

The study presented in this paper was supported by the California Department of Conservation, California Geological Survey, Strong Motion Instrumentation Program, Contract 1005-833. This support is gratefully acknowledged. The authors also wish to thank Rudi Roodsari and Robert Walker of the US Army Corps of Engineers, Los Angeles District, for providing geotechnical reports and project background information, and Aram Eftekhari of the Orange County Flood Control District for providing data on reservoir levels.

### **References**

- Bendat, J.S. and Piersol, A.G. (1980). Engineering applications of correlation and spectral analysis, John Wiley and Sons.
- Boulanger, R.W., Bray, J.D., Merry, S.M., and Mejia, L.H. (1995). "Three-dimensional dynamic response analyses of Cogswell dam." Canadian Geotechnical Journal, 32(3), 452-464.
- Dakoulas, P. (1993). Earth dam-canyon interaction effects for obliquity incident SH waves," Journal of Geotechnical and Geoenvironmental Engineering, ASCE, 119(11), 1696-1716.

Hardin, B.O., and Kalinski, M.E.. (2005). "Estimating the shear modulus of gravelly soils," *Journal of Geotechnical and Geoenvironmental Engineering*, ASCE, 131(7), 867-875.

Itasca (2005) *FLAC, Fast Lagrangian Analysis of Continua, User's Guide*. Minneapolis, Minnesota, USA.

Makdisi, F.I., Roodsari, A.T., Madianos, M.N. and Wang, Z.-L. (1996). "Evaluation of Seismic Stability of Seven Oaks Dam," Sixteenth Annual USCOLD Lecture Series, Los Angeles, California, July 22-26.

Mejia, L.H. and Seed, H.B. (1983). "Comparison of 2-D and 3-D dynamic analyses of earth dams," *Journal of the Soil Mechanics and Foundation Division*, ASCE, 109, GT11, 1383-1398.

Mejia, L.H., Sykora, D.W., Hynes, M.E., Fung, K., Koester, J. (1991). "Measured and calculated dynamic response of rockfill dam," *Proceedings, 2<sup>nd</sup> International Conference on Recent Advances in Geotechnical Earthquake Engineering and Soil Dynamics*, March, St. Louis, Mo., 1063-1070.

Mejia, L.H., and Dawson, E.M. (2006). "Earthquake deconvolution for FLAC," *Proceedings, Fourth International FLAC Symposium on Numerical Modeling in Geomechanics*, Madrid, Spain, May.

Mejia, L.H., and Dawson, E.M. (2007). "Analysis of seismic response of Seven Oaks Dam," Report prepared for the California Geological Survey, Strong Motion Instrumentation Program (SMIP), URS Corporation, Oakland, California.

Rollins, K.M., Evans, M.D., Diehl, N.B., and Daily, W.D. (1998). "Shear modulus and damping relationships for gravels," *Journal of Geotechnical and Geoenvironmental Engineering*, ASCE, 124(5), 396-405.

Seed, H.B. and Idriss, I.M. (1970). "Soil moduli and damping factors for dynamic response analysis," Report No. EERC 70-10, University of California, Berkeley, Earthquake Engineering Research Center.

Seed, H.B., Wong, R.T., Idriss, I.M. and Tokimatsu, K. (1986). "Moduli and damping factors for dynamic analyses of cohesionless soils," *Journal of Geotechnical and Geoenvironmental Engineering*, ASCE, 112(11), 1016-1032.

U.S. Army Corps of Engineers (USACE). (1992). "Design Memorandum No. 8, Feature Design – Seven Oaks Dam, Embankment and Spillway, Volume 2 – Appendix A, Dynamic Analysis Supplement," Report prepared by the USACE, Los Angeles District, December.

Table 1. Properties for Dynamic Analysis of Seven Oaks Dam

Material	Moist Unit Weight (lbs/ft <sup>3</sup> )	Saturated Unit Weight (lbs/ft <sup>3</sup> )	K <sub>2max</sub>	Poisson's Ratio <sup>1</sup>	Modulus Reduction	Damping
Core	136	138	70	0.45 (0.48)	S&I Sands Ave <sup>2</sup>	S&I Sands ALB <sup>3</sup>
Rockfill	142	148	160	0.33 (0.45)	Seed et al Gravels Ave <sup>4</sup>	Seed et al Gravels Ave
Alluvial Fill	146	149	175	0.33 (0.45)	Seed et al Gravels Ave	Seed et al Gravels Ave
Foundation Alluvium	146	149	275	0.33 (0.45)	Seed et al Gravels Ave	Seed et al Gravels Ave
Weathered Rock <sup>5</sup>	165	170	V <sub>s</sub> = 3000 ft/sec	0.33 (0.4)	Idriss W. Rock <sup>6</sup>	Idriss W. Rock
Bedrock	170	170	V <sub>s</sub> = 6000 ft/sec	0.33 (0.33)	Elastic	0.5%

Notes: <sup>1</sup> Values of Poisson's ratio in parenthesis are for saturated materials.  
<sup>2</sup> Average relationship for sands by Seed and Idriss (1970). For effective mean stresses greater than 10 tsf, the upper bound relationship was used.  
<sup>3</sup> Intermediate between the average and lower bound curves by Seed and Idriss (1970). For effective mean stresses greater than 10 tsf, the lower bound relationship was used.  
<sup>4</sup> Average relationship for gravels by Seed et al. (1986). For effective mean stresses greater than 10 tsf, the upper bound modulus reduction and intermediate lower bound damping relationships were used.  
<sup>5</sup> For analysis of downstream free-field motions.  
<sup>6</sup> Average relationship for weathered rock by Idriss (personal communication).

Table 2. Peak accelerations recorded at Seven Oaks Dam Site (g's)

Instrument	2005 Yucaipa Eq.			2001 Big Bear Lake Eq.		
	360°	90°	UP	360°	90°	UP
Center crest Surface	0.196	0.188	0.110	0.026	0.029	0.025
Center crest downhole	0.086	0.078	0.036	0.014	0.017	0.018
Right crest	NA	NA	0.110	0.029	0.025	0.011
Right abutment	0.208	0.127	0.095	0.011	0.011	0.009
Tunnel chamber	0.054	0.045	0.027	0.005	0.007	0.004
Downstream surface	0.290	0.224	0.173	0.041	0.060	0.017
Downstream downhole	0.075	0.079	0.038	0.007	0.020	0.006

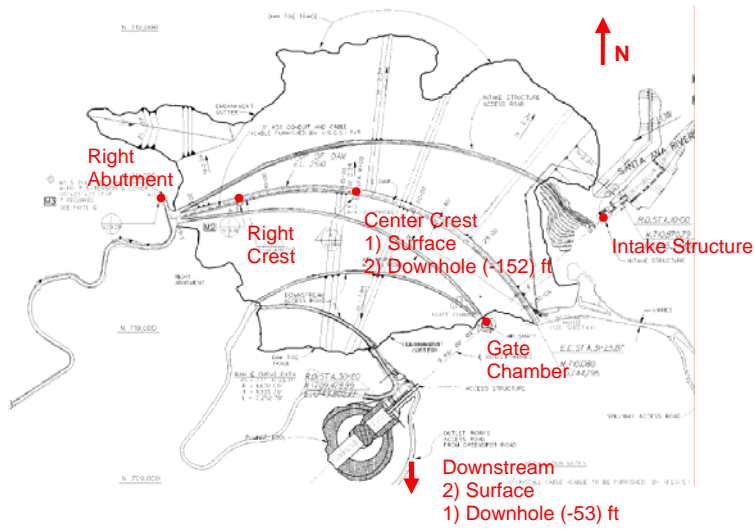


Figure 1. Plan view of Seven Oaks Dam showing accelerographs locations

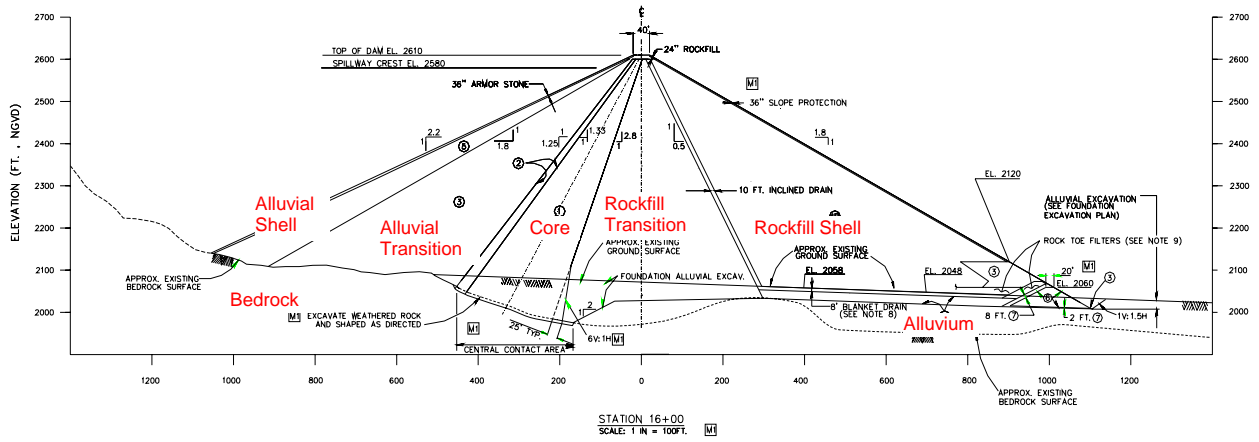


Figure 2. Maximum cross section of Seven Oaks Dam

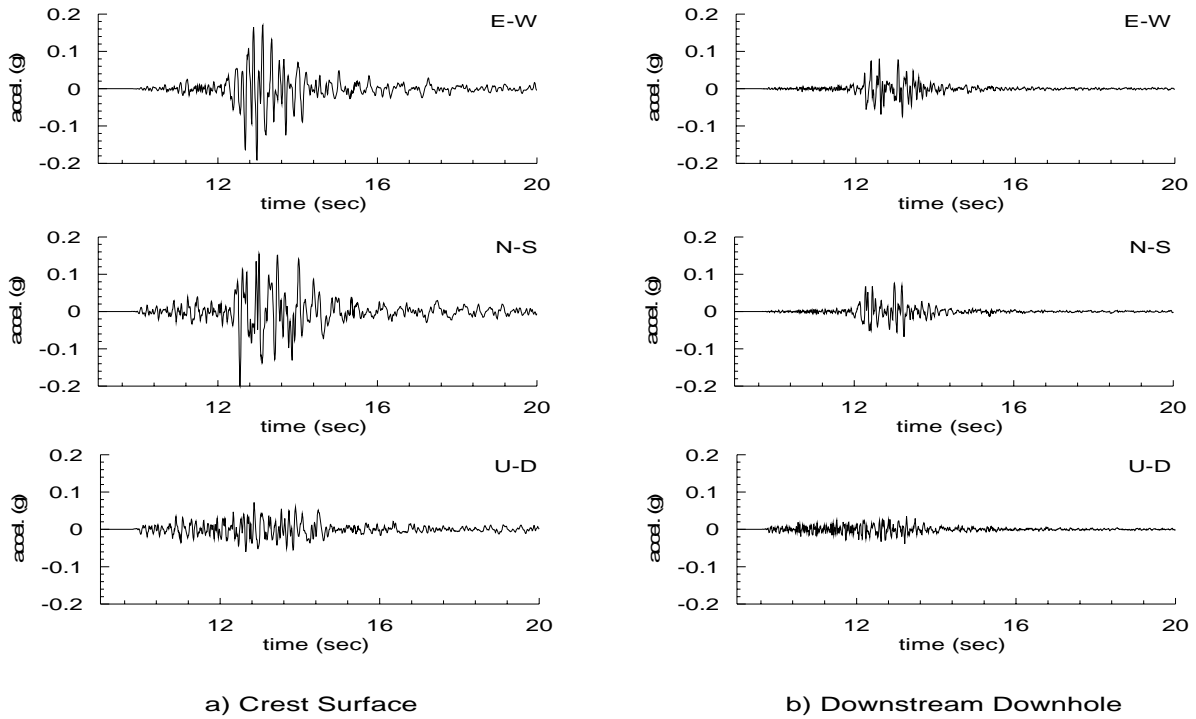


Figure 3. Acceleration time histories recorded at dam crest and downstream downhole instruments during the Yucaipa earthquake

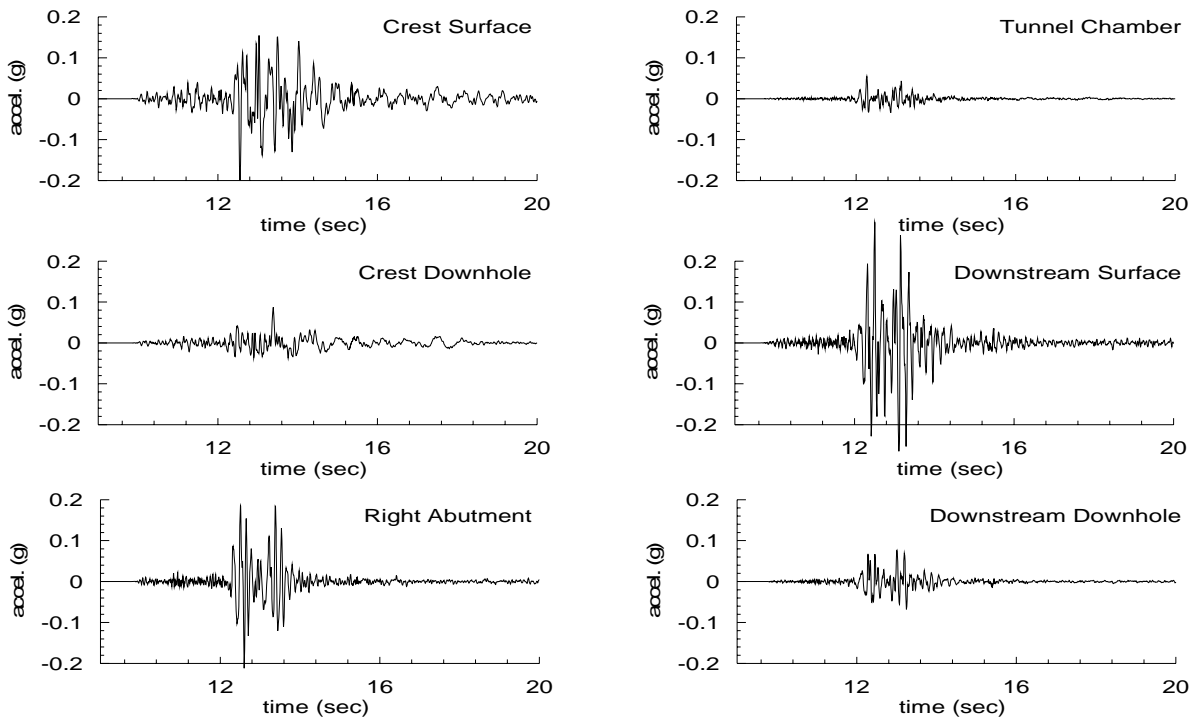


Figure 4. North-south acceleration time histories recorded at selected dam-site and downstream locations during the Yucaipa earthquake

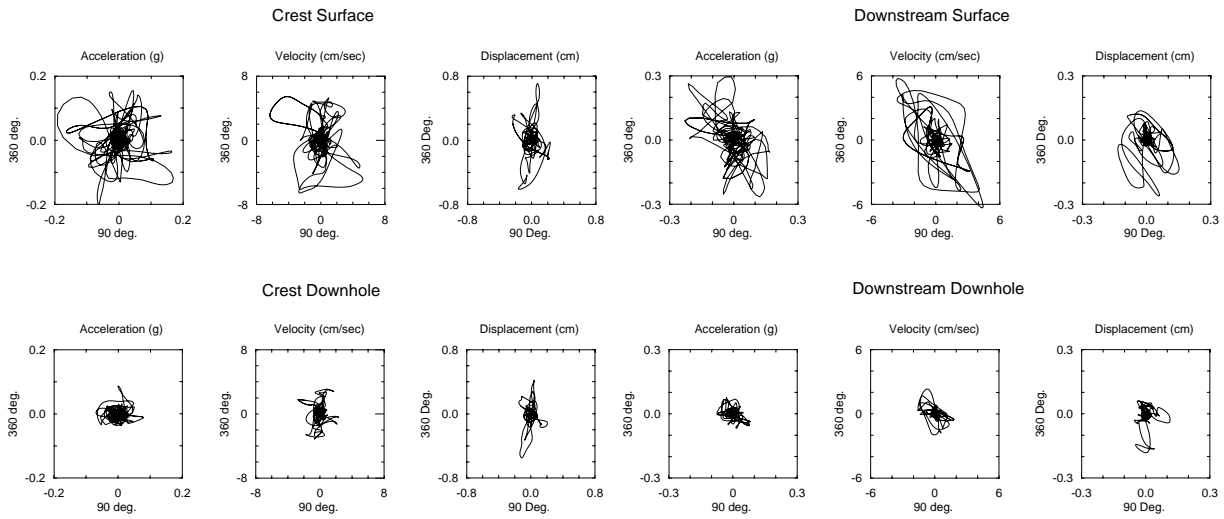


Figure 5. Horizontal particle acceleration, velocity and displacement at the crest surface and downhole instruments during the Yucaipa earthquake

Figure 6. Horizontal particle acceleration, velocity and displacement at the downstream surface and downhole instruments during the Yucaipa earthquake

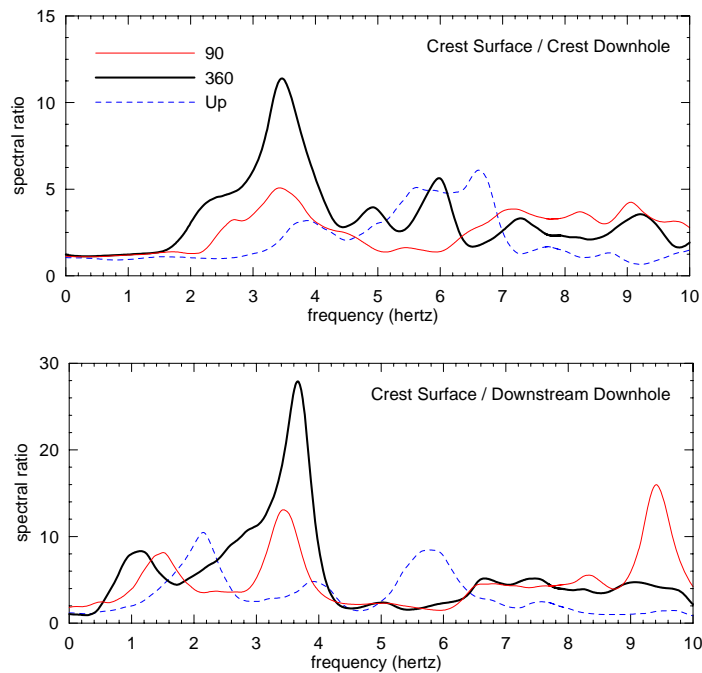


Figure 7. Fourier spectral ratios between selected acceleration records from the Yucaipa earthquake

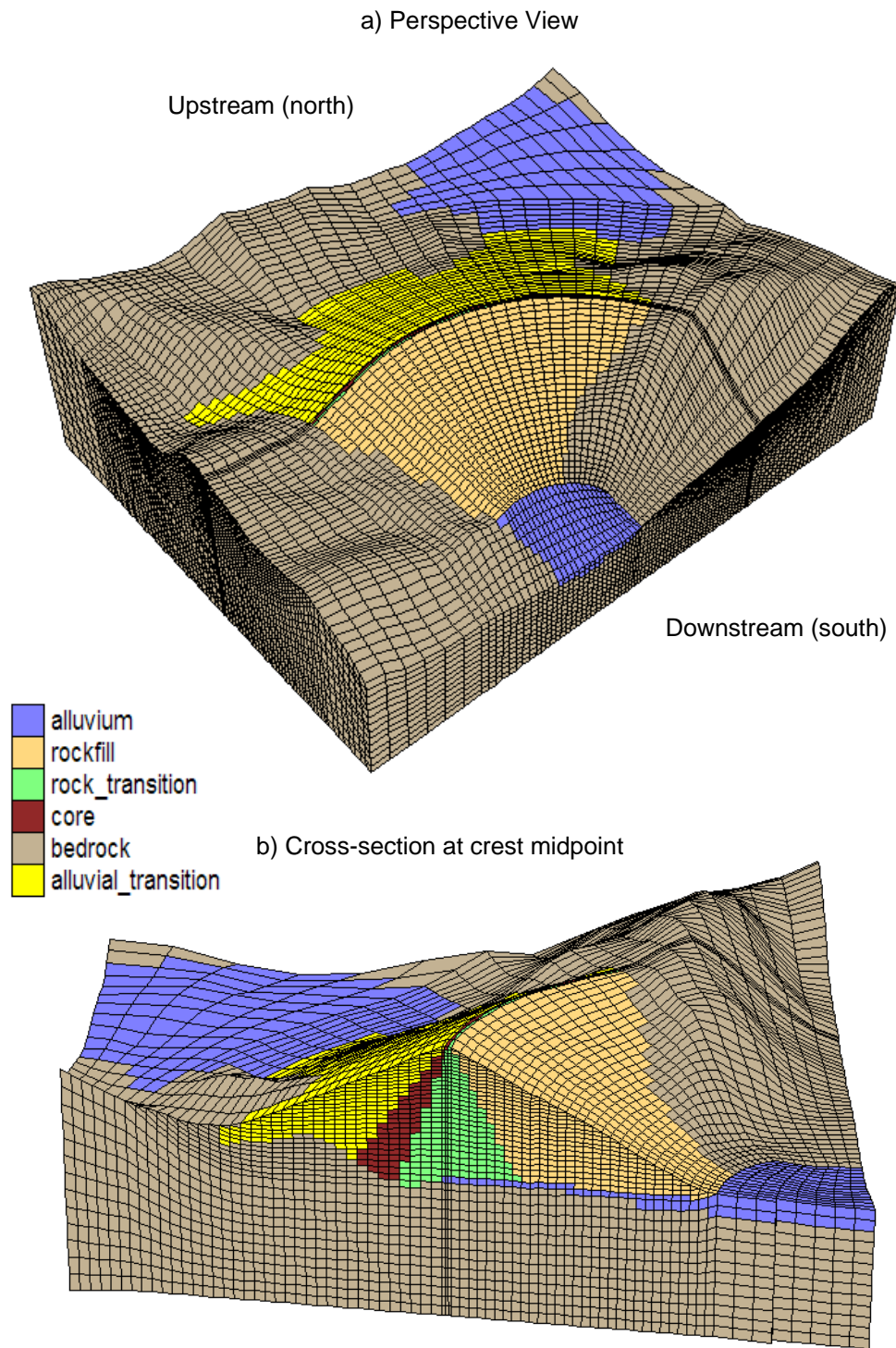


Figure 8. Three-dimensional finite element mesh of dam

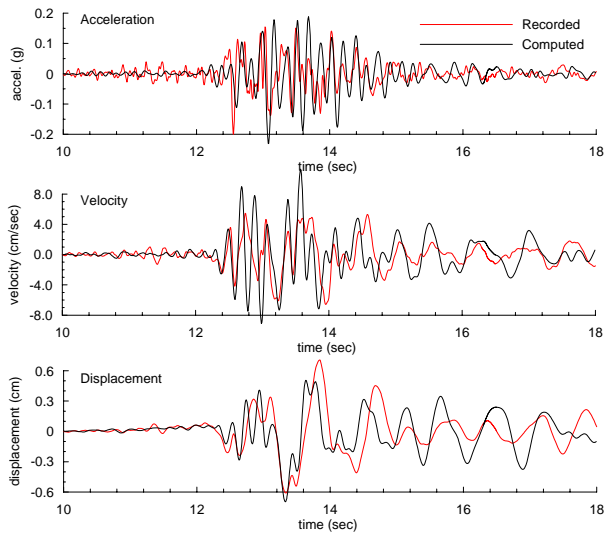


Figure 9. Calculated and recorded N-S time histories at crest surface for the Yucaipa earthquake – 3-D analysis

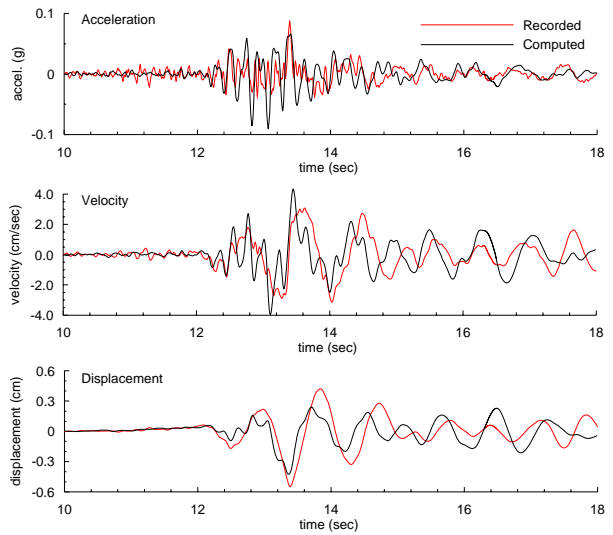


Figure 10. Calculated and recorded time histories at the crest downhole instrument for the Yucaipa earthquake – 3-D analysis

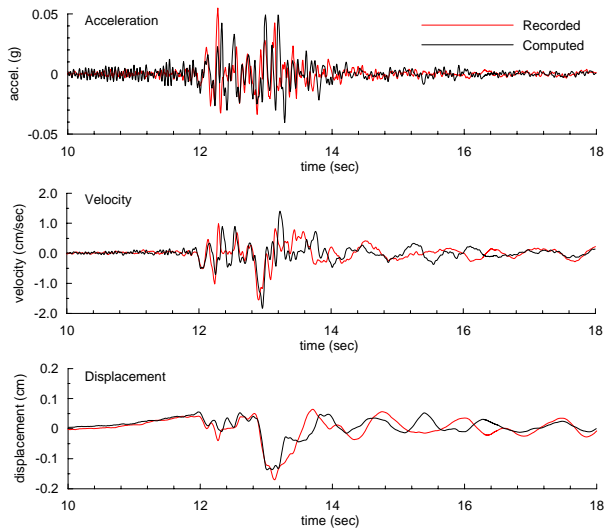


Figure 11. Calculated and recorded N-S time histories at the tunnel chamber for the Yucaipa earthquake – 3-D analysis

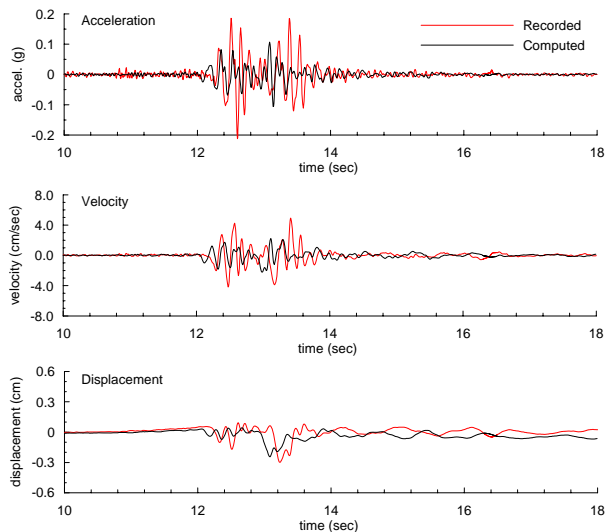


Figure 12. Calculated and recorded N-S time histories at the right abutment for the Yucaipa earthquake – 3-D analysis



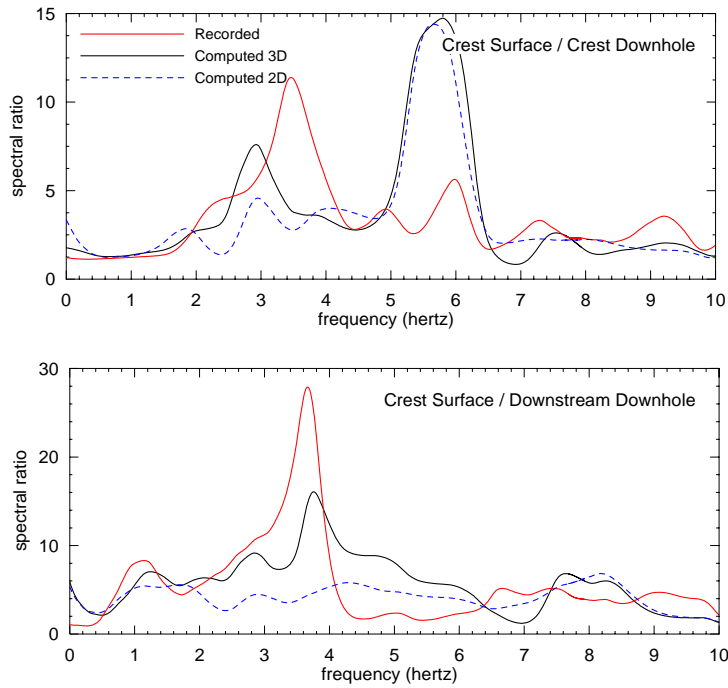


Figure 13. Comparison of N-S spectral ratios calculated from 3-D and 2-D analyses for the Yucaipa earthquake with recorded ratios

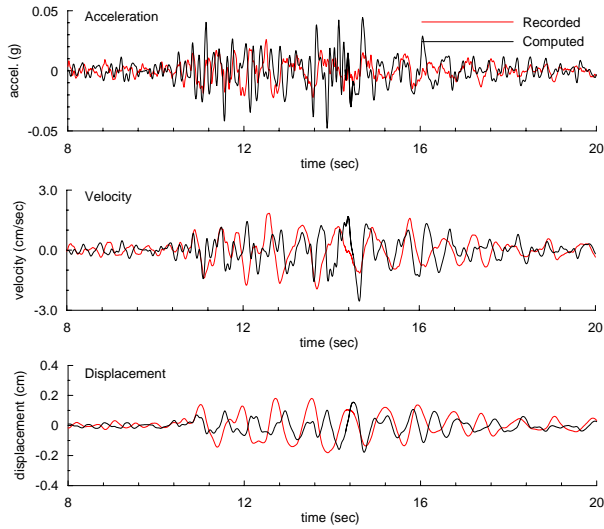


Figure 14. Calculated and recorded time histories at the crest surface for the Big Bear Lake earthquake – 3-D analysis

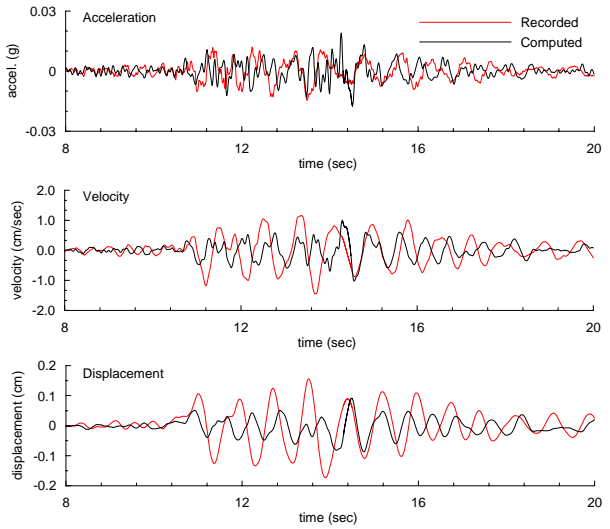


Figure 15. Calculated and recorded time histories at the crest downhole instrument - Big Bear Lake earthquake – 3-D analysis

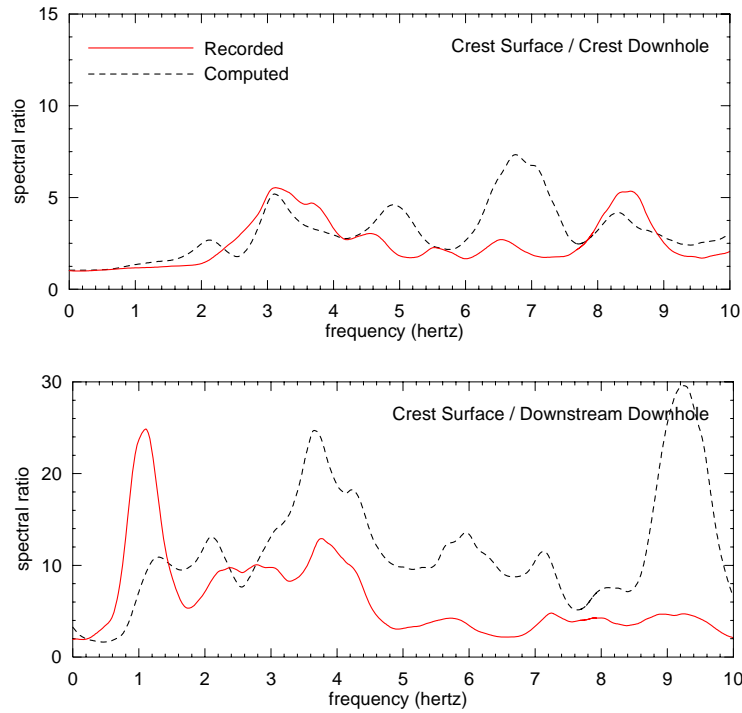


Figure 16. Calculated and recorded N-S acceleration Fourier spectral ratios for the Big Bear Lake earthquake – 3-D analysis

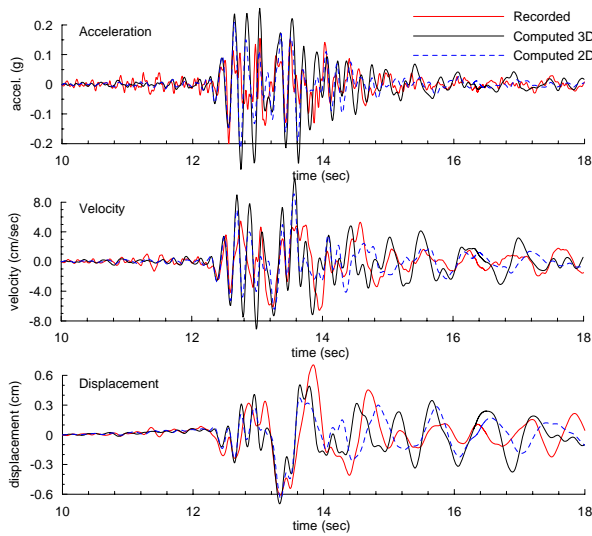


Figure 17. Comparison of N-S motions calculated at the crest surface from 2-D and 3-D analyses with recorded motions – Yucaipa earthquake

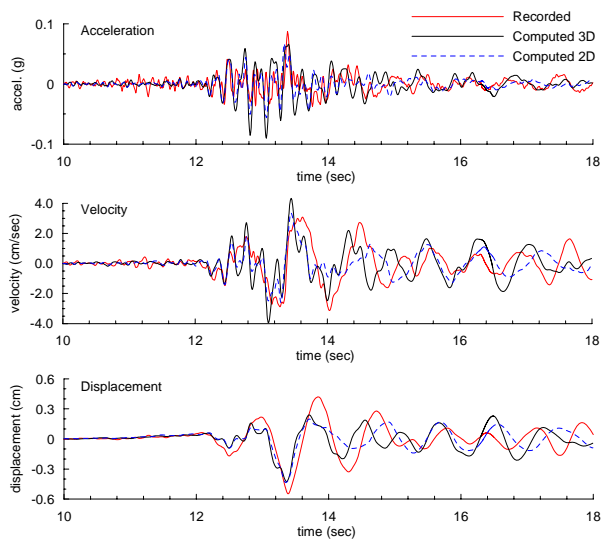


Figure 18. Comparison of N-S motions calculated at the crest downhole from 2-D and 3-D analyses with recorded motions – Yucaipa earthquake

**U.S. NATIONAL CENTER FOR ENGINEERING STRONG MOTION DATA (NCESMD)**

Hamid Haddadi<sup>1</sup>, Anthony Shakal<sup>1</sup>, William Savage<sup>2</sup>, Christopher Stephens<sup>2</sup> and Moh Huang<sup>1</sup>

1 Strong Motion Instrumentation Program, California Geological Survey

2 National Strong Motion Project, U.S. Geological Survey

**Abstract**

The U.S. Geological Survey (USGS) and the California Geological Survey (CGS) have established a cooperative U.S. National Center for Engineering Strong Motion Data (NCESMD), which will have mirrored operational centers in Sacramento and Menlo Park, CA. The National Center integrates earthquake strong-motion data from the CGS California Strong Motion Instrumentation Program, the USGS National Strong Motion Project, and the regional networks of the USGS Advanced National Seismic System (ANSS), thus serving as a provider of uniformly processed strong-motion data for seismic engineering applications. The NCESMD builds on the Engineering Data Center of the California Integrated Seismic Network, and so will continue to serve the California region while expanding to serve other ANSS regions. The National Center will assimilate the Virtual Data Center, which was developed at U.C. Santa Barbara with support from the Consortium of Strong Motion Observation System (COSMOS), NSF and SCEC. A Center Management Group with input from an external Advisory Committee manages the NCESMD. Products will be generated by both CGS and USGS facilities, thus ensuring robustness. Each ANSS region is responsible and credited for the data recorded by its regional network. The National Center is co-hosted by CGS and USGS at [www.strongmotioncenter.org](http://www.strongmotioncenter.org).

**Introduction**

The U.S. National Center for Engineering Strong Motion Data was recently established as a single, unified facility to provide earthquake strong motion data for engineering applications. The goal of the Center is to provide timely, quality-controlled, and easily accessible data for domestic and foreign earthquakes of engineering interest. The Center is responsible for receiving data from field stations, uniformly processing data, rapidly releasing data through the web site, and archiving data. It also provides a search engine to facilitate selection of data from its archive. The National Center evolved from the TriNet Engineering Strong Motion Data Center (Shakal and Scrivner, 2000; Shakal et al, 2002) and the California Integrated Seismic Network Engineering Data Center (CISN EDC) (Shakal et al, 2003; Huang et al, 2004), and includes the California strong motion data of the CISN EDC as well as that of the other ANSS regions of the US. This paper describes the National Center's web site, its available functions, and plan for further developments.

## National Center Web Site

The National Center web site, hosted by CGS at <http://www.strongmotioncenter.org>, consists of three major sections: Internet Quick Reports (IQR), Internet Data Reports (IDR), and the Search Engine. Figure 1 shows the home page of the National Center. In addition to serving as a data source, the National Center will also notify users when important new data are available, and when important pages are updated.

The NCESMD web site has removed some of the limitations of the CISN EDC site. The NCESMD's web site is a dynamic web site in which all the web pages are generated on-the-fly. Data are retrieved from a database in real time when users open web pages. The dynamic nature of the database-driven system makes it much easier to ensure that tables and maps will always contain updated data.

### The Internet Quick Reports

The National Center, like its predecessor CISN EDC, continues to provide the most current strong motion data of engineering significance through the Internet Quick Reports (IQR) that are generated after earthquakes. The Internet Quick Reports are intended primarily for post-earthquake response and analyses. The first version of the IQR is usually released within a short time (the goal is less than 30 minutes) after the event. This early version may not include all the records, and more complete IQR pages are posted as data are recovered and received by the National Center. The National Center plans to automate preliminary data processing and dissemination in the near future, which will make the information available more rapidly. A snapshot of an IQR event summary page is shown in Figure 2. The user can access the Internet Quick Report for individual events by clicking on the event name on the event summary page. For example, Figure 3 shows the individual event page that is displayed by clicking on the table entry for the Chatsworth earthquake that occurred on August 9, 2007, in California.

The main feature of the IQR page for each event (e.g., Figure 3) is a table summarizing key information about the record at each station, including epicentral distance (and distance to the causative fault, if available), peak ground acceleration, velocity, and displacement, and spectral acceleration values at periods of 0.3, 1.0, and 3.0 seconds. Immediately above the table are three icons: the Earthquake Info icon on the left provides information about the location and mechanism of the earthquake; the ShakeMap icon on the right links to the corresponding ShakeMap generated by an authoritative agency; and the center icon links to an Interactive Map of strong motion stations, a new feature that is described in more detail below.

The IQR tables are now generated dynamically, which allows the entries to be sorted by station name, station number or ID, network, epicentral distance, and peak ground accelerations of the records (Figure 3).

Records from individual stations can be viewed and downloaded from the IQR page by clicking on the buttons in the appropriate columns to the right. Figure 4 shows an example of

the acceleration and displacement time histories and also response spectral accelerations for a two-story office building.

Station information is accessible by clicking on the name in the Station column of the IQR table. Figure 5 shows an example of the station information page. For structures, information about the floor plan and foundation type is provided in the station information page. The sensor layout, which shows locations of the sensors in the structure, is provided in PDF format and can be downloaded by clicking on the sensor layout image on the upper right side of the station information page. Figure 6 shows the sensor layout of the Chatsworth – 2-story Commercial Building as an example.

### **Interactive Map**

A new feature has been developed for the National Center web site that allows users to view a map of strong motion stations in addition to the standard text table format. This feature makes use of the Google Maps® web service (<http://www.google.com/apis/maps>).

An example of the map interface for an IQR page is shown in Figure 7. The map shows the earthquake epicenter and the stations that recorded the earthquake. The station symbols (circles for ground sites, squares for structures) are colored according to maximum horizontal acceleration (PGA), so a user can see at a glance where the highest ground motions were recorded. The corresponding legend of PGA values appears in the upper right corner of the map. For consistency, the colors used in the symbols correspond to the intensity coloring used on ShakeMaps for that acceleration. Many standard features of Google Maps® are also present. For example, the inset at the lower right corner of the map provides regional context, a scale bar is displayed at the lower left corner of the map, standard navigation tools (zoom, translation) appear in the upper left of the map, and the base map view (Map, Satellite, Hybrid) can be selected at the upper right. These features allow the user to interactively drag or pan the map around using either the left mouse button (click and drag), or the arrows at the upper left corner of the map. The button in the middle of those arrows (the one with four arrows pointing inward) will bring the user back to the previous map coverage. The map can also be panned by clicking and dragging the blue rectangle inside the regional overview map.

When the mouse hovers over a station on the map, a photo of the station appears beside the map to the lower right, along with some information about the station. The user can also click on the station to open a pop-up window containing basic information about the station and links to the station's time history, station page, and strong motion data. Clicking on the epicenter opens a pop-up window providing the basic information on the earthquake. Once an information window has been opened, it can be closed by using the "X" button in its upper right corner, or by clicking anywhere on the map background.

A feature has been added in the Interactive Map that allows users to download a file with station information in KML format so that it can be viewed in three dimensions in the Google Earth® viewer (<http://earth.google.com>). In contrast to the 2-dimensional Google Maps viewer, which can be incorporated within an organization's web site, Google Earth is a standalone 3-D geospatial exploration system that a user must download from Google and install locally.

### **Internet Data Reports**

While the IQR is used to provide strong motion records of the most recent earthquakes, archived records are available in the Internet Data Reports (IDR). The IDR pages are sorted by event date (most recent on top). The layout of the IDR pages is the same as that of the IQR pages, so a user who is familiar with the IQR will find it easy to use the IDR pages. Figure 8 shows the front page of the Internet Data Reports.

Concurrent with the accumulation of data from new and recent events, the NCESMD also will be adding significant historic records to the to the IDR archive.

### **Search for Data**

Strong motion records of the National Center are searchable using the “Search for Data” button on the National Center’s front page. Clicking on this button will display the search page shown in Figure 9, which currently includes two search options, one for the NCESMD and one for the COSMOS Virtual Data Center (VDC). Currently these two options are needed because both the extent and scope of data holdings and search options of these two data centers are incongruent (presently the VDC provides access to worldwide and historical US data not yet available through the NCESMD). Eventually, however, the National Center will incorporate the Virtual Data Center (VDC) so that users will then be able to access US and significant international data through the NCESMD web site.

The current search engine of the NCESMD for US structural and ground response data is shown in Figure 10. The records in the NCESMD archive are searchable in several ways, depending upon a user’s interests. In general, the search parameters can be a combination of earthquake, station, and record parameters. The searchable earthquake parameters are earthquake name, magnitude and date. The station parameters are station city, station name, number, and type. The station type parameters are ground stations, buildings, bridges, dams, geotechnical arrays, and other station types that are not specified. For building stations, additional search parameters include material (such as wood, steel, concrete, masonry), whether or not there is base-isolation, and height (low, mid, and high rise). An example of a search result is shown in Figure 11. The search table can be sorted the same way as an IQR or IDR table. The search table is linked to the station pages and to the corresponding IDR pages. The records are also directly viewable and downloadable from the search result table.

### **Future Developments**

The National Center is currently engaged in the process of transitioning the Virtual Data Center (VDC) to the National Center to provide all users with a better and more convenient one-stop portal to both US and significant international strong motion data. Concurrently, the NCESMD is working to implement modifications and enhancements to existing search options and display features in response to suggestions from an external Advisory Committee, and also working to implement automatic data collection and preliminary processing and dissemination. The goal is to provide at least preliminary versions of US strong motion data through the

National Center within a few minutes after a significant event and fully vetted data soon afterwards. The records from all ANSS strong motion networks will be uniformly processed and provided in the COSMOS format. The National Center will notify registered users when important new pages are posted and/or when an existing page is significantly updated.

### Summary

- The National Center for Engineering Strong Motion Data, NCEM, is a cooperative effort of the California Geological Survey and the US Geological Survey to establish a unified strong motion data center for engineering applications. The National Center integrates earthquake strong-motion data from the CGS California Strong Motion Instrumentation Program, the USGS National Strong Motion Project, and the regional networks of the USGS Advanced National Seismic System (ANSS).
- A Center Management Group manages the NCEM with guidance from an external Advisory Committee.
- Products will be generated by both CGS and USGS facilities, thus ensuring robustness. Each ANSS region is responsible for and credited for the data recorded by its regional network.
- The National Center is working to incorporate the COSMOS Virtual Data Center to provide one-stop convenient and effective access to US and significant international strong motion data.
- The web portal of the National Center has evolved from the CISN EDC site. It is now a database-driven site with dynamic pages and new map features that facilitate the use of strong-motion data.

### Acknowledgements

The Google Map® feature of the National Center was implemented by Peter Roffers with the assistance of Jessica Zhang. The efforts of Jessica Zhang in adopting a database for the National Center and designing the new dynamic web pages are acknowledged. We would also like to acknowledge the National Center advisory committee and others for their input and advice on improving the functionality and effectiveness of the National Center.

### References

- Shakal, A. and C. Scrivner (2000). TriNet Engineering Strong-Motion Data Center, *Proceedings of SMIP2000 Seminar on Utilization of Strong-Motion Data*, p. 115-124.
- Lin, Kuo-wan, A. Shakal, M. Huang, C. Stephens and W. Savage (2002). Dissemination of Strong-Motion Data Via the Internet Quick Report and the Internet Data Report at the CISN Engineering Data Center, *Proceedings of SMIP2002 Seminar on Utilization of Strong-Motion Data*, p. 115-126.

Shakal, A., K. Lin, M. Huang, C. Stephens and W. Savage (2003). Rapid Post-earthquake Strong-Motion Data via Internet Quick Report and the CISN Strong Motion Data Center, *Proceedings of SEAOC 2003 Convention*, September 18-19, 2003.

Huang, M., A. Shakal, K. Lin, C. Stephens and W. Savage (2004). Rapid Post-earthquake Strong-Motion Data from the CISN Engineering Strong Motion Data Center, *Proceedings of the 13th World Conference on Earthquake Engineering*, Vancouver, B.C., Canada, August 1-6, 2004.

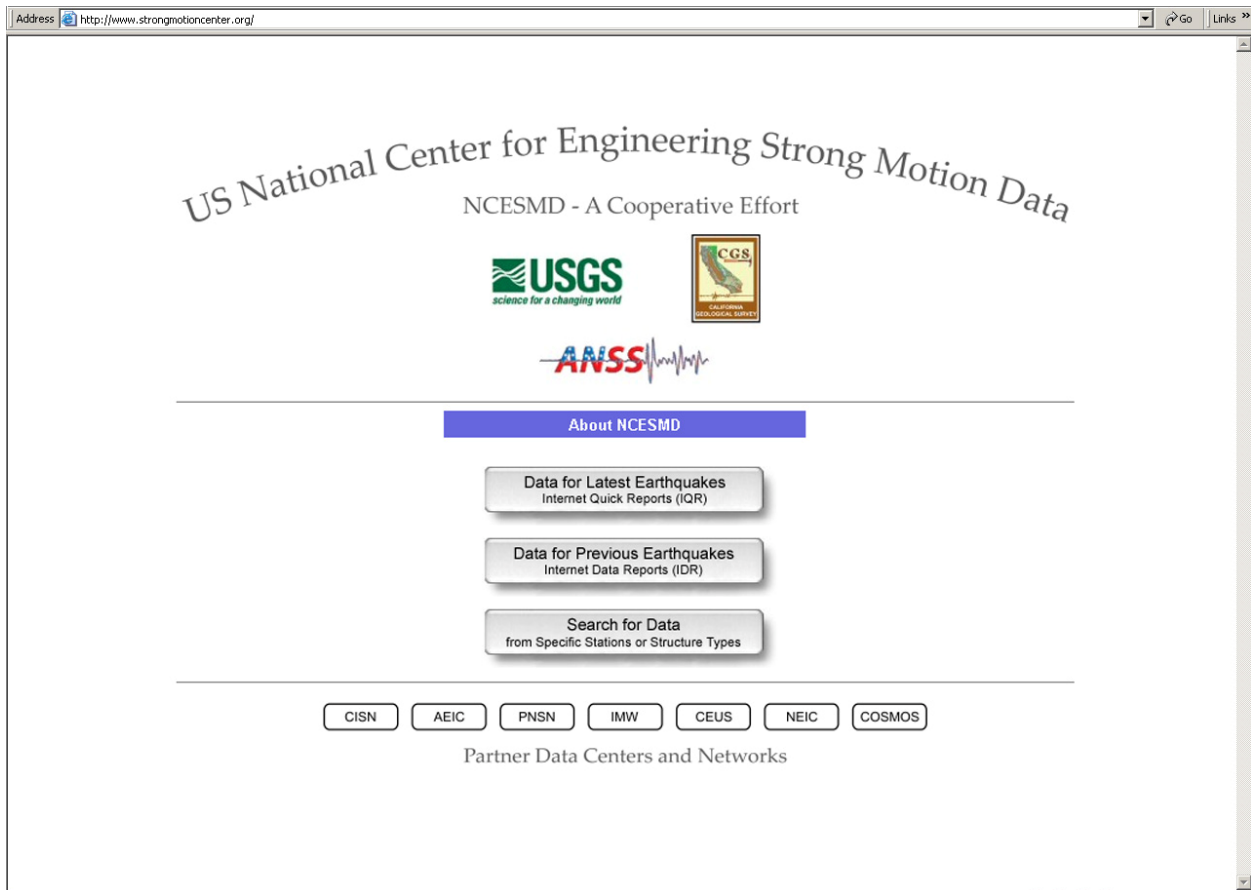


Figure 1. The home page of the National Center's web site.



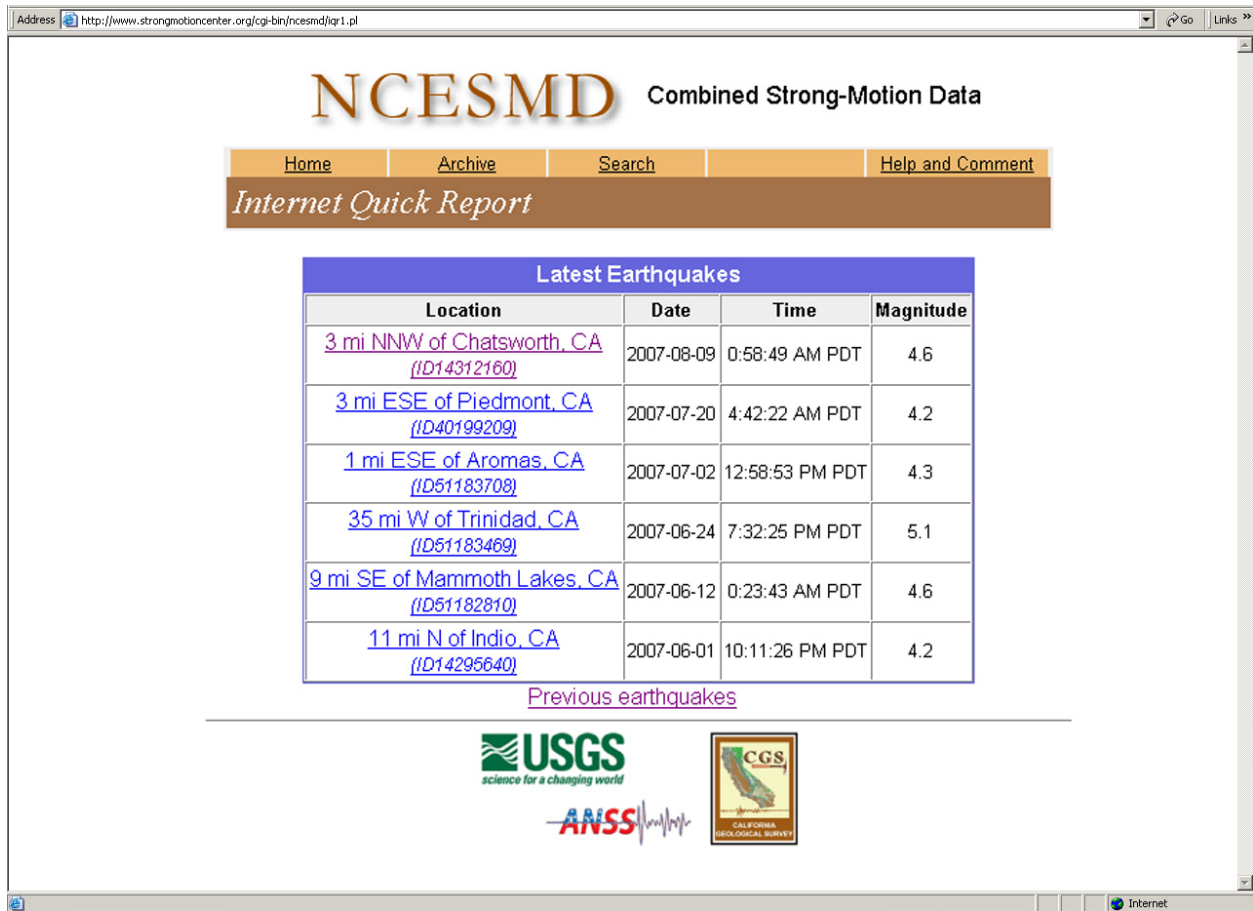


Figure 2. The Internet Quick Report summary page listing the latest earthquakes.

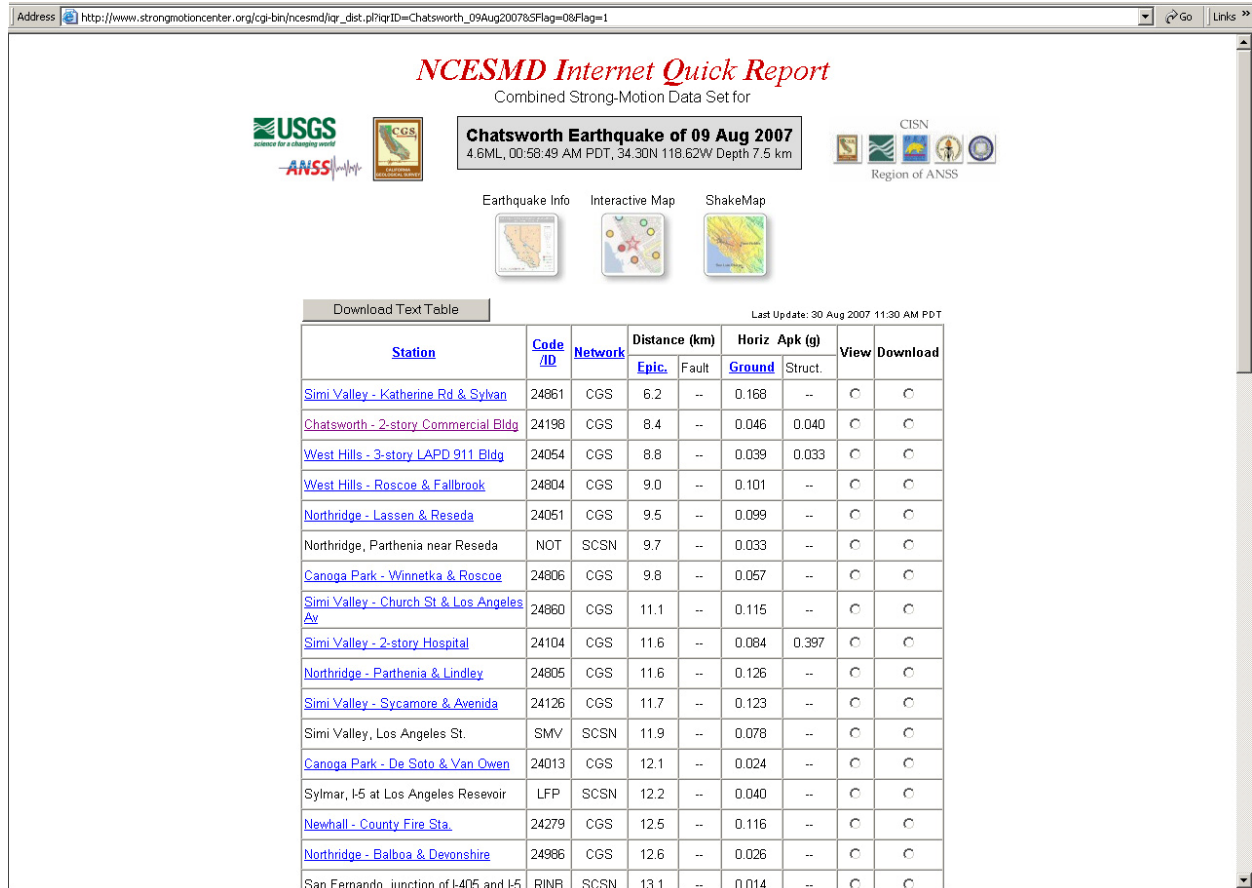


Figure 3. Internet Quick Report (IQR) table for the Chatsworth earthquake of August 9, 2007.

# SMIP07 Seminar Proceedings

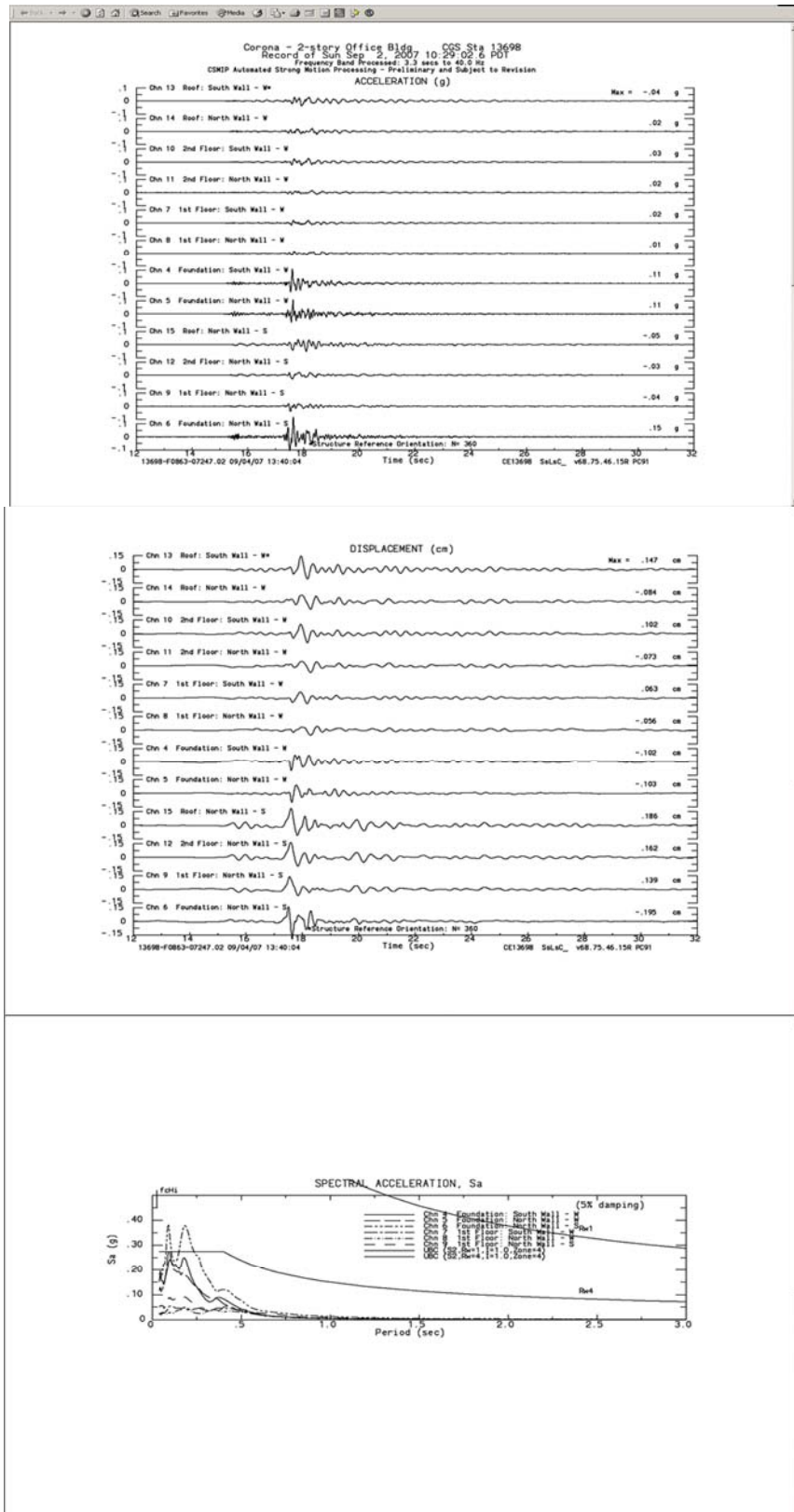



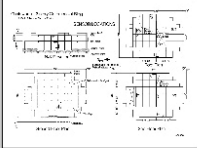
Figure 4. An example of the acceleration, displacement, and response spectral acceleration plots in the Data Center's Internet Quick Reports and Data Reports.

Address <http://www.strongmotioncenter.org/cgi-bin/ncesmd/station.html.pl?stationID=C24198&network=CGS> Go Links >>

### NCESMD Information for Strong-Motion Station Chatsworth - 2-story Commercial Bldg CGS - CSMIP Station No. 24198



(Station Photograph - click to enlarge)



(Sensor Layout - click to see PDF File)

Latitude	34.24 N
Longitude	118.565 W
Elevation (m)	261
Site Geology	Alluvium
Vs30 (m/sec)	--
Site Class	--
Remarks	--

No. of Stories above/below ground	2/0
Plan Shape	Rectangular with plan setbacks.
Base Dimensions	208 x 295 ft (63.4 x 89.9 m)
Typical Floor Dimensions	208 x 295 ft (63.4 x 89.9 m)
Design Date	1990
Instrumentation	2002. 12 accelerometers, on 3 levels in the building.

Vertical Load Carrying System	Concrete slabs on metal deck supported on steel beams and columns.
Lateral Force Resisting System	Three interior steel moment frames in E/W direction and perimeter steel moment frames in N/S direction.
Foundation Type	Cast-in-place concrete piles. Typical 4" slab-on-grade.
Remarks	--

Done Internet

Figure 5. An example Station Information Page, for the Chatsworth, California, 2-story Commercial Building.

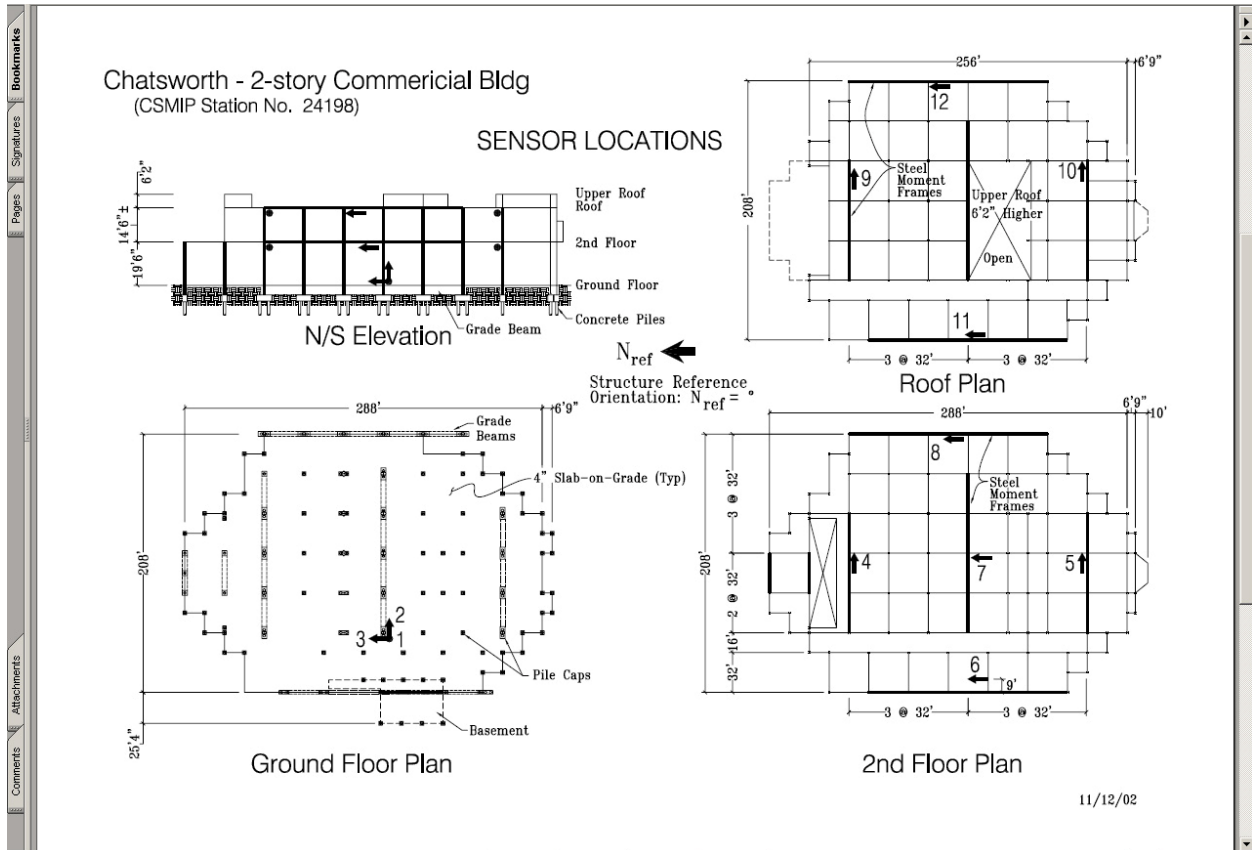


Figure 6. Sensor layout for the CGS station, Chatsworth, California, 2- story Commercial Building.

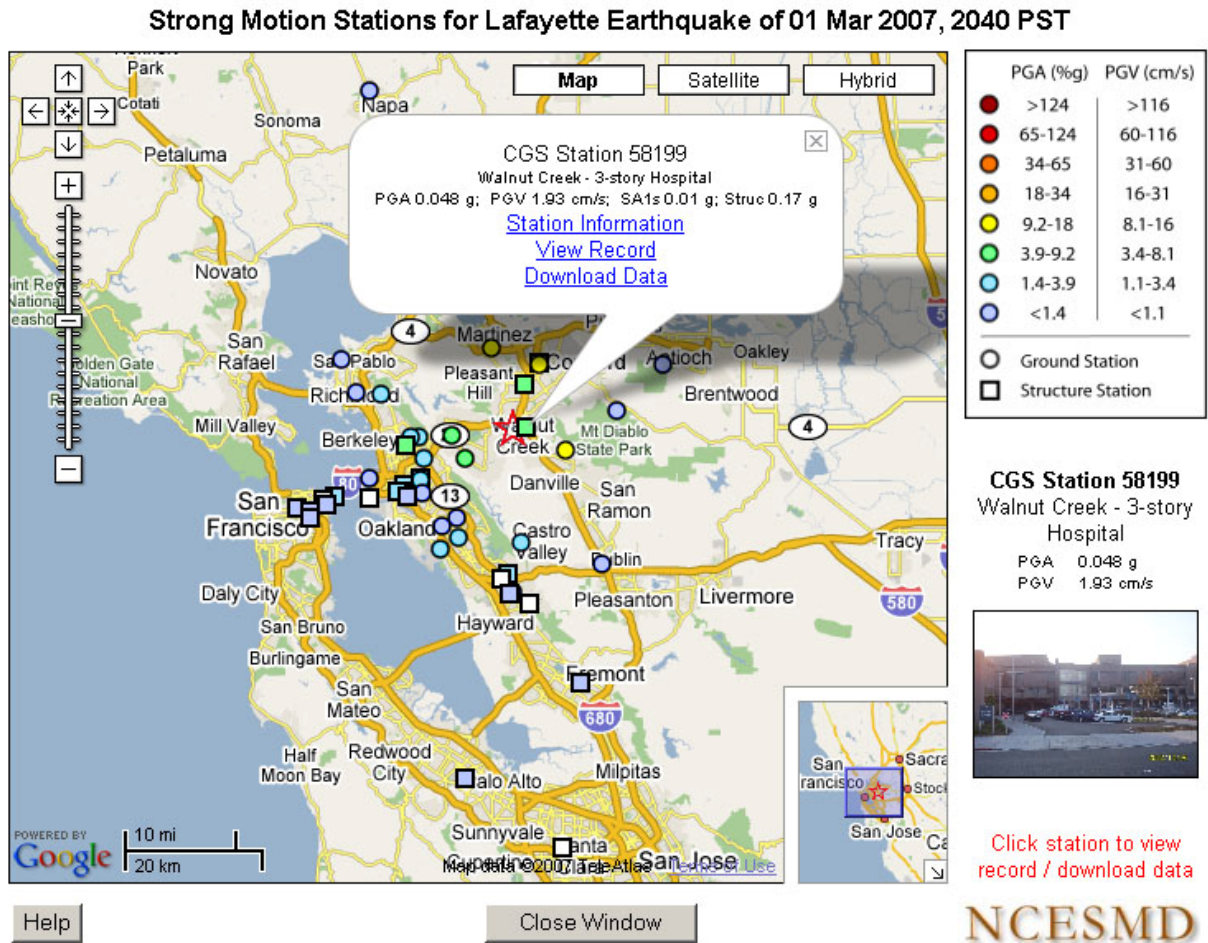


Figure 7. The IQR Interactive Map, generated for the Lafayette Earthquake of March 1, 2007.

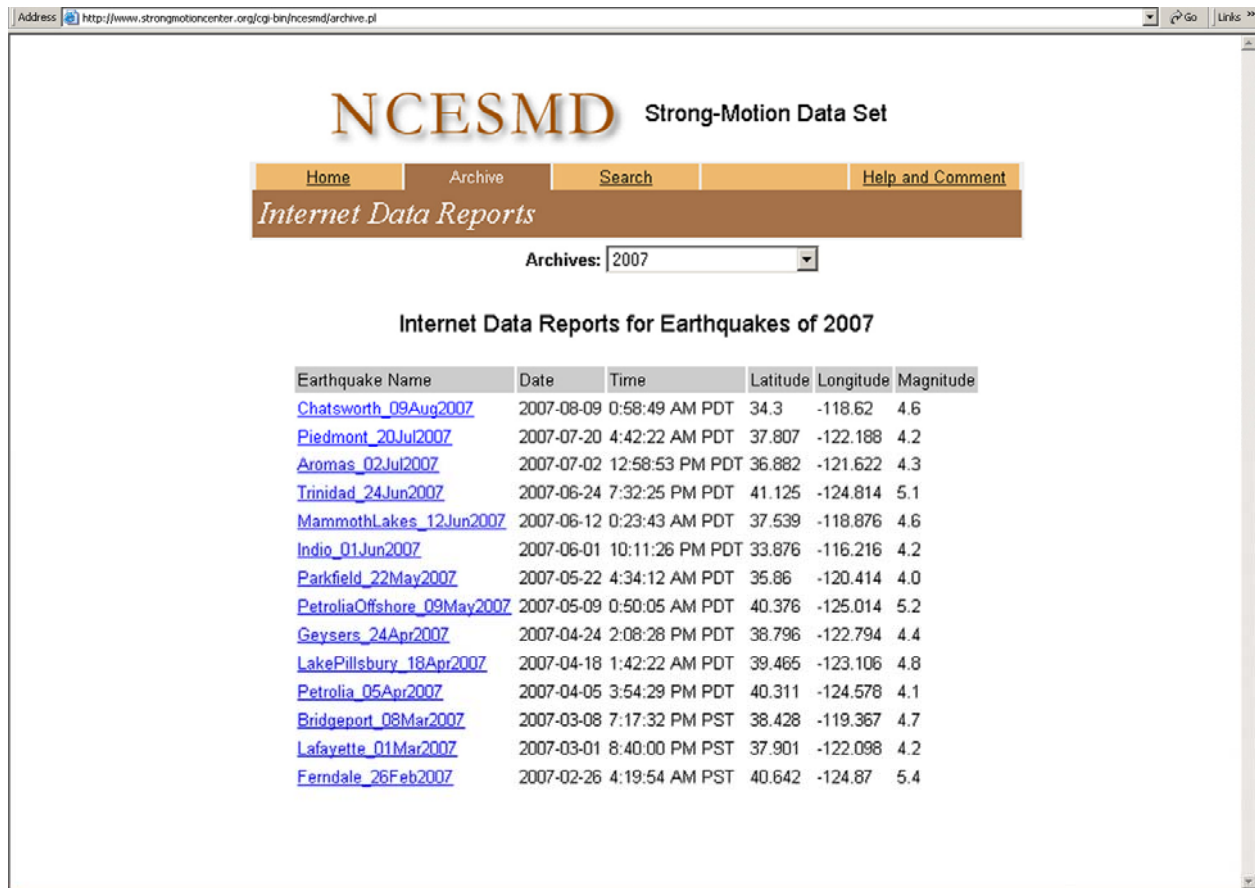


Figure 8. The Internet Data Report (IDR) page of the National Center. Data are grouped by the event year in the archive.

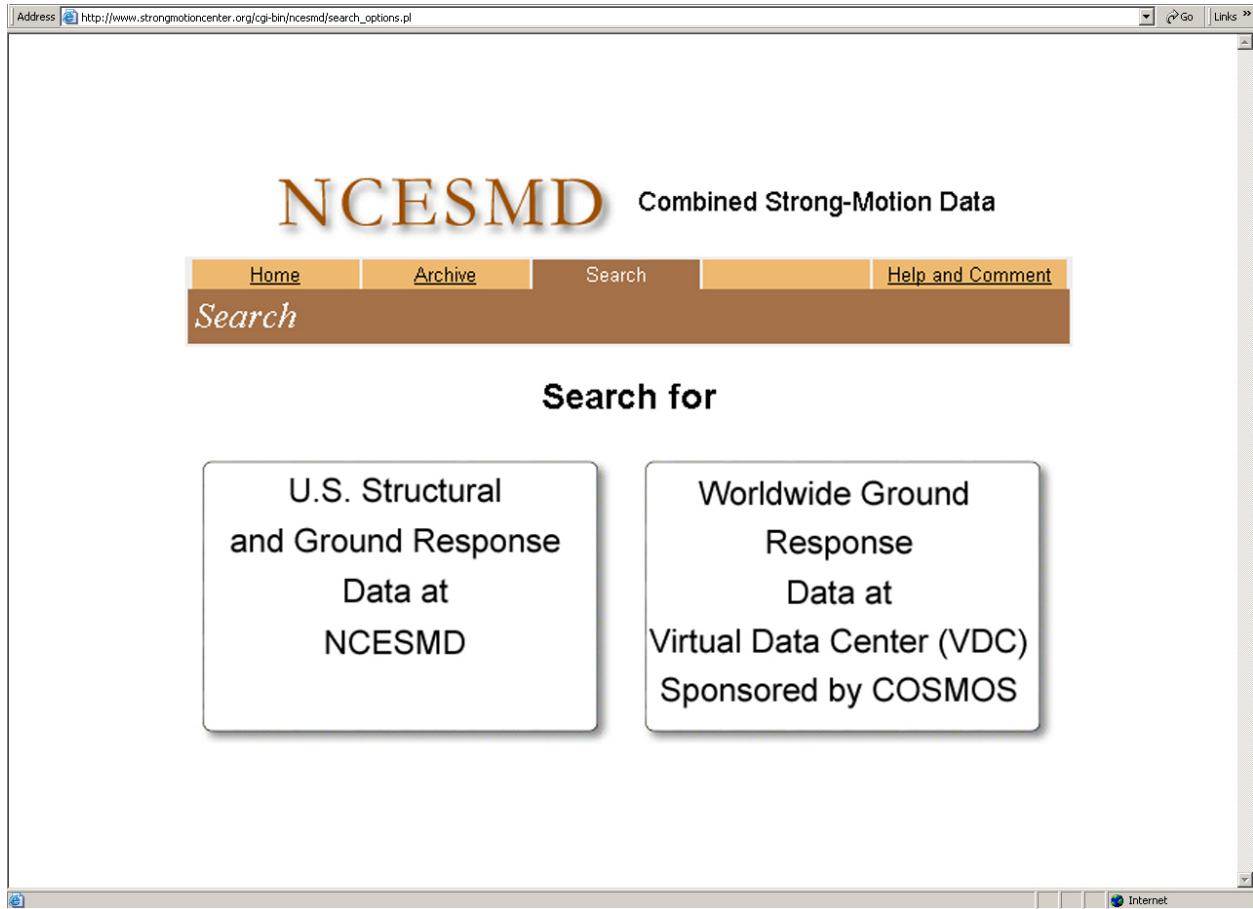


Figure 9. Search for Data in the National Center and the Virtual Data Center (VDC)'s search facility. The two functions will be integrated to provide "one-stop shopping" for earthquake strong motion data.



The screenshot shows a web browser window with the address bar containing the URL `http://www.strongmotioncenter.org/cgi-bin/ncesmd/search1.pl`. The main content area features the NCESMD logo and the text "Combined Strong-Motion Data". Below this is a navigation bar with buttons for "Home", "Archive", "Search", and "Help and Comment". A prominent "Search" button is also visible. The search form is titled "Search for Data" and includes a note: "Note: Leave fields blank that do not apply to your search." The form contains several input fields and dropdown menus: "Earthquake Name:" with a text box; "Magnitude:" with two text boxes separated by "to"; "Year (4-digit):" with two text boxes separated by "to"; "Station (City, Name, or No.):" with a text box; "Station Type:" with a dropdown menu showing "Building"; "Material:" with a dropdown menu showing "Any"; "Height:" with a dropdown menu showing "Any"; "PGA (g):" with two text boxes separated by "to"; and "Epicentral Dist. (km):" with two text boxes separated by "to". At the bottom of the form are "Search" and "Reset" buttons.

Figure 10. The National Center's search engine interface, showing the available search parameters.

**NCESMD** Combined Strong-Motion Data

[Home](#) | [Archive](#) | [Search](#) | [Help and Comment](#)

*Search*

**60 records match your search**

StaNo	Station	Network	Epic. (Fault) Dist.(km)	Horiz Apk (g)		Earthquake	View	Down-load
				Ground	Struct.			
24054	<a href="#">West Hills - 3-story LAPD 911 Bldg</a>	CGS	8.8(-)	0.039	0.033	<a href="#">Chatsworth 09Aug2007</a>	⊙	⊙
23788	<a href="#">Colton - 3-bldg Hospital Complex</a>	CGS	10.2(-)	0.121	0.116	<a href="#">Fontana 06Jan2005</a>	--	--
23497	<a href="#">Rancho Cucamonga - 4-story Justice Cntr</a>	CGS	12.1(-)	--	0.240	<a href="#">Upland 28Feb1990</a>	⊙	⊙
58197	<a href="#">San Francisco - 4-story Office Bldg</a>	CGS	15.6(-)	0.005	0.025	<a href="#">PiedmontArea 20Dec2006</a>	⊙	⊙
24605	<a href="#">Los Angeles - 7-story Univ. Hospital</a>	CGS	16.8(-)	0.027	--	<a href="#">WHollywood 9Sep2001</a>	⊙	⊙
58197	<a href="#">San Francisco - 4-story Office Bldg</a>	CGS	17.9(-)	0.007	0.038	<a href="#">Piedmont 20Jul2007</a>	⊙	⊙
24723	<a href="#">Los Angeles - 2-story County EOC Bldg</a>	CGS	19.0(-)	0.011	--	<a href="#">WHollywood 9Sep2001</a>	--	⊙
14724	<a href="#">Los Angeles - 5-story Hospital</a>	CGS	21.1(-)	0.006	--	<a href="#">WHollywood 9Sep2001</a>	--	⊙
	"		21.1(-)	0.017	--	<a href="#">WHollywood 9Sep2001</a>	--	⊙
58769	<a href="#">Hayward - 4-story City Hall</a>	CGS	22.8(-)	0.008	0.023	<a href="#">Berkeley 05Sep2003</a>	⊙	⊙
	"		25.6(-)	0.008	0.027	<a href="#">Lafayette 01Mar2007</a>	⊙	⊙
24580	<a href="#">Los Angeles - 2-story Fire Command Cntr</a>	CGS	28.0(-)	0.080	0.110	<a href="#">SierraMadre91</a>	⊙	⊙
58197	<a href="#">San Francisco - 4-story Office Bldg</a>	CGS	28.6(-)	0.004	0.025	<a href="#">Lafayette 01Mar2007</a>	⊙	⊙
24605	<a href="#">Los Angeles - 7-story Univ. Hospital</a>	CGS	29.0(-)	0.160	--	<a href="#">SierraMadre91</a>	--	--

Figure 11. The search engine results are displayed in a table that can be sorted like the IQR table. The records obtained through the search are viewable and downloadable directly, in the same way as for the IQR and IDR pages.

**EVALUATION OF CURRENT NONLINEAR STATIC PROCEDURES FOR  
CONCRETE BUILDINGS USING RECORDED STRONG-MOTION DATA**

Rakesh K. Goel and Charles Chadwell

Department of Civil and Environmental Engineering  
California Polytechnic State University, San Luis Obispo

**Abstract**

This paper evaluates current Nonlinear Static Procedures (NSPs) specified in the FEMA-356, ASCE-41, ATC-40, and FEMA-440 documents using strong-motion data from reinforced-concrete buildings. For this purpose, peak roof (or target node) displacements estimated from the NSPs are compared with the value derived from recorded motions. It is shown that: (1) the NSPs either overestimate or underestimate the peak roof displacement for several of the buildings considered in this investigation; (2) the ASCE-41 Coefficient Method (CM), which is based on recent improvements to the FEMA-356 CM suggested in FEMA-440 document, does not necessarily provide better estimate of roof displacement; and (3) the improved FEMA-440 Capacity Spectrum Method (CSM) generally provides better estimates of peak roof displacements compared to the ATC-40 CSM. However, there is no conclusive evidence of either the CM procedures (FEMA-356 or ASCE-41) or the CSM procedure (ATC-40 or FEMA-440) leading to better estimate of the peak roof displacement when compared with the value derived from recorded motions.

**Introduction**

Estimating seismic demands at low performance levels, such as life safety and collapse prevention, requires explicit consideration of inelastic behavior of the structure. While nonlinear response history analysis (RHA) is the most rigorous procedure to compute seismic demands, current structural engineering practice prefers to use the nonlinear static procedure (NSP) or pushover analysis. The two key steps in estimating seismic demands in NSP are: (1) estimation of the target node displacement; and (2) pushover analysis of the structure subjected to monotonically increasing lateral forces with specified height-wise distribution until the target displacement is reached. Both the force distribution and target displacement are typically based on the assumption that the response is controlled by the fundamental mode and that the mode shape remains unchanged after the structure yields.

The two widely used procedures to estimate the target displacement are: (1) the Coefficient Method (CM) defined in the FEMA-356 document (ASCE, 2000); and (2) the Capacity Spectrum Method (CSM) specified in ATC-40 document (ATC-40, 1997). The CM utilizes a displacement modification procedure in which several empirically derived factors are used to modify the response of a linearly-elastic, single-degree-of-freedom (SDOF) model of the structure. The CSM is a form of equivalent linearization. This technique uses empirically derived relationships for the effective period and damping as a function of ductility to estimate the response of an equivalent linear SDOF oscillator.

Various researchers have found that the CM and CSM may provide substantially different estimates of target displacement for the same ground motion and the same building (Aschheim et al., 1998; Akkar and Metin, 2007; Chopra and Goel, 2000; Goel, 2007; Miranda and Ruiz-Garcia, 2002) and have proposed improved procedures for estimating the target displacement. The ATC-55 project, which led to publication of the FEMA-440 document (ATC-55, 2003), undertook a comprehensive examination of the existing research in this area and has proposed improvements to both the CM and CSM.

Most previous investigations on development and evaluation of NSPs are based on numerical modeling studies; a comprehensive list of previous investigations is available in the FEMA-440 document (ATC-55, 2003). Recorded motions of strongly shaken buildings, especially those deformed into the inelastic range, provide a unique opportunity to evaluate such procedures. Therefore, the principal objective of this investigation is to evaluate the current NSPs for seismic analysis and evaluation of building structures using strong-motion records of reinforced-concrete buildings. The NSPs to be evaluated are: (1) Coefficient Method in the FEMA-356 document; (2) Capacity Spectrum Method in the ATC-40 report; and (3) improved Coefficient Method in ASCE-41 document; and (4) improved Capacity Spectrum Method proposed in the FEMA-440 document. The accuracy of these NSPs is evaluated by comparing the peak roof (or target node) displacement computed from various NSPs with that derived directly from recorded motions.

### **Selected Buildings and Strong-Motion Data**

Recorded motions of buildings that were strongly shaken and potentially deformed beyond the yield limit during the earthquake are required for this investigation. For this purpose, five concrete buildings, ranging from low-rise to high-rise, have been selected (Table 1). The strong-motion data used in this investigation are also identified in Table 1 for each building. These data are available from the US National Center for Engineering Strong Motion Data (NCESMD) (<http://www.strongmotioncenter.org>). Following is a brief description of each of the five selected buildings.

Table 1. Five concrete buildings selected.

<b>Buildings name</b>	<b>CSMIP Station</b>	<b>Number of Stories</b>	<b>Strong-Motion Data from</b>
Imperial County Services Building, El Centro	01260	6/0	1979 Imperial Valley Earthquake
13-Story Commercial Building, Sherman Oaks	24322	13/2	1994 Northridge Earthquake
20-Story Hotel, North Hollywood	24464	20/1	1994 Northridge Earthquake
4-Story Commercial Building, Watsonville	47459	4/0	1989 Loma Prieta Earthquake
3-Story UCSB Office Building, Santa Barbara	25213	3/0	1978 Santa Barbara Earthquake

### 6-Story Imperial County Services Building in El Centro

This building has open first story and five occupied stories (Figure 1). Designed in 1968, its vertical load carrying system consists of 12.7 cm (5 inch) reinforced-concrete (RC) thick slabs supported by RC pan joists spanning in transverse direction which in turn are supported by RC frame spanning in the longitudinal direction. The lateral load system consists of RC shear walls in the transverse direction and moment resisting frames in the longitudinal direction. The shear walls are offset in the first story compared to upper stories. The foundation system consists of piles under each column with pile caps connected with RC beams.

The Imperial County Services building was instrumented in 1976 with 13 sensors at four levels of the building and 3 sensors at a reference free-field site. The sensors in the building measure horizontal accelerations at ground floor, 2<sup>nd</sup> floor, 4<sup>th</sup> floor, and roof; and vertical acceleration at ground floor (Figure 1). The recorded motions of this building are available only for the 1979 Imperial Valley earthquake, during which this building was damaged and subsequently demolished. The peak recorded accelerations during this earthquake were 0.34g at the ground floor and 0.58g at the roof level.

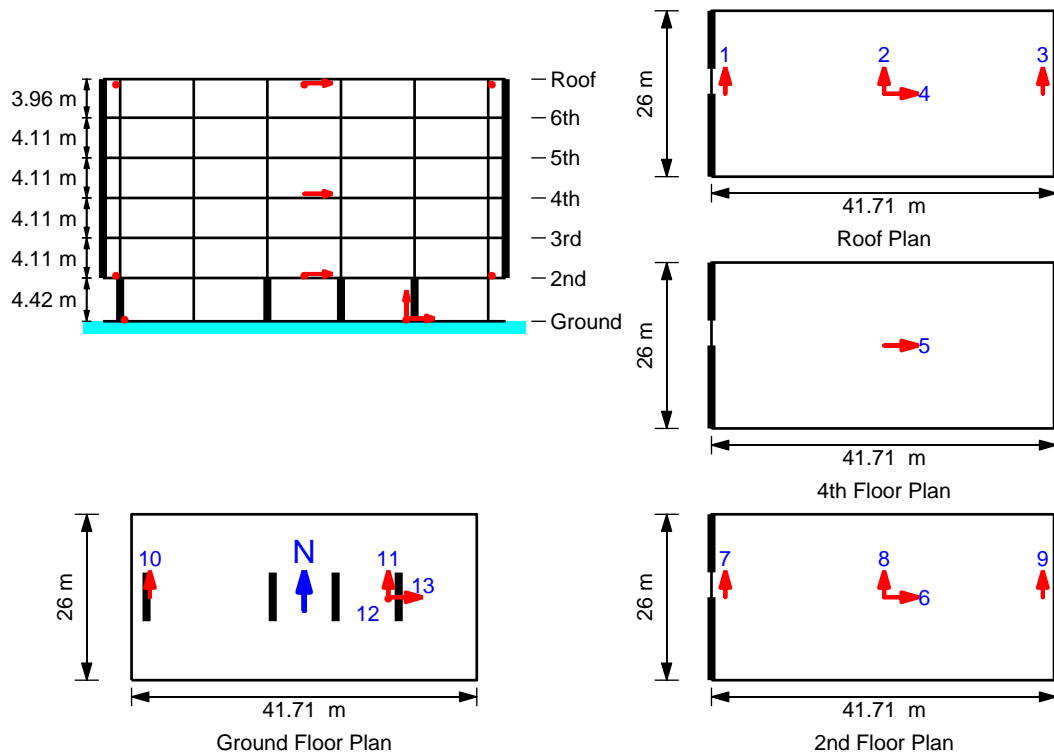


Figure 1. Imperial County Services Building.

### 13-Story Commercial Building in Sherman Oaks

This building has 13 stories above and two floors below the ground (Figure 2). Designed in 1964, its vertical load carrying system consists of 11.4 cm (4.5 inch) thick slabs supported by concrete beams, girders, and columns. The lateral load system consists of moment resisting

concrete frames in the upper stories and concrete shear walls in the basements. The foundation system consists of concrete piles.

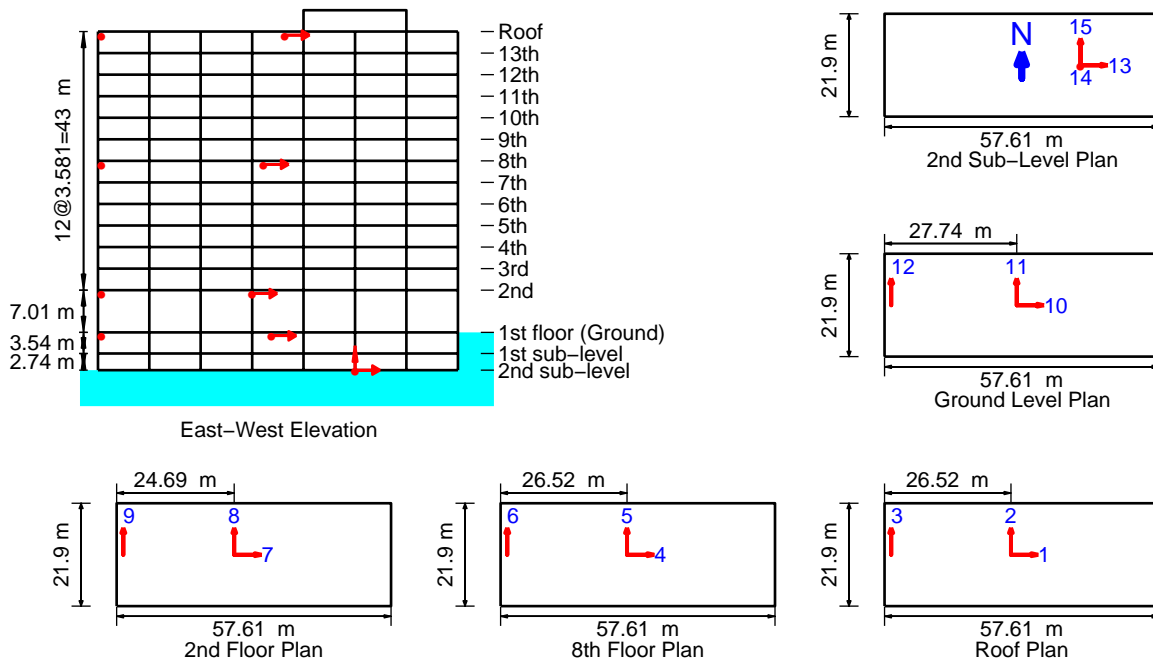


Figure 2. 13-Story Commercial Building in Sherman Oaks.

This building was instrumented in 1977 with 15 sensors on five levels of the building. The sensors in the building measure horizontal accelerations at the 2<sup>nd</sup> sub-basement level, ground level, 2<sup>nd</sup> floor, 8<sup>th</sup> floor, and roof level; and vertical accelerations at the 2<sup>nd</sup> sub-basement (Figure 2). Although this building yielded recorded motions during four major earthquakes – 1994 Northridge, 1992 Landers, 1991 Sierra Madre, and 1987 Whittier – the strongest shaking occurred during the 1994 Northridge earthquake when peak recorded accelerations were 0.46g at the basement and 0.65g in the structure. The strong-motion data from this earthquake has been used in this investigation. The building is reported to have suffered cracks at many beam-column joints during the 1994 Northridge earthquake (Shakal et al., 1994) and has subsequently been strengthened with friction dampers.

### 20-Story Hotel in North Hollywood

This building has 20 stories above and one floor below the ground (Figure 3). Designed in 1966, its vertical load carrying system consists of 11.4 cm (4.5 inch) to 15 cm (6 inch) thick RC slabs supported by concrete beams and columns. The lateral load system consists of ductile moment resisting concrete frames in both directions. The foundation system consists of spread footing below columns.

This building was instrumented in 1983 with 16 sensors on five levels of the building. The sensors in the building measure horizontal accelerations at the basement level, 3<sup>rd</sup> floor, 9<sup>th</sup> floor, 16<sup>th</sup> floor, and roof level; and vertical acceleration at the basement (Figure 3). Although this building yielded recorded motions during three major earthquakes – 1994 Northridge, 1991

Sierra Madre, and 1987 Whittier – the strongest shaking occurred during the 1994 Northridge earthquake when peak recorded accelerations were 0.33g at the basement and 0.66g in the structure. The data from 1994 Northridge earthquake has been used in this investigation.

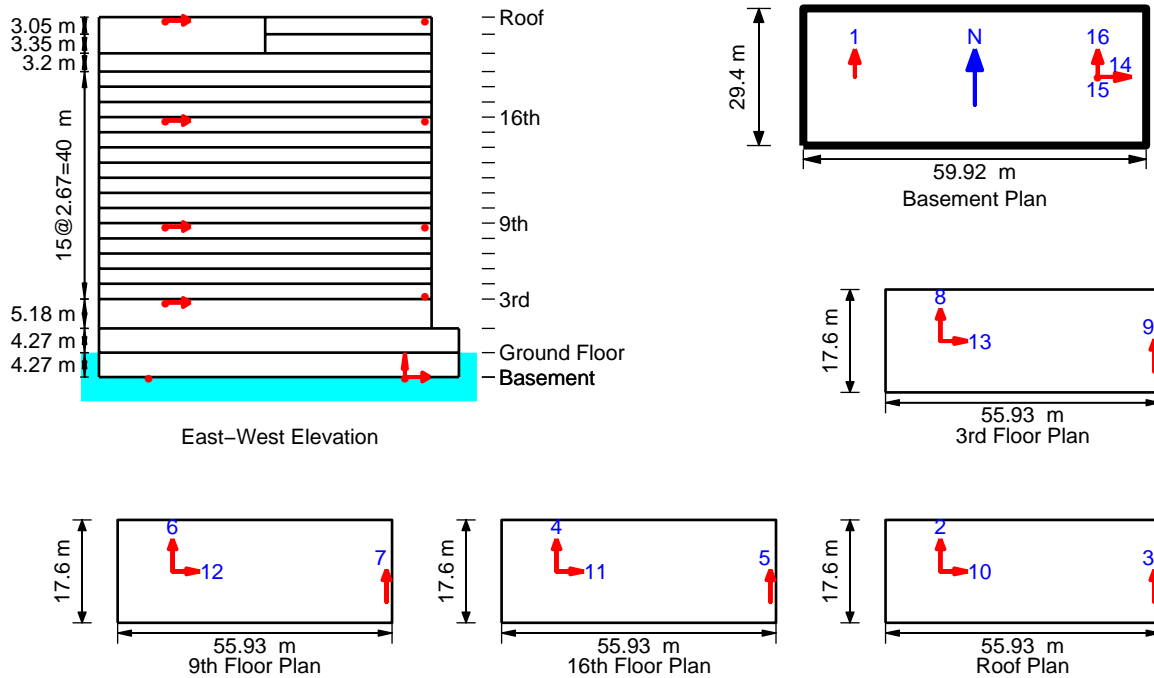


Figure 3. 20-Story Hotel in North Hollywood.

#### 4-Story Commercial Building in Watsonville

This commercial building has 4 stories above the ground (Figure 4). Originally designed and constructed in 1948 as a three-story building, the fourth story was added in 1955. Its vertical load carrying system consists of concrete slabs supported by composite concrete-steel columns. The lateral load system consists of concrete shear walls in both directions. The foundation system consists of spread footing below shear walls.

This building was instrumented in 1982 with 13 sensors on three levels of the building. The sensors in the building measure horizontal accelerations at the ground floor, 3<sup>rd</sup> floor, and roof level; and vertical accelerations at four corners of the building at the ground floor (Figure 4). This building yielded recorded motions during 1989 Loma Prieta earthquake with peak accelerations of 0.66g at the ground level and 1.24g in the structure.

#### 3-Story UCSB Office Building in Santa Barbara

This office building on the campus of University of California at Santa Barbara has 3 stories above the ground (Figure 5). Originally designed and constructed in 1960, this building was strengthened in 1975 with shear walls in both directions. The vertical load carrying system of the original building consists of concrete slabs supported by joists and RC/masonry columns. The lateral load system of the strengthened building now consists of concrete shear walls in both

directions. The foundation system consists of caissons under columns with tie beams and 10 cm (4 inch) thick slab.

This building was instrumented in 1975 with 9 sensors on three levels of the building, and 3 sensors at a reference free-field site. The sensors in the building measure horizontal accelerations at the ground floor, 3<sup>rd</sup> floor, and roof level; and vertical acceleration at the ground floor (Figure 5). This building yielded recorded motions during 1978 Santa Barbara earthquake with peak accelerations of 0.4g at the ground level and 1g in the structure.

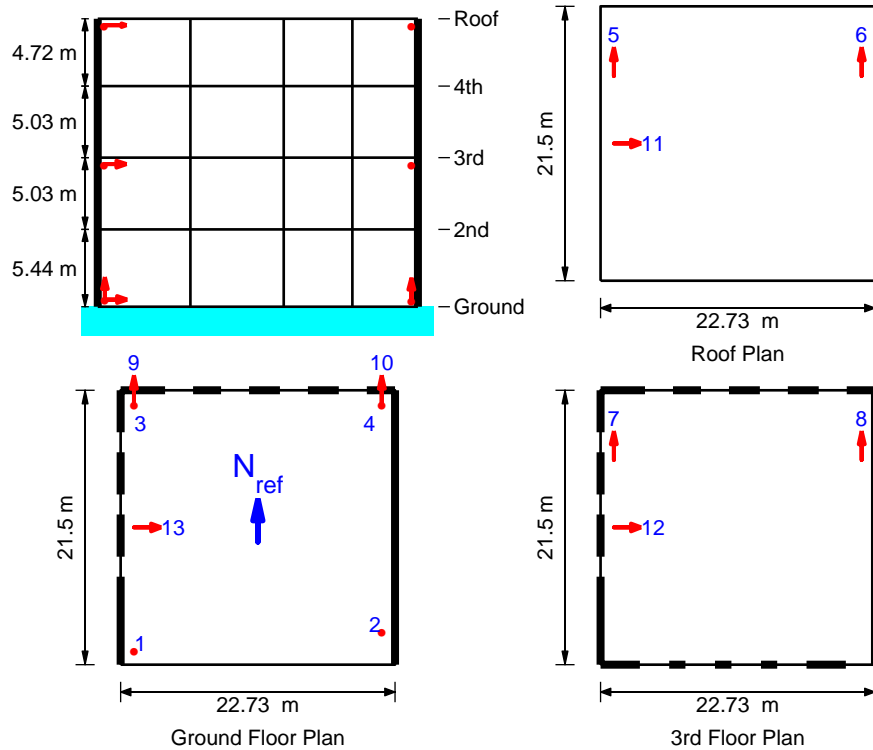


Figure 4. 4-Story Commercial Building in Watsonville.

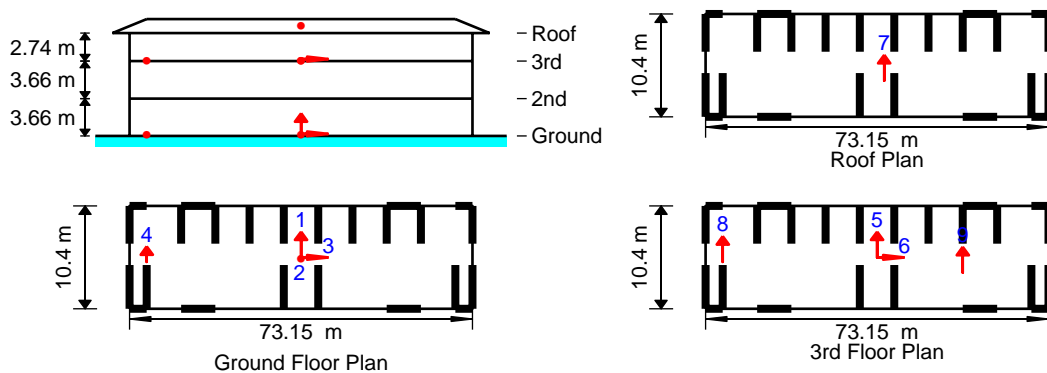


Figure 5. 3-Story Office Building in Santa Barbara.



### Current Nonlinear Static Procedures (NSPs)

NSPs in the FEMA-356, ATC-40, FEMA-440, and ASCE-41 documents require development of a pushover curve which is defined as the relationship between the base shear and lateral displacement of a control node. The height-wise distributions of lateral loads for pushover analysis is typically selected from: (1) Equivalent lateral force (ELF) distribution:  $s_j^* = m_j h_j^k$  (the floor number  $j = 1, 2 \dots N$ ) where  $s_j^*$  is the lateral force and  $m_j$  the mass at jth floor,  $h_j$  is the height of the jth floor above the base, and the exponent  $k = 1$  for fundamental period  $T_1 \leq 0.5$  sec,  $k = 2$  for  $T_1 \geq 2.5$  sec; and varies linearly in between; (2) Fundamental mode distribution:  $s_j^* = m_j \phi_{j1}$  where  $\phi_{j1}$  is the fundamental mode shape component at the jth floor; and (3) Response Spectrum Analysis (RSA) distribution: the vector of lateral forces  $\mathbf{s}^*$  is defined by the lateral forces back-calculated from the story shears determined by linear response spectrum analysis of the structure including sufficient number of modes to capture 90% of the total mass; and (4) “Uniform” distribution:  $s_j^* = m_j$  in which  $m_j$  is the mass and  $s_j^*$  is the lateral force at jth floor. The FEMA-356 NSP requires development of the pushover curve for two height-wise distributions of lateral forces: one selected from the first three of the aforementioned distributions and the second selected as the “Uniform” distribution. The ATC-40, FEMA-440, and ASCE-41 NSP require development of the pushover curve only for the fundamental mode distribution.

The structure is pushed statically to a target displacement at the control node to check for the acceptable structural performance. The NSP in the FEMA-356, FEMA-440, ATC-40, and ASCE-41 documents differ primarily in computation of this target displacement. These methods are summarized next.

#### FEMA-356 Coefficient Method

The target displacement in the Coefficient Method (CM), specified in the FEMA-356 document is computed from

$$\delta_t = C_0 C_1 C_2 C_3 S_a \frac{T_e^2}{4\pi^2} g \quad (1)$$

where  $S_a$  = Response spectrum acceleration at the effective fundamental vibration period and damping ratio of the building under consideration;  $g$  = Acceleration due to gravity;  $T_e$  = Effective fundamental period of the building in the direction under consideration computed by modifying the fundamental vibration period from elastic dynamic analysis, e.g., eigen-value analysis,  $T_i$ , by:

$$T_e = T_i \sqrt{\frac{K_i}{K_e}} \quad (2)$$

in which  $K_i$  is the elastic stiffness of the building and  $K_e$  is the effective stiffness of the building obtained by idealizing the pushover curve as a bilinear relationship;  $C_0$  = Modification factor that relates the elastic response of a Single-Degree-of-Freedom (SDF) system to the elastic displacement of the Multi-Degree-of-Freedom (MDF) building at the control node taken as the first mode participation factor or selected from tabulated values in FEMA-356;  $C_1$  = Modification factor that relates the maximum inelastic and elastic displacement of the SDF system computed from

$$C_1 = \begin{cases} 1.0; & T_e \geq T_s \\ \frac{1.0 + (R-1)T_s/T_e}{R}; & T_e < T_s \\ 1.5; & T_e < 0.1s \end{cases} \quad (3)$$

in which  $R$  is the ratio of elastic and yield strengths and  $T_s$  is the corner period where the response spectrum transitions from constant pseudo-acceleration to constant pseudo-velocity;  $C_2$  = Modification factor to represent the effects of pinched hysteretic shape, stiffness degradation, and strength deterioration selected either from tabulated values depending on the framing system (see FEMA-356 for details of various framing systems) and the performance level or taken as one for nonlinear analysis; and  $C_3$  = Modification factor to represent increased displacement due to P-delta effects computed from

$$C_3 = \begin{cases} 1.0; & \alpha \geq 0 \\ 1.0 + \frac{|\alpha|(R-1)^{3/2}}{T_e}; & \alpha < 0 \end{cases} \quad (4)$$

in which  $\alpha$  is the ratio of the post-yield stiffness to effective elastic stiffness.

### **ATC-40 Capacity Spectrum Method**

The target displacement in the Capacity Spectrum Method (CSM) specified in the ATC-40 document is computed as the maximum displacement of a linearly-elastic SDF system with equivalent period,  $T_{eq}$ , and equivalent damping ratio,  $\zeta_{eq}$  given by:

$$T_{eq} = T_o \sqrt{\frac{\mu}{1 + \alpha\mu - \alpha}}; \quad \zeta_{eq} = \zeta_o + \kappa \frac{1(\mu-1)(1-\alpha)}{\pi \mu(1 + \alpha\mu - \alpha)} \quad (5)$$

in which  $T_o$  is the initial period of vibration of the nonlinear system,  $\alpha$  is the post-yield stiffness ratio,  $\mu$  is the maximum displacement ductility ratio, and  $\kappa$  is the adjustment factor to approximately account for changes in hysteretic behavior of reinforced concrete structure. The ATC-40 document defines three types of hysteretic behaviors – Type A with stable, reasonably full hysteretic loops; Type C with severely pinched and/or degraded loops; and Type B between

Types A and C – and provides equations for computing  $\kappa$  for each of the three types of hysteretic behavior.

Since the equivalent linearization procedure requires prior knowledge of the displacement ductility ratio (see Eq. 5), ATC-40 document describes three iterative procedures: Procedures A, B, and C. Procedures A and B are the most transparent and convenient for programming, whereas Procedure C is purely a graphical method that is not suitable for programming. Details of these procedures are available in ATC-40 document and are not presented here for brevity.

### **ASCE-41 Coefficient Method**

The ASCE-41 CM is based on the improvements to the FEMA-356 CM (Eq. 1) proposed in the FEMA-440 document. In the ASCE-41 CM, the coefficient  $C_1$  is given by

$$C_1 = \begin{cases} 1.0; & T_e > 1.0\text{s} \\ 1.0 + \frac{R-1}{aT_e^2}; & 0.2\text{s} < T_e \leq 1.0\text{s} \\ 1.0 + \frac{R-1}{0.04a}; & T_e \leq 0.2\text{s} \end{cases} \quad (6)$$

in which  $a$  is equal to 130 for site class A and B, 90 for site class C, and 60 for site classes D, E, and F (see ASCE-41 for details of various site classes), respectively. The coefficient  $C_2$  is given by

$$C_2 = \begin{cases} 1.0; & T_e > 0.7\text{s} \\ 1 + \frac{1}{800} \left( \frac{R-1}{T_e} \right)^2; & T_e \leq 0.7\text{s} \end{cases} \quad (7)$$

Finally, ASCE-41 CM has dropped the coefficient  $C_3$  but imposes a limitation on strength to avoid dynamic instability. This limitation on strength is specified by imposing a maximum limit on  $R$  given by

$$R_{\max} = \frac{\Delta_d}{\Delta_y} + \frac{|\alpha_e|^{-h}}{4}; \quad h = 1.0 + 0.15 \ln(T_e) \quad (8)$$

in which  $\Delta_d$  is the deformation corresponding to peak strength,  $\Delta_y$  is the yield deformation, and  $\alpha_e$  is the effective negative post-yield slope given by

$$\alpha_e = \alpha_{P-\Delta} + \lambda(\alpha_2 - \alpha_{P-\Delta}) \quad (9)$$

where  $\alpha_2$  is the negative post-yield slope ratio defined in Figure 6,  $\alpha_{P-\Delta}$  is the negative slope ratio caused by  $P-\Delta$  effects, and  $\lambda$  is the near-field effect factor given as 0.8 for  $S_1 \geq 0.6$  and 0.2 for  $S_1 < 0.6$  ( $S_1$  is defined as the 1-second spectral acceleration for the Maximum Considered Earthquake). The  $\alpha_2$  slope includes  $P-\Delta$  effects, in-cycle degradation, and cyclic degradation.

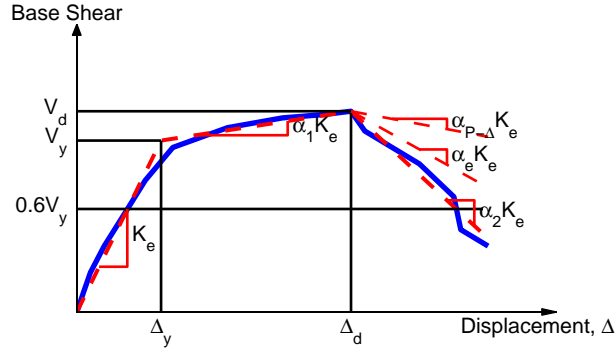


Figure 6. Idealized force-deformation curve in ASCE-41.

### FEMA-440 Capacity Spectrum Method

The improved Capacity Spectrum Method presented in FEMA-440 document includes new expressions to determine the effective period and effective damping developed by Guyader and Iwan (2006). Consistent with the original ATC-40 procedure, three iterative procedures for estimating the target displacement are also outlined. Finally, a limitation on the strength is imposed to avoid dynamic instability (Eq. 7).

The improved formulas for effective period and damping ratio in the FEMA-440 document are:

$$T_{eff} = \begin{cases} \left[ 0.2(\mu - 1)^2 - 0.038(\mu - 1)^3 + 1 \right] T_o; & \mu < 4.0 \\ \left[ 0.28 + 0.13(\mu - 1) + 1 \right] T_o; & 4.0 \leq \mu \leq 6.5 \\ \left[ 0.89 \left( \sqrt{\frac{(\mu - 1)}{1 + 0.05(\mu - 2)}} - 1 \right) + 1 \right] T_o; & \mu > 6.5 \end{cases} \quad (10a)$$

$$\zeta_{eff} = \begin{cases} 4.9(\mu - 1)^2 - 1.1(\mu - 1)^3 + \zeta_o; & \mu < 4.0 \\ 14.0 + 0.32(\mu - 1) + \zeta_o; & 4.0 \leq \mu \leq 6.5 \\ 19 \left[ \frac{0.64(\mu - 1) - 1}{0.64(\mu - 1)^2} \right] \left( \frac{T_{eq}}{T_o} \right)^2 + \zeta_o; & \mu > 6.5 \end{cases} \quad (10b)$$

These formulas apply for periods in the range of 0.2 and 2.0s. The FEMA-440 document also provides formulas with constants  $A$  to  $L$  that are specified depending on the force-deformation relationships (bilinear, stiffness-degrading, strength-degrading) and the post-yield stiffness ratio,  $\alpha$ ; these formulas are not included here brevity.

### Analytical Model

The three-dimensional analytical models of the selected buildings were developed using the structural analysis software Open System for Earthquakes Engineering Simulation (*OpenSees*) (McKenna and Fenves, 2001). Two models were developed for each building: linearly elastic model for computing the mode shapes and frequencies (or vibration periods), and a nonlinear model for pushover analysis. The beams, columns, and shear walls in the linear elastic model were based on effective section properties recommended in the FEMA-356 document. The size of the rigid-end offset at connection between beam and columns were varied between zero and one times the half the joint size in the appropriate direction. The size of the rigid-end offset was based on matching the computed vibration periods with those identified from recorded motions. The beams, columns, and shear walls were modeled using *elasticBeamColumn* element in *OpenSees*.

The beams, columns, and shear walls in the nonlinear model were modeled either with *beamWithHinges* or *nonlinearBeamColumn* element in *OpenSees*. Both elements used fiber sections containing confined concrete, unconfined concrete, and steel reinforcing bars. The stress-strain behavior of concrete, both confined and unconfined, was modeled with *Concrete04* material in *OpenSees* (Fig. 7a). This material model, compared to the traditionally used *Concrete01* material model with residual strength (or stress capacity) after crushing strain, enabled capturing of the rapid strength loss after the building's peak strength (see Fig. 6). The crushing strain of the unconfined concrete was selected to be equal to 0.004 and that for confined concrete was selected to be that corresponding to the rupture of confining steel using the well established Mander model. The stress-strain behavior of steel was modeled with *ReinforcingSteel* material in *OpenSees* (Fig. 7b). The strength of concrete and steel was selected based on the values specified in the structural drawings. The P-Delta effects were included in the pushover analysis by applying the gravity loads prior to application of the lateral loads.

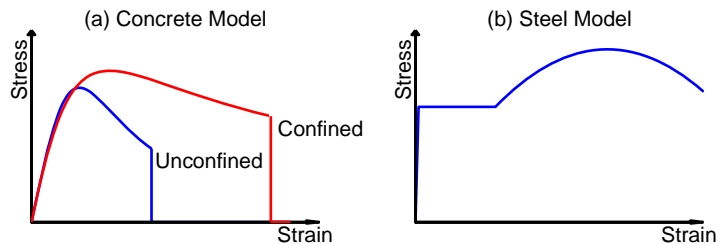


Figure 7. Material models used for nonlinear analysis.

For two of the five selected buildings – 4-Story Commercial Building in Watsonville and 3-Story UCSB Office Building in Santa Barbara – the foundation flexibility was expected to significantly influence the response during strong ground shaking because lateral load resisting system of these two low-rise buildings consists of shear walls in both directions. The foundation

flexibility was included in analytical models of these buildings by attaching six linear springs – three along the x-, y-, and z-translation, two about the x- and y- rocking, and one about the z-torsion – at the base as per the FEMA-356 recommendations.

In addition to all five buildings being modeled in *OpenSees*, a few selected buildings were also modeled using other computer programs: (1) a three dimensional model of the Imperial County Services Building was developed in *CANNY* (Li, 2004); (2) a two dimensional model in the longitudinal direction of the Imperial County Services Building was developed in *CAPP* (Chadwell, 2007); and (3) a two dimensional model in the longitudinal direction of the North Hollywood building was developed in *Peform3D* (CSI, 2006). These models were used to verify the pushover curves from *OpenSees* and investigate the variability in the pushover curves from different analytical programs. This paper presents results from models developed in *OpenSees*; results from models in other programs would be presented in a comprehensive report.

### Pushover Curves

Pushover curves for the selected building in the transverse (North-South) and longitudinal (East-West) directions were developed for the fundamental-mode height-wise distribution of lateral loads. These pushover curves are shown in Figs. 8 to 13 with thick solid line along with their idealization, shown in thick dashed line. The idealization is developed from the procedure specified in the FEMA-356 and ASCE-41 documents. Based on the elastic stiffness,  $K_i$ , and effective stiffness,  $K_e$ , shown as the initial elastic slope of the pushover curve and initial elastic slope of the bilinear idealization, the “effective” period,  $T_e$ , was computed from Eq. 2 and is also shown in these figures. Also included is the base-shear strength as a fraction of the total building weight, and the peak roof (or target node) displacement,  $u_t$ , recorded during the selected earthquake.

### Imperial County Services Building

The pushover curve in the longitudinal direction shows that the Imperial County Services Building begins to rapidly lose strength in the longitudinal direction at roof displacement of about 13 cm (Fig. 8a). This rapid loss of strength is an indication of initiation of failure (or collapse) of the building. The strong-motion data from the 1979 Imperial Valley earthquake indicated a peak roof displacement in the longitudinal direction of 23.58 cm, which far exceeded the displacement capacity of the building in this direction. As a result, the building is expected to collapse during the selected earthquake, an observation which is consistent with the field report (ATC-9, 1984) that this building collapsed primarily due to motions in the longitudinal direction. The pushover curve in the transverse direction, however, does not indicate collapse as the building’s displacement capacity exceeded the displacement demand of 5.57 cm (Fig. 8b).

It must be noted that the failure of the building in the longitudinal direction could only be predicted by considering concrete model with crushing in compression. Pushover analysis of analytical models in *OpenSees* or *CANNY*, which did not consider a concrete model with complete loss of strength immediately after crushing, did not predict the building failure prior to the peak roof displacement.

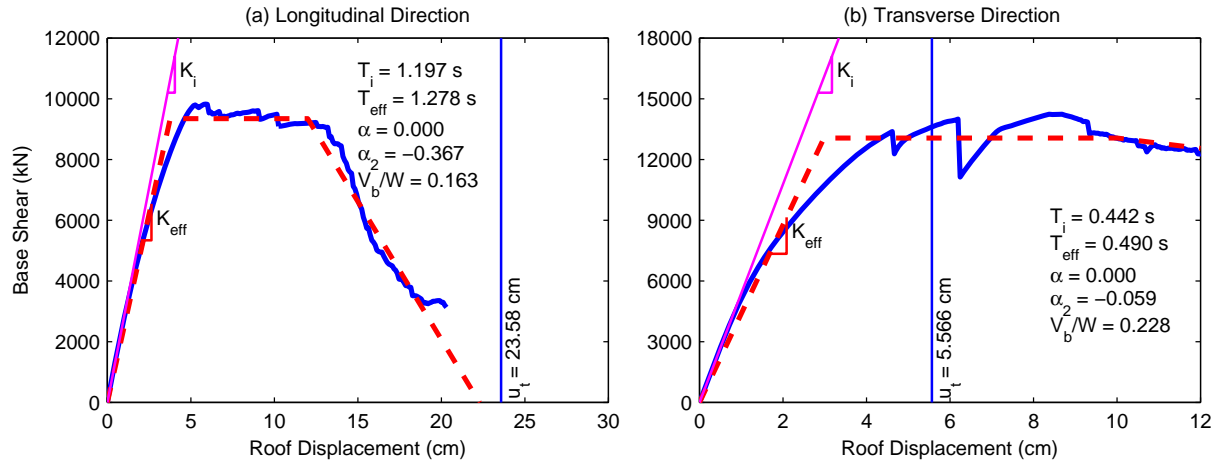


Figure 8. Pushover curves for Imperial County Services Building.

### 13-Story Commercial Building in Sherman Oaks

The pushover curve of the Sherman Oaks building in the longitudinal direction indicates that the building was deformed beyond the elastic limit during the 1994 Northridge earthquake: the peak roof displacement of 33.6 cm is slightly larger than the effective yield displacement of about 20 cm (Fig 9a). The pushover curve, however, suggests that the building would have collapsed if the roof displacement in the longitudinal direction were to exceed approximately 45 cm due to initiation of rapid loss of strength after this value of roof displacement. The pushover curve in the transverse direction indicates that the building essentially remained elastic in this direction during the 1994 Northridge earthquake as the peak roof displacement is slightly lower than the effective yield displacement (Fig. 9b).

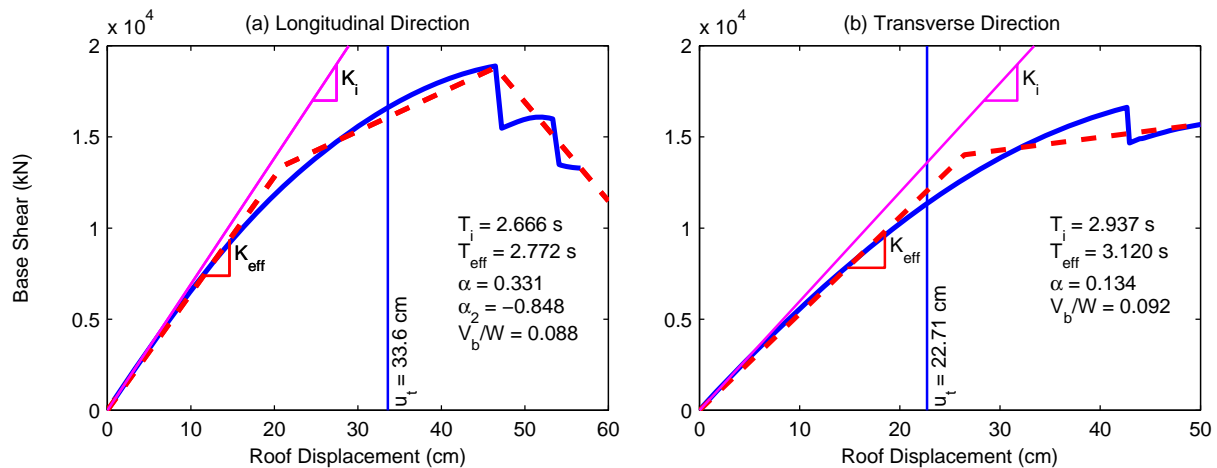


Figure 9. Pushover curves for 13-Story Commercial Building in Sherman Oaks.

In addition to the pushover curves for the entire building (Fig. 9), it is also useful to examine the force-deformation behavior of individual frames. Such results presented in Fig. 10 for the Sherman Oaks building indicate that the strength of interior frame is significantly larger than that of the exterior frame: exterior frame is about 2.5 times stronger in the longitudinal

direction and about 2.0 times stronger in the transverse direction compared to the interior frame. More importantly, the interior frame remains essentially elastic during the 1994 Northridge earthquake, whereas the exterior frame experienced significant nonlinear action.

It must be noted that the Sherman Oaks building suffered significant cracks at many beam-column joints (Shakal et al., 1994). The pushover curves, in particular, in the longitudinal direction clearly indicate the possibility of such damage.

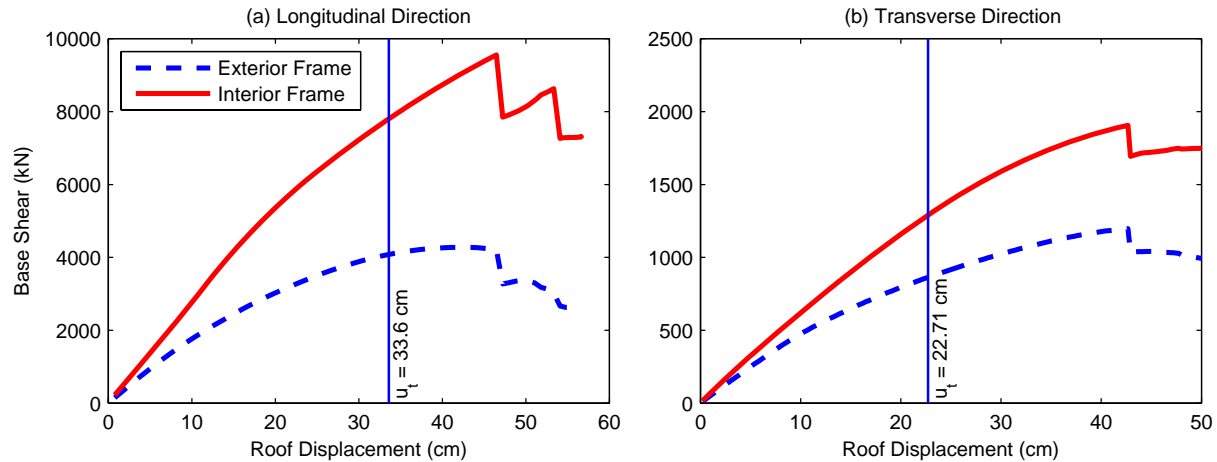


Figure 10. Force-deformation behavior of typical exterior and interior frames of the 13-Story Commercial Building in Sherman Oaks.

### 20-Story Hotel in North Hollywood

The pushover curves for the North Hollywood Hotel indicate that the building remained well within the linear elastic range both in the longitudinal as well as transverse direction during the 1994 Northridge earthquake (Fig. 11). This building is reported to have suffered heavy nonstructural and content damage but no significant structural damage (Naeim, 1999). The lack of structural damage is consistent with the observations from pushover curves in Fig. 11.

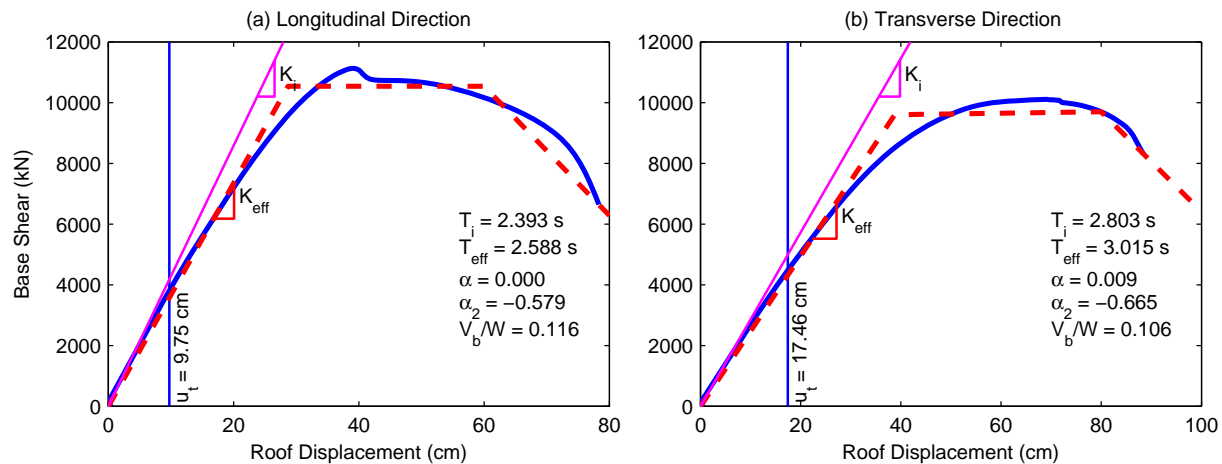


Figure 11. Pushover curves for 20-Story Hotel in North Hollywood.



### 4-Story Commercial Building in Watsonville

The pushover curves for the Watsonville building indicates that the strength of the building in the longitudinal direction is much lower compared to that in the transverse direction: the building strength is about  $0.125W$  in the longitudinal direction compared to  $0.310W$  in the transverse direction (Fig. 12). Such is the case because the south face of the building has essentially open first story as opposed to shear walls on the remaining three faces. Furthermore, the building was deformed slightly beyond the elastic range in the longitudinal (or East-West) direction but remained essentially elastic in the transverse (or North-South) direction during the 1989 Loma Prieta earthquake.

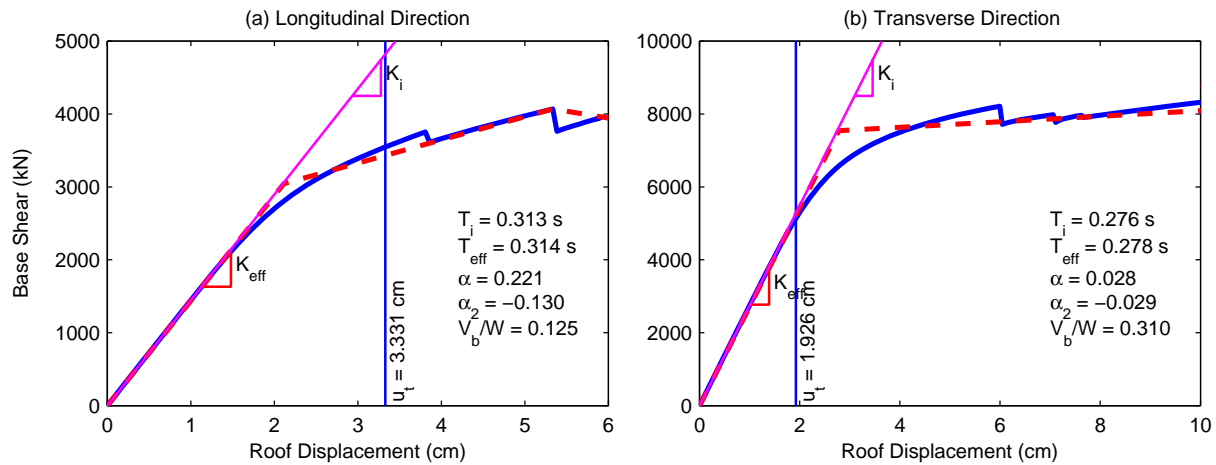


Figure 12. Pushover curves for 4-Story Commercial Building in Watsonville.

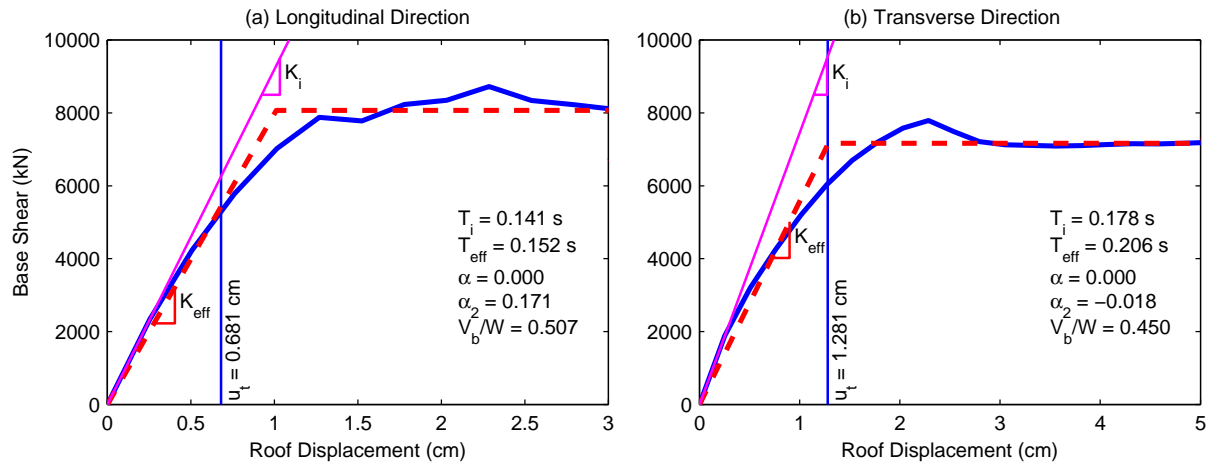


Figure 13. Pushover curves for 3-Story UCSB Office Building in Santa Barbara.

### 3-Story UCSB Office Building in Santa Barbara

The pushover curves for the Santa Barbara building indicate significant strength of the building compared to what may be expected in typical buildings designed in California: the building strength is  $0.507W$  and  $0.450W$  in the longitudinal and transverse directions,

respectively (Fig. 13). Such higher strengths are due to strengthening of the building with large number of shear walls in both directions in 1975. This building remains well within the linear elastic limit in the longitudinal direction but reaches just about the effective elastic limit in the transverse direction during the 1978 Santa Barbara earthquake.

### **Evaluation of Current NSPs**

Current NSPs are evaluated next by comparing the estimates of peak roof (or target node) displacement from the four NSP methods – FEMA-356 CM, ASCE-41 CM, ATC-40 CSM, and FEMA-440 CSM – with the value derived from recorded motions of the selected buildings. The procedure to compute derived roof displacement from recorded motions is available elsewhere (Goel, 2005).

It must be noted that the FEMA-356 CM, ASCE-41 CM, ATC-40 CSM, and FEMA-440 CSM are typically restricted to buildings that respond primarily in the fundamental mode. In this investigation, however, these NSPs were applied to buildings that may have significant contributions from higher modes, e.g., Imperial County Services Building, 13-Story Commercial Building in Sherman oaks, and 20-Story Hotel in North Hollywood. Furthermore, The peak roof displacement in the FEMA-356 and ASCE-41 NSP CM was computed from the 5%-damped elastic response spectrum at vibration period  $T_e$ . Similarly, the peak roof displacement is estimated from the damped elastic response spectrum for  $\zeta_{eq}$  and  $T_{eq}$  for the ATC-40 CSM, and for  $\zeta_{eff}$  and  $T_{eff}$  for the FEMA-440 CSM. For each case, the elastic response spectrum is developed for the acceleration recorded at the base of the building in the appropriate direction.

The application of the FEMA-356 CM, ASCE-41 CM, ATC-40 CSM, and FEMA-440 CSM to estimate the peak is illustrated in Figures 14 and 15 for one selected building: 13-Story Commercial Building in Sherman Oaks. The peak roof displacements for all buildings from the various NSP are summarized in Table 2. Errors in the peak roof displacements from various NSP, compared to the peak roof displacements derived from recorded motions, are presented in Fig. 16 with the error defined as

$$E = 100 \times \frac{u_c - u_t}{u_t} \quad (11)$$

in which  $u_c$  is the peak roof (or target node) displacement computed from the NSP, and  $u_t$  is the corresponding value derived from recorded motions. Note that the peak roof (or target node) displacement derived from recorded motions is considered to be the exact value in computing the error.

The presented results indicate that the roof displacements of the Sherman Oaks building in the longitudinal direction computed from the FEMA-356 and ASCE-41 CM are identical: the roof displacement is 28.04 cm (Figs. 14a and 14b). Such is the case because coefficient  $C_1$  and  $C_2$  in the two NSP are equal to one due to relatively long fundamental vibration period ( $= 2.67$  s) of this building in this direction. This is consistent with the equal-displacement rule, i.e., equal displacements of nonlinear and linear SDF systems, applicable for systems with long vibration

period. The two CSM procedures, however, lead to slightly different values of the roof displacement: ATC-40 CSM gives a value of 24.25 cm (Fig. 14c) and the FEMA-440 CSM provides a value of 27.05 cm (Fig. 14d). The difference between the roof displacements from the two CSM procedures are due to different values of effective period and damping ratio used in these CSM procedures (see Eqs. 5 and 10). Furthermore, the roof displacements from the CM procedures differ from the values from the CSM procedures.

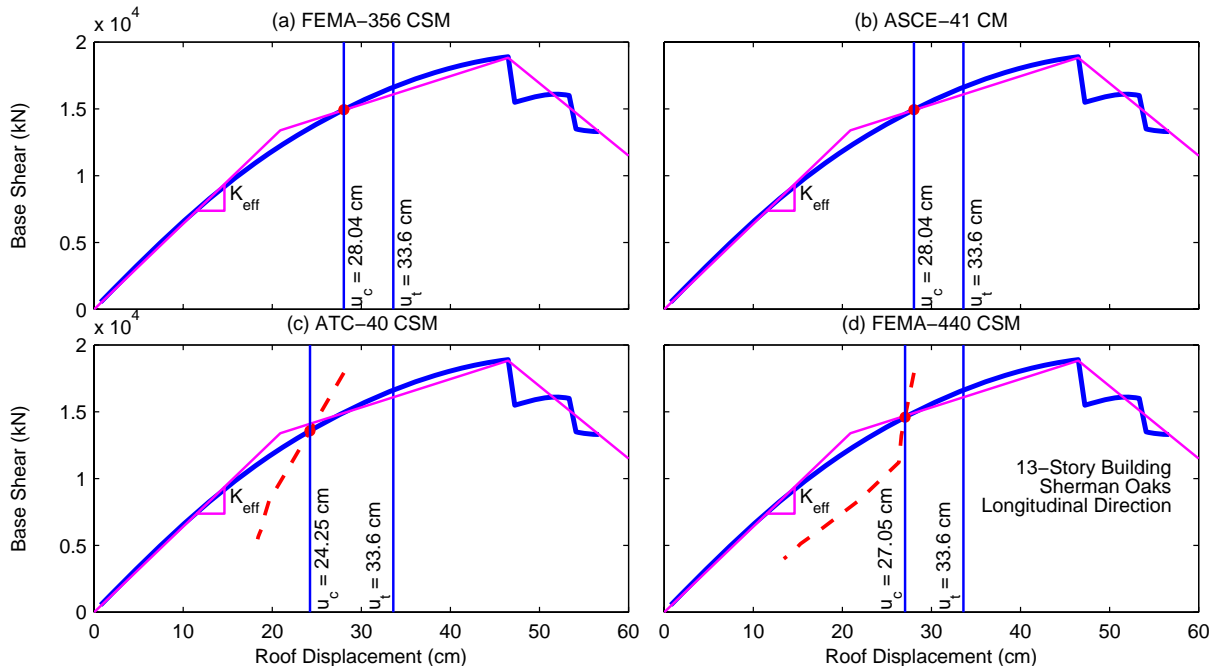


Figure 14. Computation of peak roof displacement in the longitudinal direction of the 13-Story Commercial Building in Sherman Oaks.

All NSP lead to identical peak roof displacement in the transverse direction: the peak roof displacement from various NSP is equal to 17.98 cm (Fig. 15). Such is the case because the building in the transverse direction remains in the linear elastic range. Recall that the coefficients  $C_1$ ,  $C_2$ , and  $C_3$  in the FEMA-356 NSP (Eqs. 3 and 4) as well as the coefficients  $C_1$  and  $C_2$  in the ASCE-41 NSP (Eqs. 6 and 7) are equal to one for a linearly-elastic SDF system, i.e.,  $R = 1$ . Furthermore, the additional terms in the effective vibration period and damping ratio in both the ATC-40 CSM (Eq. 5) and FEMA-440 CSM (Eq. 10) vanish for a linearly-elastic SDF system for  $\mu = 1$ . Obviously, the target displacement from all NSP would be identical.

The presented results also indicate that the peak roof displacements from NSPs for the Sherman Oaks building are less than those from recorded motions. Such is the case because the NSPs attempt to capture the response only due to the fundamental mode. Such procedures, obviously, can not capture the response due to higher modes; several higher modes contribute to the response of the 13-Story Commercial Building in Sherman Oaks.

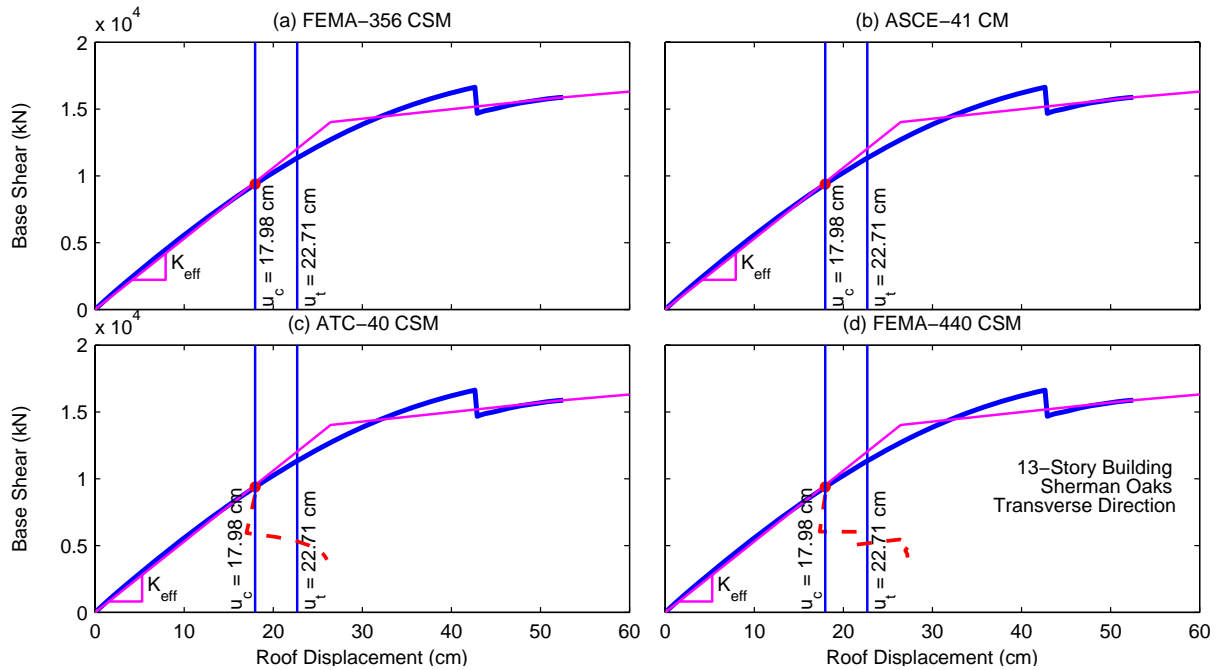


Figure 15. Computation of peak roof displacement in the transverse direction of the 13-Story Commercial Building in Sherman Oaks.

The peak roof displacements estimated from various NSP, along with the value derived from recorded motions, are summarized in Table 2. Note that peak roof displacements for the Imperial County Services Building and the Watsonville Commercial Building in the longitudinal direction could not be computed from various NSP and hence are denoted as not available (N/A).

Table 2. Peak roof displacements from various NSP.

<b>Peak Roof Displacement (cm)</b>					
	<b>Rec.</b>	<b>FEMA-356 CM</b>	<b>ASCE-41 CM</b>	<b>ATC-40 CSM</b>	<b>FEMA-440 CSM</b>
<b>Imperial County Services Building (IC)</b>					
Longitudinal (EW)	23.58	N/A	N/A	N/A	N/A
Transverse (NS)	5.57	6.99	7.60	5.64	5.46
<b>Sherman Oaks Commercial Building (SO)</b>					
Longitudinal (EW)	33.60	28.04	28.04	24.25	27.05
Transverse (NS)	22.71	17.98	17.98	17.98	17.98
<b>North Hollywood Hotel (NH)</b>					
Longitudinal (EW)	9.75	10.17	10.17	10.17	10.17
Transverse (NS)	17.46	14.33	14.33	14.33	14.33
<b>Watsonville Commercial Building (WT)</b>					
Longitudinal (EW)	3.33	N/A	N/A	N/A	N/A
Transverse (NS)	1.93	1.66	1.56	2.58	2.61
<b>Santa Barbara Office Building (SB)</b>					
Longitudinal (EW)	0.68	0.45	0.38	0.67	0.67
Transverse (NS)	1.28	1.08	0.93	1.06	1.19

It is expected that the various NSPs, which primarily should differ only for buildings responding in the nonlinear range, should provide identical values of peak roof displacements. While this expectation is confirmed for the Sherman Oaks Commercial Building in the transverse direction and the North Hollywood Building in both directions, such is not the case for the Watsonville Commercial Building in the transverse direction and the Santa Barbara Office Building in both directions (Table 2). Recall that these buildings (in indicated directions) did not deform beyond the linear elastic range during the selected earthquake; see pushover curves for Sherman Oaks Building in the transverse direction (Fig. 9b), North Hollywood Hotel in both directions (Figs. 11a and 11b), Watsonville Commercial Building in the transverse direction (Fig. 12b), and Santa Barbara Office Building in both directions (Figs. 13a and 13b). The primary difference between these buildings is the length of the fundamental vibration period: the taller Sherman Oaks Commercial Building and the North Hollywood Building have fundamental vibration periods that exceed 2.0 s whereas the shorter Watsonville Commercial Building and the Santa Barbara Office Building have fundamental vibration periods that are less than 0.5 s. Therefore, the presented results indicate that the various NSP provide identical estimates of peak roof displacement for a long-period, linearly-elastic building but may lead to different estimates for a short-period, linearly-elastic building.

The aforementioned discrepancy in roof displacement from various NSPs for short-period, linearly-elastic buildings occurs due to high sensitivity of the  $R$  value in the CM procedures and the  $\mu$  value in the CSM procedure to even very small errors in estimating the period and damping ratio. It is well known that the linearly-elastic response spectrum tends to be very jagged in the short-period range. As a result, estimates of the peak response of the linearly-elastic SDF system tends to be sensitive to errors in the vibration period and damping ratio. For the FEMA-356 CM and ASCE-41 CM, even the slight errors in estimating the vibration period and damping ratio may lead to the value of  $R$  needed in estimating the various coefficients (see Eqs. 3, 4, 6, and 7) to be larger than one. For similar reasons, the  $\mu$  needed in the ATC-40 CSM and FEMA-440 CSM to compute the effective period and effective damping ratio (see Eqs. 5 and 10) may become larger than one. Recall that for linearly-elastic buildings, values of both  $R$  and  $\mu$  should be equal to one. Depending on by how much the  $R$  and  $\mu$  values differ from one, the various NSPs would obviously lead to different values of the peak roof displacement for short-period, linearly-elastic buildings. Since the linearly-elastic response spectrum in the long-period range tends to be smooth, errors in vibration period and damping ratio do not affect the peak roof displacement estimate, and hence the  $R$  and  $\mu$  values, of the long-period, linearly elastic systems.

The FEMA-356 CM and ASCE-41 CM provide identical values of the peak roof displacements for the two flexible buildings – Sherman Oaks Commercial Building and the North Hollywood Building. As noted previously, this occurs because the coefficients  $C_1$  and  $C_2$  for these buildings are identical in the two NSP due to fundamental vibration periods being longer than 1 s. For the remaining three stiff buildings – Imperial County services Building (transverse direction only), Watsonville Commercial Building and Santa Barbara Office Building – however the two NSP lead to different estimates of peak roof displacements as the coefficients  $C_1$  and  $C_2$  differ between the two NSP for short-period buildings.

Figure 16 presents the percent error (see Eq. 11) in the peak roof displacement from various NSPs when compared to the value derived from recorded motions. These results indicate significant errors in the estimate of peak roof displacement from current NSPs. These errors range from about 40% underestimation, e.g., as is the case for ASCE-41 CM for the Santa Barbara building (see SB-EW in Fig. 16), to about 40% overestimation, e.g., FEMA-440 iterative CSM for the Watsonville building (see WT-NS in Fig 16) .

Among the two CM procedures, the ASCE-41 CM, which is based on the improvements suggested recently in the FEMA-440 document, does not necessarily provide improved estimates for the selected buildings. For example, the ASCE-41 CM leads to larger overestimation for the Imperial County Services Building (see IC-NS in Fig. 16) and larger underestimation for Watsonville and Santa Barbara buildings (see WT-NS, SB-EW, and SB-NS in Fig. 16) when compared to the results from the FEMA-356 CM.

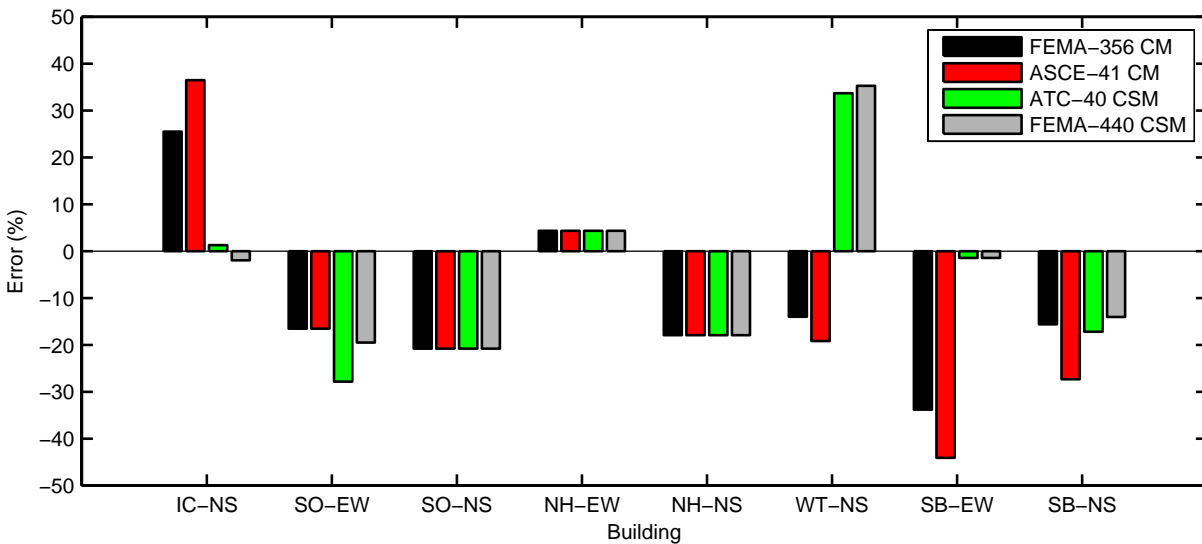


Figure 16. Percent error in peak roof displacements from various NSPs.

The FEMA-440 CSM generally provides better estimated of the peak roof displacement compared to the ATC-40 CSM (see IC-NS, SO-EW, and SB-NS in Fig. 16). This indicates that the improvements to the CSM procedure suggested in the FEMA-440 document are likely to lead to better estimated of peak roof displacement.

Finally, there is no clear evidence of whether the CM procedure (FEMA-356 or ASCE-41) or the CSM procedure (ATC-40 or FEMA-440) provides better estimate of peak roof displacement when compared with the value derived from recorded motions. The CSM procedure lead to better estimates for some building (see IC-NS and SB-EW in Fig. 16) but worse estimates for other (see SO-EW and WT-NS in Fig. 16) compared to the CM procedure. For other buildings, the two procedures lead to essentially similar level of accuracy (see SO-NS, NH-EW, and NH-NS in Fig. 16).

### Conclusions

This investigation on evaluation of the FEMA-356 CM, ASCE-41 CM, ATC-40 CSM, and FEMA-440 CSM using strong-motion records of five reinforced-concrete building have led to the following conclusions:

1. The pushover curve for the entire building that is used in implementation of the NSP may not truly reveal the extent of nonlinearity in the building during an earthquake. This may occur for buildings in which strength and stiffness properties of lateral-load resisting elements (such as frames, walls) differ significantly.
2. The various NSPs may lead to either significant overestimation or underestimation of the peak roof displacement.
3. It is expected that various NSPs provide identical estimates of peak roof displacement for buildings responding in the linearly-elastic range during an earthquake. While this expectation is found to be valid for flexible (long-period) buildings, it may not be valid for stiff (short-period) buildings.
4. The ASCE-41 CM, which is based on recent improvements to the FEMA-356 CM suggested in FEMA-440 document, does not necessarily provide better estimate of roof displacement for the buildings considered in this investigation.
5. The improved FEMA-440 CSM generally provides better estimates of peak roof displacements compared to the ATC-40 CSM.
6. There is no conclusive evidence that the CM procedures (FEMA-356 or ASCE-41) lead to better estimates of the peak roof displacement compared to the CSM procedure (ATC-40 or FEMA-440) or vice-versa.

It must be emphasized that the NSPs are typically designed to be used with smooth spectrum. Ideally, these procedures must be evaluated using a suite of design spectrum compatible ground motions, a wide range of buildings, and statistical analysis of results. Although, the evaluation of various NSPs in this investigation is conducted based on limited data – five buildings and one set of strong motion records for each building – and this investigation has led to some useful observations, it is still not possible to draw definitive conclusions about all aspects of various NSPs. More definitive conclusions may be drawn as additional data becomes available in future.

### Acknowledgment

This investigation is supported by the California Department of Conservation, California Geological Survey, Strong Motion Instrumentation Program, Contract No. 1005-832. This support is gratefully acknowledged. Also acknowledged is the contribution to this research investigation by Matthew Hazen and Joey Givens, undergraduate students at Cal Poly, San Luis Obispo, and by Dr. Dae-Han Jun, Visiting Professor from Dongseo University, Korea.

## References

- ASCE (2000). Prestandard and Commentary for the Seismic Rehabilitation of Buildings. *Report No. FEMA-356*, Building Seismic Safety Council, Federal Emergency Management Agency, Washington, D.C.
- Aschheim, M. A., Maffei, J. and Black, E. (1998). "Nonlinear Static Procedures and Earthquake Displacement Demands." *Proceedings of 6th U.S. National Conference on Earthquake Engineering*, Earthquake Engineering Research Institute, Seattle, WA.
- Akbar, S. and Metin, A. (2007). "Assessment of Improved Nonlinear Static Procedures in FEMA-440." *Journal of Structural Engineering*, **133**(9): 1237-1246.
- ATC-40 (1997). Seismic Evaluation and Retrofit of Concrete Buildings. *Report No. ATC-40*, Applied Technology Council, Redwood City, CA.
- ATC-55 (2003). Improvement of Inelastic Seismic Analysis Procedures: Draft Report for Atc-55 Project. *Report No. FEMA-440*, Applied Technology Council, Redwood City, CA.
- ATC-9 (1984). An Evaluation of the Imperial County Services Building: Earthquake Response and Associated Damage. *Report No. ATC-9*, Applied Technology Council, Palo Alto, CA.
- Chadwell, C. (2007). Capacity Analysis and Pushover Program (Capp): Version 1.04. Imbsen & Associates, Inc., ([www.imbsen.com](http://www.imbsen.com)).
- Chopra, A. K. and Goel, R. K. (2000). "Evaluation of NSP to Estimate Seismic Deformation: SDF Systems." *Journal of Structural Engineering*, **126**(4): 482-490.
- CSI (2006). Perform3D: Nonlinear Analysis and Performance Assessment for 3d Structures: Version 4. Computers and Structures, Inc., Berkeley. ([www.csiberkeley.com](http://www.csiberkeley.com)).
- Goel, R. K. (2005). "Evaluation of Modal and FEMA Pushover Procedures Using Strong-Motion Records of Buildings." *Earthquake Spectra*, **21**(3): 653-684.
- Goel, R.K. (2007). "Evaluation of Current Nonlinear Static Procedures Using Strong Motion Records," *Proceedings of the 2007 Structures Congress, Long Beach, CA*, American Society of Civil Engineers, Reston, VA.
- Guyader, A. C. and Iwan, W. D. (2006). "Determining Equivalent Linear Parameters for Use in a Capacity Spectrum Method." *Journal of Structural Engineering*, **132**(1): 59-67.
- Li, K. (2004). CANNY: 3-Dimensional Nonlinear Static/Dynamic Structural Analysis Computer Program: CANNY Consultant PTE LTD, Singapore.
- McKenna, F. and Fenves, G. (2001). The Opensees Command Language Manual: 1.2. Pacific Earthquake Engineering Center, University of California, Berkeley, (<http://opensees.berkeley.edu>).
- Miranda, E. and Ruiz-Garcia, J. (2002). "Evaluation of Approximate Methods to Estimate Maximum Inelastic Displacement Demands." *Earthquake Engineering and Structural Dynamics*, **31**(3): 539-560.
- Naeim, F. (1999). "Lessons Learned from Performance of Nonstructural Components During the January 17, 1994 Northridge Earthquake -- Case Studies of Six Instrumented Multistory Buildings." *Journal of Seismology and Earthquake Engineering*, **2**(1): 47-57.



Shakal, A. F., Huang, M. and Darragh, R. B. (1994). "Some Implications of Strong-Motion Records from the 1994 Northridge Earthquake." *Proceedings of SMIP94 Seminar on Utilization of Strong-Motion Data*, Strong Motion Instrumentation Program, CDMG, Sacramento, CA.



**PREDICTIVE CAPABILITY OF NONLINEAR STATIC ANALYSIS PROCEDURES FOR SEISMIC EVALUATION OF BUILDINGS**

Dionisio Bernal<sup>1</sup> and Arash Nasser<sup>2</sup>

<sup>1</sup> Civil and Environmental Engineering Department, Center for Digital Signal Processing, Northeastern University, Boston, MA.

<sup>2</sup> Graduate Student, Northeastern University, Boston, MA,

**Abstract**

The recorded response of a number of reinforced concrete buildings to real earthquakes are used to test the predictive capability of nonlinear static procedures (NSP). Response parameters such as drifts and inter-story shears are obtained by blending measured acceleration signals and model based information, using an observer. The buildings are represented by 3D nonlinear Finite Element models with elastic stiffness updated from eigenproperties identified from small amplitude response. The fidelity of the models for behavior at large amplitudes is validated by contrasting time history predictions with measured strong motion acceleration response. As one anticipates from theoretical considerations, the prediction accuracy of NSP is found to be significantly higher in the lower levels of the buildings considered. The ratio of “measurements” to predictions over the full height for the cases analyzed has a mean and coefficient of variation of around {1.05 and 0.22} for shears and {1.2 and 0.45} for inter-story drifts. Differences in predictive capability between the various NSP are found statistically insignificant.

**Introduction**

Many existing concrete buildings in the US were designed and built without the benefit of the modern understanding of behavior for severe seismic loading. Since an across the board policy of condemnation or mandatory retrofit of the old stock is economically unacceptable, a case by case determination of vulnerability has proven necessary. The framework that has evolved is one where building performance is explicitly quantified in terms of anticipated damage and decisions are made on this basis. Ideally the anticipated performance would be evaluated by subjecting a refined nonlinear model of the structure to an ensemble of multi-component excitations representing the appropriate level of shaking. At present, however, the nonlinear dynamic approach is considered impractical for routine applications. The procedures that have emerged as a compromise between a code-based evaluation and time history analysis of nonlinear Finite Element models have been labeled Nonlinear Static Procedures (NSP).

In NSP the connection between structural behavior and response amplitude is modeled explicitly but, as the name indicates, the dynamics are avoided by assuming that the results of interest can be taken from configurations reached when the structure is pushed laterally using one or more prescribed lateral load distributions. Recently the Applied Technology Council (ATC) undertook a study to examine the variability of predictions from different guidelines and suggested changes geared towards reducing the differences between the techniques currently in

vogue [1]. This paper summarizes some results obtained in a CSMIP funded project whose objective was to examine the relative merit of NSP in light of empirical data available from the response of structures to real earthquakes. This assessment has two distinct components, namely:

1. Obtaining the NSP predictions
2. Obtaining estimates of the quantities of interest from the acceleration data.

The uncertainties that appear in item#1 due to modeling difficulties are well appreciated but the issues connected with item#2 are less so. It is, in fact, not uncommon in the literature to find references to “measured base-shear” or to “measured inter-story drift” even though these quantities are not actually measured. In this regard the paper shows that the procedure used to make inferences from the acceleration data can have an important effect on accuracy. In this study the response is reconstructed from the measurements using an observer having a gain that accounts for the fact that the bulk of the discrepancies between measurements and open loop model estimates arise (in this application) from modeling errors [2]. The rest of the paper is organized as follows. The first section summarizes the conceptual support of NSP and the next outlines the observer. Results for the 13-story Sherman Oaks building, the 6-story Imperial County Services building and a 4-story telephone building in Watsonville are presented subsequently. Two other structures are presented in the final report of the project to CSMIP, namely, a 3-story building in Santa Barbara and a 20-story structure in North Hollywood [3]. The paper closes with a brief critical review of the material presented.

### Nonlinear Static Procedures

Assume the performance of a structure during earthquakes is some function of a set of variables  $r_1(t)$   $r_2(t)$  ...  $r_n(t)$  and that an approximate but practically useful decision on the structural state can be made by looking at some metric from each variable separately, typically the maximum value. Say these metrics are  $r_1, r_2 .. r_n$ . The objective of NSP is to provide and estimate of  $r_j$  from a static analysis of the structure subjected to a prescribed lateral load distribution. In principle the lateral load distribution can be different for each  $r_j$ , but in practice only a few load patterns, and many times only one, are used. NSP differ on the criterion that is used for deciding the magnitude of the load at which the analysis is terminated. At present all techniques provide termination in terms of the attainment of a roof displacement that is referred to as the target displacement or the performance point. There are two NSP in vogue: the coefficient method CM and the capacity spectrum method CSM.

#### The Coefficient Method (FEMA-356 and FEMA-440 CM)

In this method the target displacement is determined using the formula

$$\delta_t = C_o C_1 C_2 C_3 S_a \frac{T_e^2}{4\pi^2} g \quad (1)$$

where  $C_o$ = ratio between the MDOF roof displacement and the SDOF elastic spectral response,  $C_1$  = ratio between the expected maximum displacement of the inelastic SDOF oscillator with

elastic perfectly plastic (EPP) hysteretic to the displacements calculated for linear elastic response,  $C_2$  = factor that accounts for deviations of the hysteretic response from the ideal EPP behavior and  $C_3$  = amplification factor for P- $\Delta$  effects. The factor  $C_3$  has been suspect to be near one since the early work of Husid, and Jennings and Husid [4,5] and the extensive MDOF studies in the 1990's by Bernal provide further confirmation [6,7]. In the newest version of the coefficient method  $C_3$  has been eliminated and replaced by a minimum strength requirement and the numerical values of the coefficients  $C_1$  and  $C_2$  have been adjusted [8]. The remaining variables in eq.1 are  $S_a$  = elastic response spectrum acceleration at the fundamental period  $T_e$  of the building, and  $g$  = acceleration of gravity.

### **Capacity-Spectrum Method (ATC-40 and FEMA-440 Linearization)**

The basic assumption here is that the target displacement can be estimated from the maximum displacement of a linear elastic SDOF system having a damping and period that are larger than the values connected with the first mode of the elastic model of the building. The values of effective period and damping in the CSM need to be obtained iteratively because the "correct values" depend on the performance point and this is unknown at the outset. As noted in FEMA-440, many engineers prefer to work with the CSM because the graphical nature of the procedure is intuitively appealing. It is worth noting, however, that the impression of precision that comes from a solution that is obtained at the intersection of demand and capacity lines is not substantiated by examination of the theory. The new version of the CSM presented in FEMA-440 involves changes in the expression for the linearization parameters.

### **Applicability of NSP**

Since NSP are founded on the assumption that the response can be "reasonably" approximated using a SDOF they become progressively less tenable as the influence of higher mode increases. FEMA 356 explicitly states that NSP shall be permitted for structures in which the effects of higher modes are not significant [9]. According to FEMA 356 the effects of higher modes are deemed significant if the story shear obtained from a response spectral analysis that captures at least 90% of the mass participation is  $\geq$  than 1.3 times the same story shear obtained from a modal analysis based on the 1<sup>st</sup> mode. If the effect of higher modes is large, however, an NSP evaluation is still permitted by FEMA-356 but it must be accompanied by linear dynamic analysis. Acceptance criteria for the linear dynamic analysis are also provided. In the equivalent linearization procedures applicability is indirectly imposed by limiting the range of the expressions for the equivalent parameters to buildings with fundamental periods that do not exceed 2.0 seconds.

### **Estate Estimation in Earthquake Engineering**

The sensors available on instrumented buildings do not provide a direct measurement of most of the quantities of interest and it is thus necessary to bring analytical tools to obtain estimations. Needless to say, if one had a perfect model and a very accurate description of the excitation all quantities could be taken from a simulated response. This, however, is far from the

situation that prevails in practice. The classical tool used for blending measurements with model information is known as an observer. A classical full order observer has the form

$$\hat{x}_{k+1} = A \hat{x}_k + Bu_k + G(y_k - \hat{y}_k) \quad (2)$$

where  $\hat{x}$  is the state vector estimate,  $y$  is the measured output,  $\hat{y}$  is the estimated output and the system is assumed to be described by the triple  $\{A, B, C\}$  where these matrices are, in the order given: the system matrix, the input to state matrix and the state to output matrix, respectively [10]. Eq.2 can also be written as

$$\hat{x}_{k+1} = (A - GC) \hat{x}_k + Bu_k + Gy_k \quad (3)$$

where  $G$  is selected to attain specific goals. In particular, when uncertainties arise because of unknown initial conditions  $G$  is selected to bring the poles of the matrix in parenthesis in eq.3 close to the origin. When the bulk of the uncertainty arises because there are unmeasured disturbances (unmeasured inputs, for example) then, provided the disturbances are broad band the optimal gain is the Kalman Filter. In the application of interest here, however, much of the uncertainty comes from model errors and as a consequence the Kalman Filter (at least in standard form) is not applicable. An observer explicitly designed for the situation of large modeling error was recently proposed in [2] and has the form

$$\hat{x}_{k+1} = (I - C^T C)A\hat{x}_k + (I - C^T C)Bu_k + C^T y_{k+1} \quad (4)$$

where

$$A = \begin{bmatrix} 0 & I \\ -M^{-1}K & -M^{-1}C_D \end{bmatrix} \quad B = \begin{bmatrix} 0 \\ -r \end{bmatrix} \quad C = [0 \quad L] \quad (5a,b,c)$$

In the previous expressions  $M$ ,  $C_D$  and  $K$  are the mass damping and stiffness matrices,  $u_k$  is the vector of ground accelerations,  $r$  is the pseudo-static displacement influence matrix and  $L$  is a Boolean matrix indicating which degrees of freedom (DOF) are measured. For example, if the 5<sup>th</sup> and the 9<sup>th</sup> DOF are measured then the (1,5) and (2,9) entries of  $L$  are unity and all others are zero. The form in eq.5 indicates that the state is the collection of relative displacements and relative velocities and eq.5c (in particular) shows that the measurements are assumed to be relative velocities. Needless to say, in practice the actual measurements are absolute accelerations but velocities in the bandwidth of interest can be computed with good accuracy from the accelerations and the form of the observer with velocity measurements is simpler. The feedback nature of an observer structure is illustrated schematically in Fig.1.

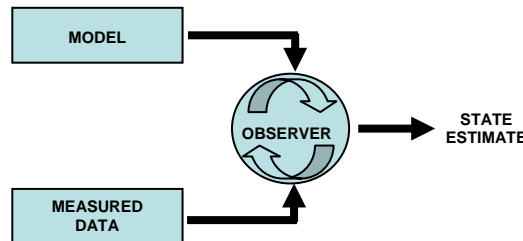


Fig.1 Schematic illustration of an observer.

### Modal Projection Estimation

A solution to the estimation problem that is simpler than the observer is a projection of the measurements in a modal basis. We comment on this solution because it is often presented in the literature as accurate, yet, as we shall illustrate next, this may or may not be the case. The projection idea is simple, namely, with the response  $y(t)$  expressed in modal coordinates  $Y(t)$  one has

$$y(t) = \Phi Y(t) \quad (6)$$

where  $\Phi$  is the modal matrix. Writing eq.6 in partitioned form

$$\begin{Bmatrix} y_m(t) \\ y_u(t) \end{Bmatrix} = \begin{bmatrix} \phi_{mm} & \phi_{mu} \\ \phi_{um} & \phi_{uu} \end{bmatrix} \begin{Bmatrix} Y_m(t) \\ Y_u(t) \end{Bmatrix} \quad (7)$$

where the subscripts  $m$  and  $u$  refer to measured and unmeasured coordinates one concludes that the responses at the unmeasured coordinates are

$$y_u(t) = \phi_{um} \phi_{mm}^{-1} y_m(t) + (\phi_{uu} - \phi_{um} \phi_{mm}^{-1} \phi_{mu}) Y_u(t) \quad (8)$$

The unmeasured coordinates in the modal projection scheme are estimated as the first term in eq.8, namely

$$\hat{y}_u(t) = \hat{\phi}_{um} \hat{\phi}_{mm}^{-1} y_m(t) \quad (9)$$

where the *hat* on the modal quantities is added to emphasize that these are not exact results but model estimates. The error in the modal projection estimation is thus given by

$$\varepsilon_u = (\phi_{um} \phi_{mm}^{-1} - \hat{\phi}_{um} \hat{\phi}_{mm}^{-1}) y_m(t) + (\phi_{uu} - \phi_{um} \phi_{mm}^{-1} \phi_{mu}) Y_u(t) \quad (10)$$

which has two parts, the first coming from error in the shapes of the  $m$  modes used to project the response and the second from the truncated space. It is shown next that for some conditions the reconstruction error in the modal projection approach can be significant.

### *Example on Estimation*

Consider a 6-story shear building where the nominal model has masses of unity and inter-story stiffness of 680 (in consistent units) but the actual inter-story stiffness and the masses are  $680 \cdot [1.2, 0.90, 0.95, 1.1, 1, 0.85]$  and  $[0.95, 1.02, 0.96, 0.97, 1, 1.1]$ . We take the real structure as having 2% modal damping while the nominal model is assigned 5%. This last discrepancy is simplistic but it is intended to stress the fact that in practice one seldom has a good characterization of the damping. One can confirm that the real structure and the nominal model have a fundamental frequency of 1 Hz (a coincidence selected to simulate the fact that the model

is likely updated to match an identified fundamental period). We assume measurements are available at coordinates #1 and #2 and that there is interest in predicting the drift in the 5<sup>th</sup> floor. Fig.2 presents the comparison of the exact solution with the following estimations: a) modal projection, b) modal projection with the output pre-filtered to the bandwidth of the first two modes, c) observer and d) nominal model in open loop.

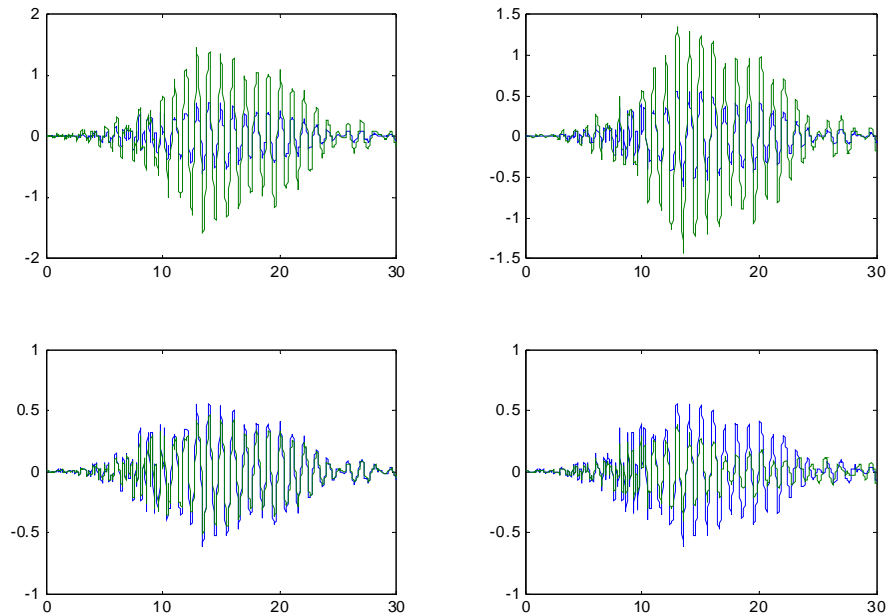


Fig.2 Drift on the 5<sup>th</sup> level: exact result in blue and predictions in green, sequentially from left to right by rows: a) MP, (b) FMP, (c) OB and (d) NM; drift in inches and time in seconds.

The superior accuracy of the observer prediction is evident by inspection.

### Shearman Oaks

The Sherman Oaks building (CSMIP station number 24322) has 13 stories above ground and two underground levels and was designed in 1964. The vertical load resisting system is concrete slabs (typically 4.5 inch thick) supported on concrete beams and columns and the lateral load resisting system is made up of moment resisting frames in both directions. The structure is on alluvium soil and the foundation is supported on concrete piles. The first floor spandrel girders were modified by post-tensioning after the 1971 San Fernando earthquake and in 1977 the building was instrumented with 15 sensors. Three sets of strong motion records are available, namely: Whittier (1987), Landers (1992) and Northridge (1994). No damage was reported due to the first two motions but the Northridge earthquake induced noticeable, yet repairable structural damage in the form of cracks in the beams, slabs, girders, and walls [11]. Fig. 3 depicts the instrumentation layout.



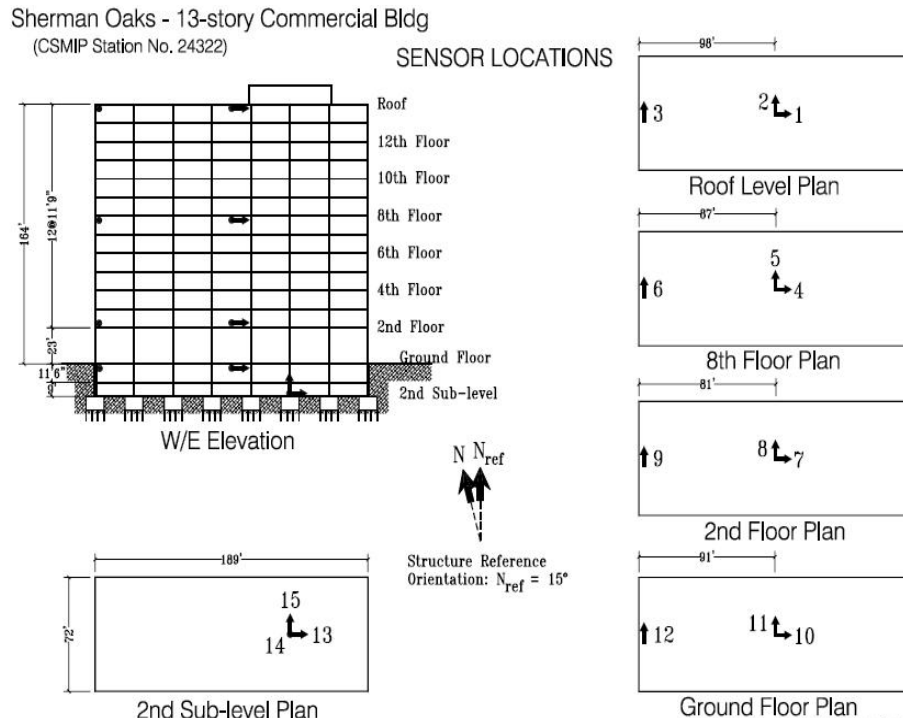


Fig.3 Layout of the sensors installed at Sherman Oaks building (taken from CSMIP web site).

**Identification of modal properties and model updating**

Identification of the quasi-linear properties of the building was done using the signals recorded during the Landers earthquake because this motion is closer in time to Northridge than Whittier and thus better captures the state of the system at the time of the shaking from Northridge. To increase confidence on the results the identification was carried out using various algorithms, in particular, ERA-OKID, Sub-ID and Reversed Time OKID [10,12]. It was found that the results for all the algorithms were quite close. The results shown in this section are those from the ERA-OKID algorithm [10].

**Longitudinal Direction**

The singular values of the Hankel matrix that is used to determine an effective model order showed 6 dominant directions, indicating 3 modes. Table1, taken directly from the ERA-OKID algorithm output summarizes the results obtained.

Table 1a. Poles in longitudinal direction

no.	Freq(Hz)	Damp%	cmi%	emac%	Mpcw%	mhp%	imp%	omp%	Msv%	mci%	moi%
1	0.386	5.363	95.6	95.6	100.0	100.0	100.0	100.0	100.0	19.5	0.2
2	1.382	6.338	9.5	9.5	99.8	76.3	76.8	99.3	52.3	41.0	0.2
3	2.520	6.839	0.0	0.0	97.8	0.0	0.0	83.1	41.6	59.5	0.1

Table 1b Mode shape amplitudes in the longitudinal direction, normalized to unity at the roof.

Level (see fig.2)	Channel #	Mode #1	Mode #2	Mode #3
2	Ch7	0.257	-0.854	0.917
8	Ch4	0.781	-0.515	-0.990
roof	Ch1	1	1	1

For a description of the quality indicators see [13].

**Transverse Direction**

Analysis showed that 3 modes could be reliably identified; results are summarized in Table 2.

Table 2a. Poles in transverse direction

no.	freq(Hz)	Damp%	cmi%	emac%	Mpcw%	mhp%	imp%	omp%	Msv%	mci%	moi%
1	0.358	4.974	90.9	90.9	100.0	99.9	99.9	100.0	100.0	15.3	0.2
2	2.357	5.814	7.6	7.7	98.9	40.4	45.8	88.3	47.6	45.9	0.2
3	1.321	6.936	43.1	43.8	98.3	85.1	85.7	99.3	53.8	35.7	0.1

Table 2b Mode shape amplitudes in the transverse direction, normalized to unity at the roof.

Level (see fig.3)	Channel #	Mode #1	Mode #2	Mode #3
2	Ch8	0.193	-0.645	1.010
8	Ch5	0.721	-0.669	-0.859
Roof	Ch2	1	1	1

**Modeling of Basement Levels**

A decision as to whether the model is to start at the ground floor or include the basement was made by looking at the Fourier amplitude spectrum of a pair of channels in each direction; one at the sublevel and one at the ground floor. The comparisons, which are shown in fig.4, illustrate that the spectra are essentially the same bellow 2.5 Hz. Since this bandwidth covers the first 3 modes in each direction a model that starts at the ground level is adequate.

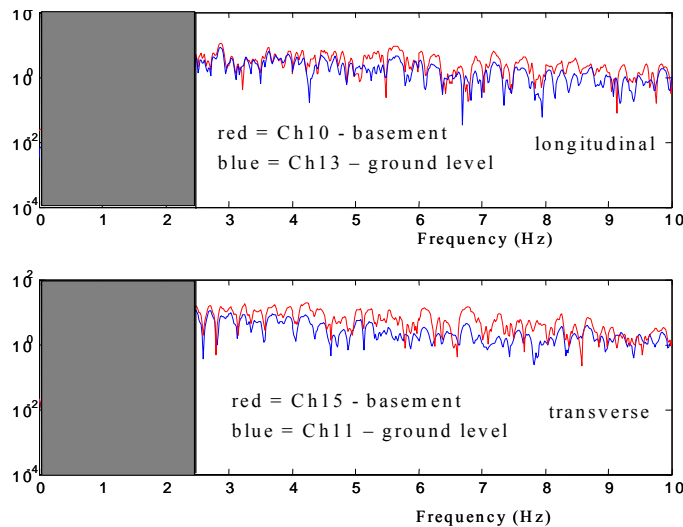


Fig.4 Fourier amplitude of channels at the lowest level (basement) and at the ground floor

***Fictive Rotational Grounding***

While the columns are taken to terminate at the ground level they cannot be treated as fixed since there is significant rotational flexibility at these points. Rotational support springs were thus included in the model. The initial stiffness of the springs was computed as the condensed flexural stiffness of a model of the basement frames. The spring constants, however, were subsequently treated as free parameters and adjusted to make the model fundamental frequency match the result from the system identification. The numerical values obtained are presented in the final report [3].

**Development of Nonlinear Model**

Nonlinear behavior was modeled with lump plasticity. The force-deformation relationship of plastic hinges was defined in terms of moment versus plastic rotation. The general force deformation relationships are as defined in FEMA 356 [9]. Strength degradation was modeled as shown schematically in fig.5.

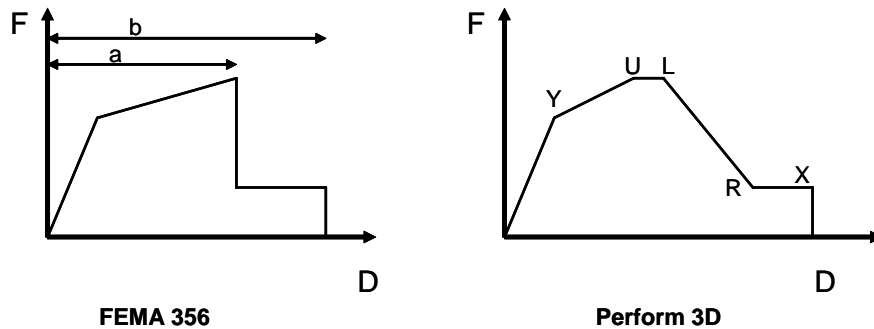


Fig.5 Comparison of load deformation relationships (left = FEMA, right = Perform3D)

***Strength Calculations and Deformation Capacities***

Over-strength values recommended by FEMA356 were implemented in the computations. For example, the moment strength of beams was computed using a 1.25 increase for the steel yield stress and 1.5 for concrete compressive strength. Calculations were done using a resistance factor of unity. Plastic hinge rotations corresponding to the onset of strength degradation and ultimate failure, as shown by parameters “a” and “b” in fig.5 are tabulated in FEMA 356 as a function of condition of transverse reinforcement, shear force on the member, percentage of tensile and compressive reinforcement and axial force (in columns). A thorough analysis for each different section was done and strength and deformations were obtained and modeled.

**Nonlinear Dynamic Analysis (NDA) and Observer Estimates**

Fig.6 (left) compares the open loop model prediction of the acceleration at the roof in the E-W direction due to Northridge with the measurement from ch1. As can be seen, the comparison is reasonable indicating that the model captures the basic features of the behavior, at least within the amplitude of the observed response. Needless to say, one does not expect the nonlinear model to give the “true” response so the targets used to judge the predictive capability

of NSP are not, as noted previously, the open loop model predictions but observer estimates. The improvements realized by the observer can be appreciated by inspecting the right side of fig.6 which shows the estimate obtained with the observer when the measurements at the roof are removed from the feedback. As can be seen, the improvement, which is a lower bound because is based on use of less than all the available information, is important.

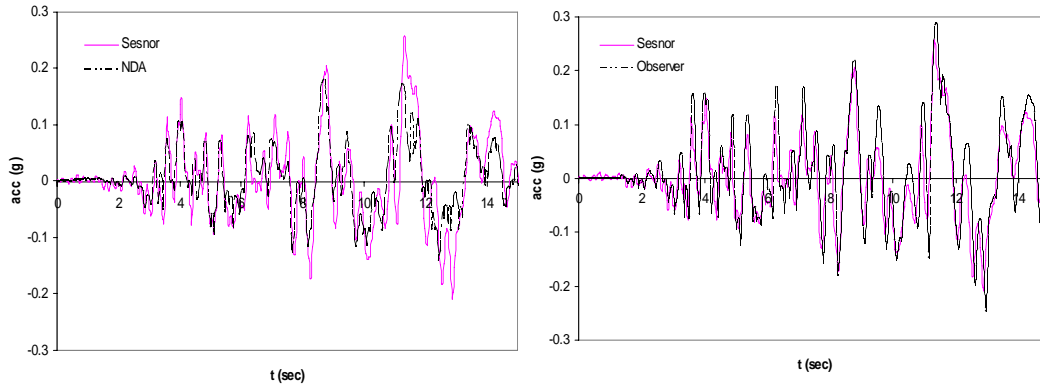


Fig.6 Ch1 acceleration in E-W direction a) NDA vs. measurements b) Observer prediction vs. measurement (obtained discarding the roof measurements)

### Performance Points and Quantities of Interest

Three different load patterns are considered: LP1= code based triangular load distribution; LP2= distribution proportional to the fundamental mode and LP3 = uniform distribution. The pushover analysis is carried out on the loaded structure so a static analysis under gravity load precedes the pushover analysis. FEMA 356 requires consideration of two gravity load combinations 1.1(D + L) and 0.9D. The mass of the structure (for inertial purposes) was taken as the mass from the dead load plus 5 percent of the live load. Concurrent seismic effects for each load pattern were considered applying simultaneously 100% of loads in the primary direction under consideration plus 30% of the loads from the other direction. The results for the Northridge earthquake are presented in Tables 3 and 4 and in fig 7. A representative pushover plot is shown in fig.8.

Table 3 Performance Point in longitudinal direction

Method	Load Pattern 1				Load Pattern 2				Load Pattern 3			
	Sa (g)	Sd (in)	V/W	drift %	Sa (g)	Sd (in)	V/W	drift %	Sa (g)	Sd (in)	V/W	drift %
ATC 40	0.103	8.507	0.085	0.52	0.1001	7.483	0.090	0.48	0.1176	6.591	0.097	0.40
FEMA 440 (Linearization)	0.116	9.650	0.089	0.60	0.1069	9.447	0.097	0.59	0.1108	9.690	0.110	0.56
FEMA 356 (CM)	0.109	11.680	0.093	0.72	0.1098	10.670	0.100	0.66	0.1201	9.786	0.111	0.58
FEMA 440 (CM)	0.119	10.790	0.091	0.66	0.1100	10.460	0.099	0.65	0.1145	10.650	0.113	0.62

Table 4 Performance Point in transverse direction

Method	Load Pattern 1				Load Pattern 2				Load Pattern 3			
	Sa (g)	Sd (in)	V/W	d %	Sa (g)	Sd (in)	V/W	d %	Sa (g)	Sd (in)	V/W	d %
ATC 40	0.100	8.330	0.074	0.53	0.0919	7.404	0.074	0.48	0.1027	5.926	0.076	0.37
FEMA 440 (Linearization)	0.104	8.465	0.076	0.54	0.0966	8.025	0.078	0.53	0.0926	7.675	0.089	0.47
FEMA 356 (CM)	0.103	9.707	0.080	0.60	0.1004	9.041	0.082	0.57	0.1082	7.771	0.091	0.47
FEMA 440 (CM)	0.109	8.916	0.078	0.57	0.1006	8.634	0.082	0.56	0.1013	9.018	0.098	0.54

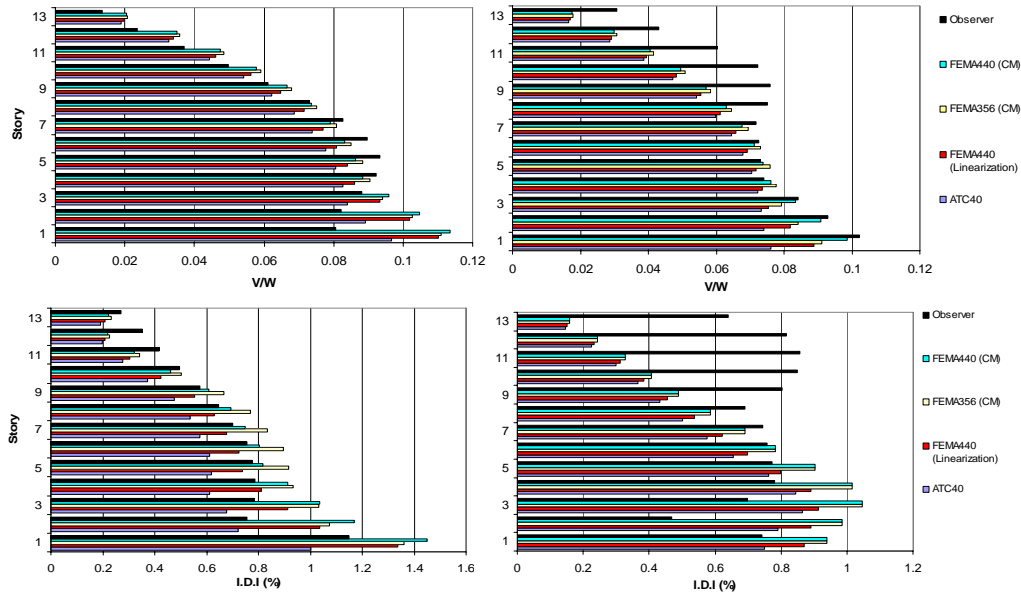


Fig.7 NSP predictions: shears on top inter-story drift index bottom: E-W and N-S (left and right)

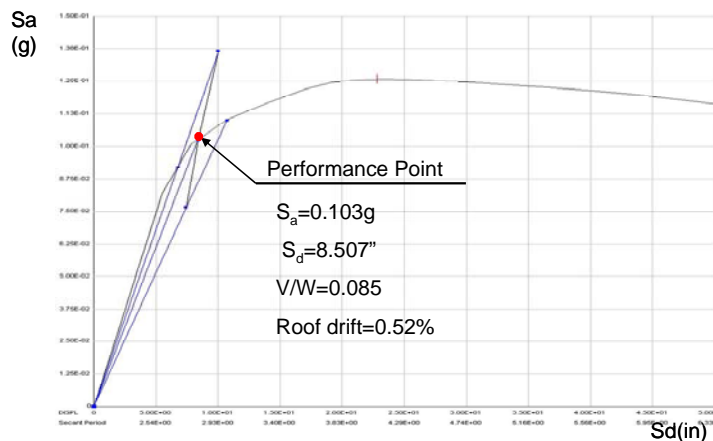


Fig.8 Pushover curve for SO building (LP1 in longitudinal direction, ATC-40 method)

**Observations**

- The differences between the estimates of the observer and the predictions of the various NSP are of the same order, although there is a small improvement in the modified versions presented in FEMA-440.
- Errors in the inter-story shears are typically less than 20% with two exceptions. A conservative estimate in E-W for the lower two floors and a significantly unconservative estimation in the upper floors in the N-S direction. This last item is easily rationalized by looking at the spectrum of the motion which shows large relative amplitudes at shorter periods and thus much more significant higher mode effects in the N-S direction (fig.9).
- Underestimation of the drift ratios in the upper floors in the N-S direction is even more pronounced than in shear. These results suggests that during the dynamic response there are instances when the shears in the upper levels are significant and the effective inter-story stiffness is much lower than the value (implicit) in the pushover. This means that

the effective inter-story stiffness is notably dependent on the load distribution, which is not surprising since the beam to column stiffness ratio is low. A detailed discussion on this matter can be found in the final report [3].

- Drifts in the lower two floors in the N-S direction are significantly overestimated, although this is not the case for the associated shears. This result indicates once again that the building has a behavior that is far from that of a shear building idealization.
- It is opportune to note that the Sherman Oaks building is outside the strict range of applicability of the current NSP since the period of the fundamental mode in both directions is larger than 2.0 seconds.

We close by noting that the base shear capacity of the building in the short direction is  $0.12W$  (including material over-strength) and that when the response base shear is computed with simple methods (such as linear interpolation of accelerations) base shears much larger than this are computed. This result points to the importance of estimating the “measured” quantities carefully since otherwise misleading observations can result.

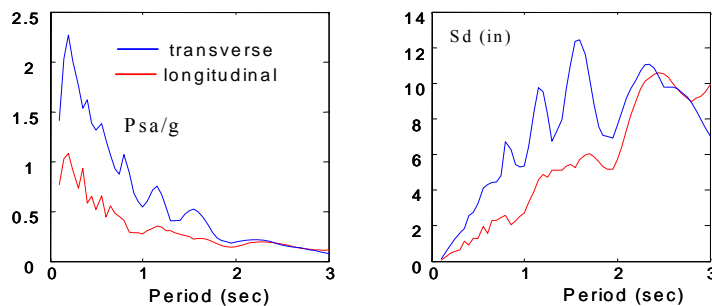


Fig 9. Elastic spectra for 5% damping (left = pseudo acceleration, right = displacement)

### Imperial County Services

The 6-story imperial county services building (CSMIP station number -1260) in El-Centro CA was built in 1969. In 1979 it suffered heavy damage from the magnitude 6.5( $M_L$ ) Imperial Valley earthquake and was subsequently demolished. A detailed description of the building and information on the extent of the damage can be found in ATC-09 [14]. Fig.10 illustrates floor plans showing the configuration of the shear walls and fig.11 shows the instrumentation set up.

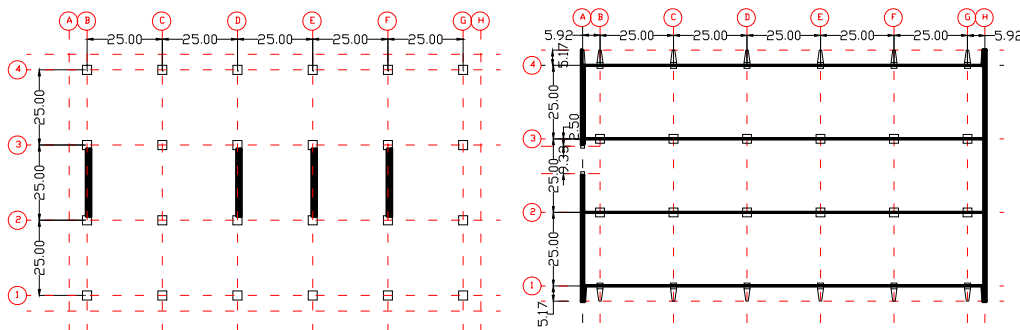


Fig.10 (left) plan view of the ground level, (right) typical plan view of stories two and above

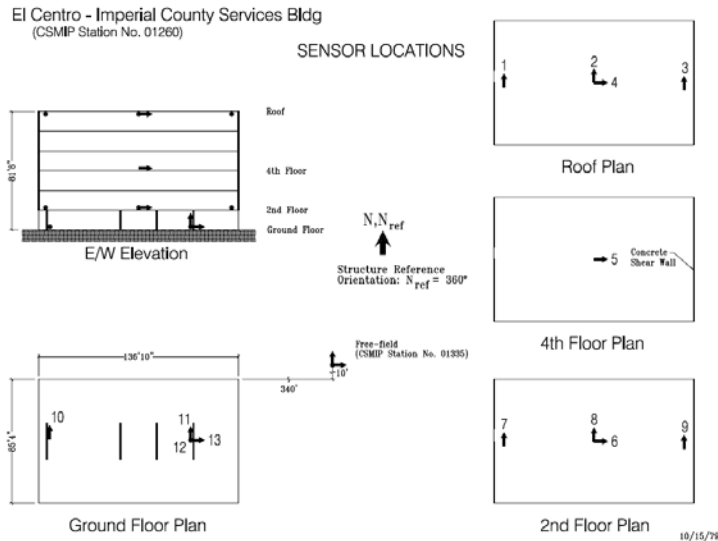


Fig.11 Layout of the sensors installed at ICS building (taken from CSMIP web site).

### System Identification and dynamic properties

The only available ground motion record on this building is the one that resulted in the heavy damage. The quasi-linear properties of the building were estimated using the early portion of the record (prior to the initiation of damage). Given the rather short time available, however, it only proved feasible to identify the fundamental mode in each direction. The results obtained are summarized in Table 5.

Table 5 Identified modal properties of the ICS building

Direction	T (sec)	$\zeta$ (%)
Longitudinal (X)	0.80	5
Transverse (Y)	0.44	8

### Analytical model and updating

Nonlinear behavior was modeled by lump plasticity in the members of the rigid frames located above the first level, while nonlinear fiber elements were used to model the walls and the columns in level #1. The elastic periods were found to be 0.84 sec in the longitudinal and 0.47 sec in the transverse direction, which are quite close to the identified values. Since the variance associated with the identified values is relatively large (due to the short available time) it was decided to use the model as formulated. In this building the item that is of paramount importance is modeling the strength degradation characteristics of the critical regions. The possibility for concrete crushing and steel bar buckling was considered. The biaxial nature of the motion is also critical in this case and was considered in all the analyses. Nominal material strengths were increase by 1.5 (concrete) and 1.25 (steel).

**Nonlinear Dynamic Analysis**

The 3D model of the building, when subjected to the recorded biaxial ground accelerations predicts an axial-flexural failure of the corner column on line G. This result matches the actual failure mode. Fig.12 shows the first 10 seconds of the acceleration response at the roof in the longitudinal and transverse direction and compares it with the measured values. As can be seen, the model tracks the measurements rather well up to about seven seconds which is the time when the northwest corner column fails. Comparisons beyond the time of failure are not meaningful since the model cannot be expected to track the post-failure state.

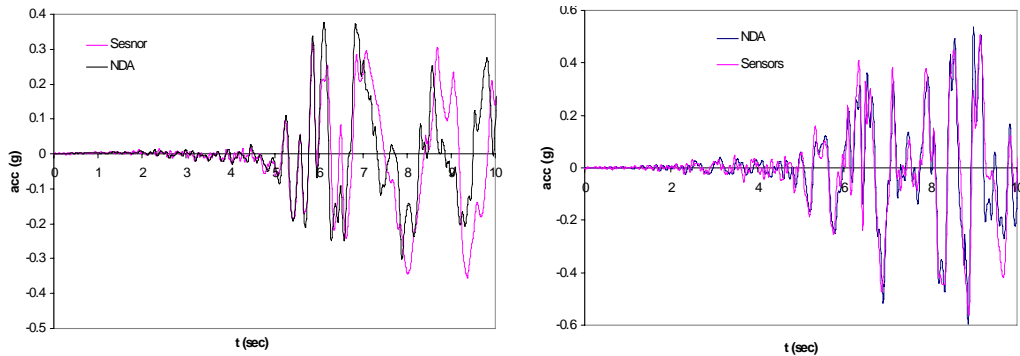


Fig.12 Acceleration response at the roof: (left) ch4, (right) ch2

**Nonlinear Static Procedure and Evaluation of the Performance Point**

Fig.13 illustrates a typical pushover curve in the longitudinal direction and the performance point for the case of the ATC-40 equivalent linearization method. As can be seen, the point falls on the softening part of the curve showing that failure is predicted. Results for all the other techniques and load distributions are summarized in Tables 6 and 7.

Table 6 Performance point evaluation in Longitudinal direction

Method	Load Pattern 1				Load Pattern 2				Load Pattern 3			
	Sa (g)	Sd (in)	V/W	drift %	Sa (g)	Sd (in)	V/W	drift %	Sa (g)	Sd (in)	V/W	drift %
ATC 40	0.208	6.264	0.165	0.79	-	-	-	-	0.278	3.339	0.219	0.42
FEMA 440 (Linearization)	0.247	3.166	0.195	0.41	0.233	3.301	0.197	0.43	0.257	3.188	0.250	0.41
FEMA 356 (CM)	0.243	3.445	0.188	0.44	0.232	3.488	0.192	4.62	0.303	2.822	0.254	0.36
FEMA 440 (CM)	0.244	3.290	0.192	0.42	0.231	3.369	0.196	0.44	0.257	3.273	0.228	0.41

Table 7 Performance point evaluation in Longitudinal direction

Method	Load Pattern 1				Load Pattern 2				Load Pattern 3			
	Sa (g)	Sd (in)	V/W	d %	Sa (g)	Sd (in)	V/W	d %	Sa (g)	Sd (in)	V/W	d %
ATC 40	0.449	1.896	0.373	0.23	0.458	1.724	0.409	0.22	0.366	2.349	0.302	0.29
FEMA 440 (Linearization)	0.410	2.844	0.352	0.26	0.477	1.817	0.415	0.24	0.323	2.840	0.379	0.26
FEMA 356 (CM)	0.412	2.793	0.334	0.28	0.520	2.094	0.430	0.26	0.389	2.716	0.456	0.20
FEMA 440 (CM)	0.425	2.997	0.345	0.26	0.508	2.133	0.444	0.28	0.328	2.964	0.362	0.27

**Observations**

- All four NSP were able to predict the observed failure.
- Convergence of ATC-40 for LP2 in the longitudinal direction proved impossible, which once again points to failure.



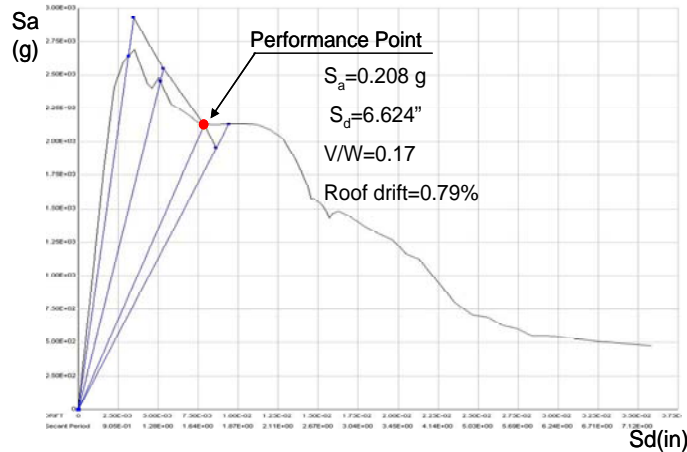


Fig.13 Performance point in longitudinal direction under LP1 by ATC-40 method

### Telephone Building in Watsonville

This building (CSMIP station 47459) was designed in 1948 and was initially build with three stories. The fourth level was added in 1955. The vertical load resisting system is concrete slabs supported by composite steel-concrete frames and the main lateral load resisting system consists of a number of solid and perforated shear walls. The foundation system is made of spread and strip footings over alluvium. Figure 14 shows the instrumentation layout.

### Soil Structure Interaction

Elastic spectra for the two available records are depicted in the E-W direction in fig.15. The Loma Prieta earthquake (LP) produced much larger response than Morgan Hill (MH) and for this reason we limit our discussions to Loma Prieta. Looking at the LP spectrum one can see two peaks bellow 0.4 seconds that are associated with feedback from strong SSI effects.

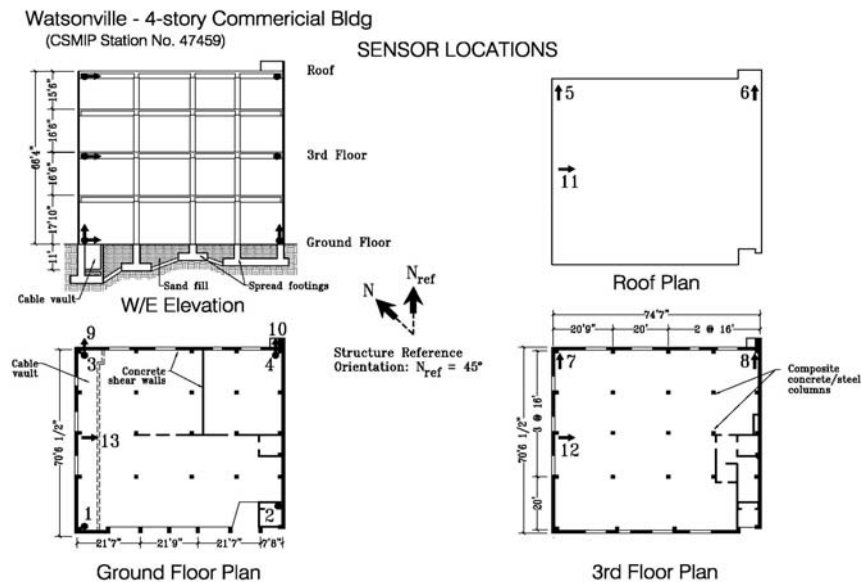


Fig.14 Instrumentation layout of Watsonville building (taken from CSMIP website)

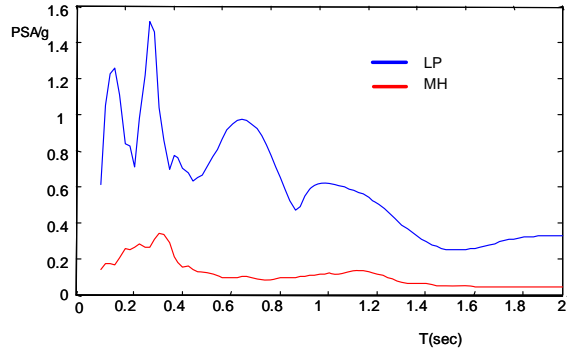


Fig15. Elastic spectra for 5% damping in the E-W direction

There are 4 vertical accelerometers at the base. To test the typical assumption of base rigidity the acceleration in ch4 was computed from the results at sensors 1, 2 and 3 (using the rigid premise) and the Fourier Spectrum of the result is compared to that of the measurements in fig.16. The result shows that the rigid assumption is accurate for frequencies up to about 2 Hz but for higher frequencies it is less accurate, especially near the resonant frequencies of the structure. While the use of the term rocking carries the rigid plane assumption one can compute approximate rocking components by least square fitting a plane to the vertical accelerations and taking the rocking as the rotations of this plane. Fig.17 shows that the contribution of this “pseudo-rocking” to the total roof acceleration is substantial.

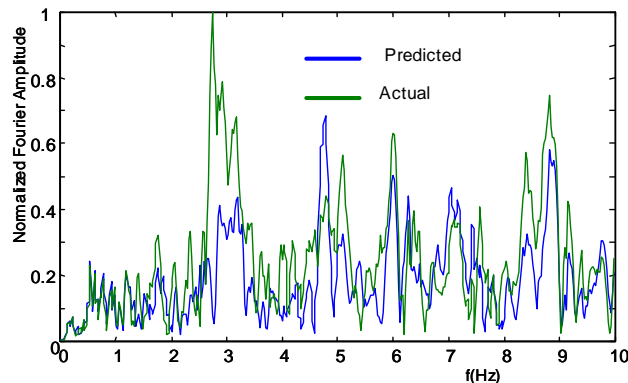


Fig.16 Spectrum of ch4 predicted from sensors 1, 2 and 3 and actual measurement (LP record).

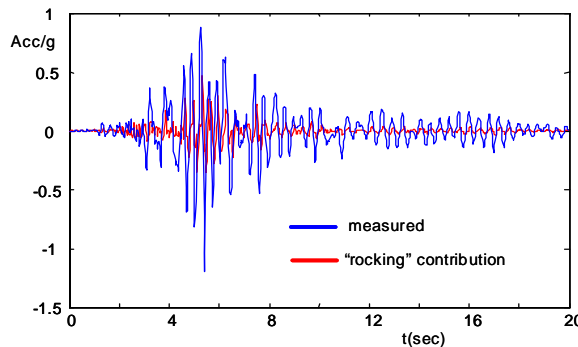


Fig.17 Acceleration in ch11 (E-W roof) for LP excitation

## System Identification

The Morgan-Hill motion was used to perform the ID because this record is the less intense of the two available and thus “quasi-linear” behavior is more closely realized. Subspace identification and the Observer Kalman Filter ID were tried but both gave results that showed significant dependency on the initial order selected, in all likelihood because the feedback effects make the input and output spectra have coincident peaks. Use of reversed time Markov Identification, however, lead to robust results. The basic idea in reversed time analysis is to flip the problem mathematically so that the stable modes become unstable. The results from the reversed time identification are:  $f_{E-W} = 3.62$  Hz  $\phi = [1, 0.52]^T$ ,  $f_{N-S} = 4.95$  Hz,  $\phi = [1, 0.61]^T$ . It is worth noting that the mode shapes in both directions are close to straight lines (at least based on the available points), which supports the previous observation regarding the fact that a significant part of the deformation is coming from base rotation.

## Analytical model and updating

To model SSI, spring and dashpots were introduced at the base. Relative values of the parameters were determined using the geometry of the foundation and the scaling was selected based on the identified frequencies. It was found that the scaling selected corresponded to a modulus of subgrade reaction of 120k/ft<sup>3</sup>. The natural frequencies of the model in the E-W and N-S directions are 3.66 Hz and 4.88 Hz. Nonlinearity, and strength loss in shear in the walls, was considered in the model. Fig.18 shows a comparison of roof acceleration obtained from NDA analysis with measured data which illustrates that the model is reasonably accurate.

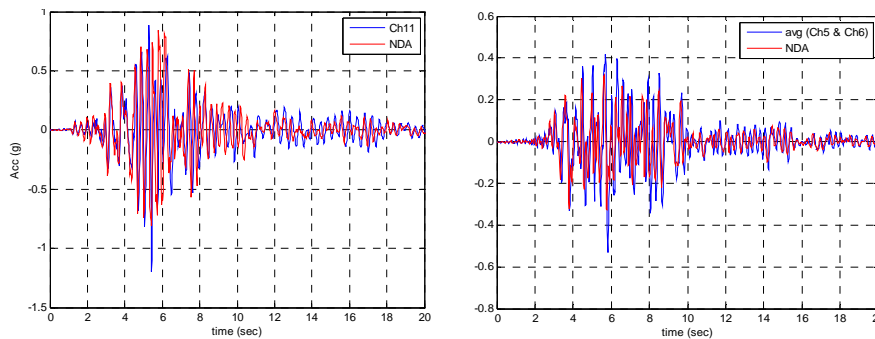


Fig.18 NDA acceleration vs measurements (left) E-W (right) N-S (LP records)

## Evaluation of the Performance Points

ATC40 and FEMA 356 adopt a simplified approach to account for SSI that considers base flexibility but not the increase in damping that arises from radiation. FEMA 440, however, offers a method to account for both effects. Table 8 summarizes the total damping due to SSI that is used in the NSP. For nonlinear dynamic analysis we included radiation damping by adding  $\beta K$  damping to the foundation springs; details are presented in [3].

Table 8 Effective damping due to SSI, used in FEMA 440 methods

Direction	Structural Damping $\beta 1 \%$	Foundation Damping $\beta f \%$	total SSI damping $\beta 0 \%$
Longitudinal (X)	5	1.99	5.36
Transverse (Y)	5	4	7

Tables 9 and 10 show the performance point evaluations in E-W and N-S directions for the Loma Prieta event. A representative push over curve with a performance point computation is depicted in fig.19 and the key results are summarized in fig.20.

Table 9 Performance point evaluation in Longitudinal (X) direction

Method	Load Pattern 1				Load Pattern 2				Load Pattern 3			
	Sa (g)	Sd (in)	V/W	drift %	Sa (g)	Sd (in)	V/W	drift %	Sa (g)	Sd (in)	V/W	drift %
ATC 40	0.661	0.682	0.339	0.109	0.6151	0.734	0.339	0.122	0.677	0.599	0.348	0.096
FEMA 440 (Linearization)	0.645	0.817	0.360	0.121	0.6257	0.835	0.349	0.136	0.633	0.811	0.372	0.107
FEMA 356 (CM)	0.627	0.686	0.340	0.109	0.6020	0.725	0.343	0.125	0.647	0.628	0.349	0.096
FEMA 440 (CM)	0.646	0.831	0.363	0.128	0.6267	0.853	0.352	0.144	0.636	0.818	0.385	0.118

Table 10 Performance point evaluation in Transverse (Y) direction

Method	Load Pattern 1				Load Pattern 2				Load Pattern 3			
	Sa (g)	Sd (in)	V/W	drift %	Sa (g)	Sd (in)	V/W	drift %	Sa (g)	Sd (in)	V/W	drift %
ATC 40	0.577	0.259	0.304	0.050	0.535	0.314	0.293	0.054	0.589	0.231	0.290	0.037
FEMA 440 (Linearization)	0.575	0.391	0.316	0.056	0.552	0.359	0.304	0.058	0.580	0.001	0.354	0.055
FEMA 356 (CM)	0.597	0.365	0.307	0.051	0.569	0.350	0.297	0.056	0.630	0.336	0.334	0.047
FEMA 440 (CM)	0.585	0.411	0.323	0.058	0.579	0.402	0.321	0.066	0.608	0.429	0.365	0.059

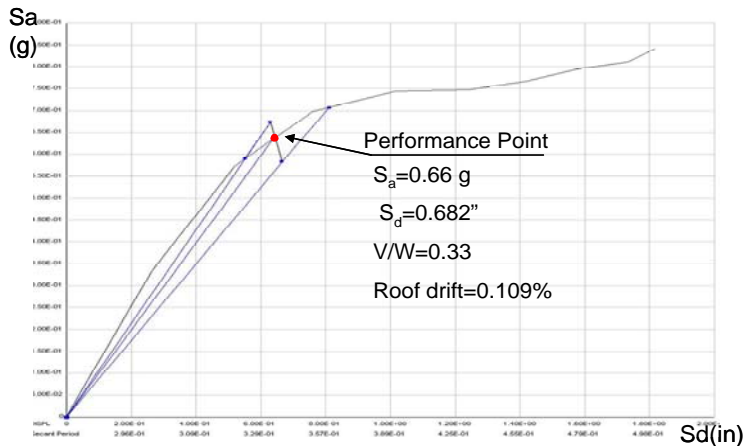


Fig.19 Performance point in longitudinal direction under LP-1 by ATC-40 method

### Predictive Capability of NSP

The mean and the coefficient of variation of the ratio of predictions to measurements are depicted in fig.21 for all the data available. The mean in the shears are not far from unity and the coefficient of variation, although not small at around 0.22, is “tolerable”. More or less the same assertion can be made for the overall displacements but the drift indices, however, are under-predicted in the mean and a representative *cv* is around 0.45, indicating a rather large spread. Although not shown here, the computation of the same statistics with the data segregated into the upper half and the lower half of the buildings shows that the accuracy in the lower half is notably better than the average and, of course, significantly worse on the upper floors. This result can be

rationalized by noting that the higher mode contributions tend to be larger in the upper levels. Differences between the various techniques do not appear statistically significant.

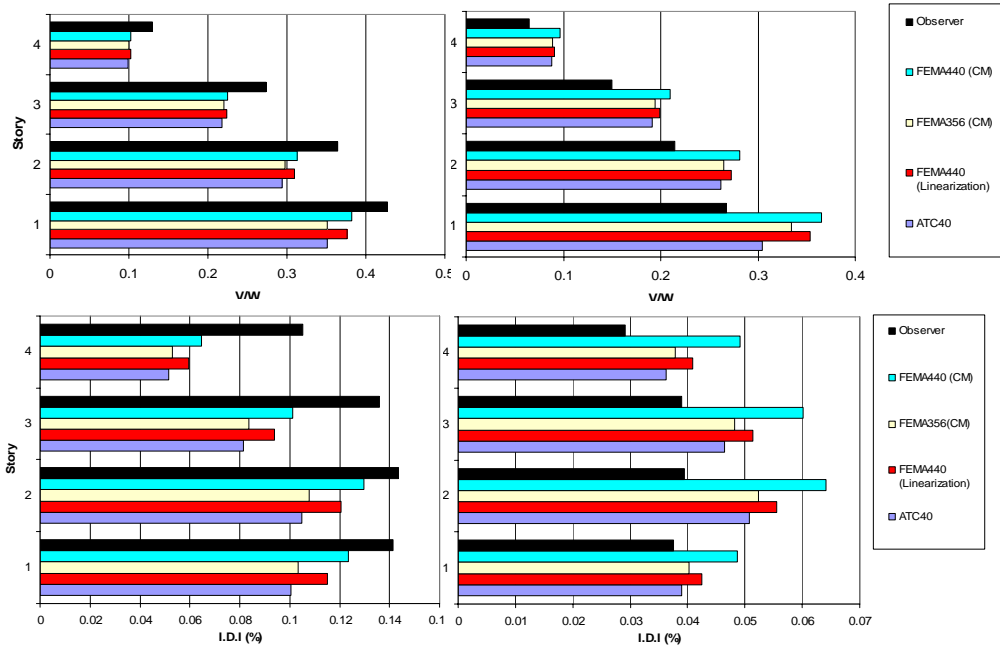


Fig.20 NSP predictions and observer predictions: (top) shears (bottom) inter-story drift index- E-W on left N-S on right.

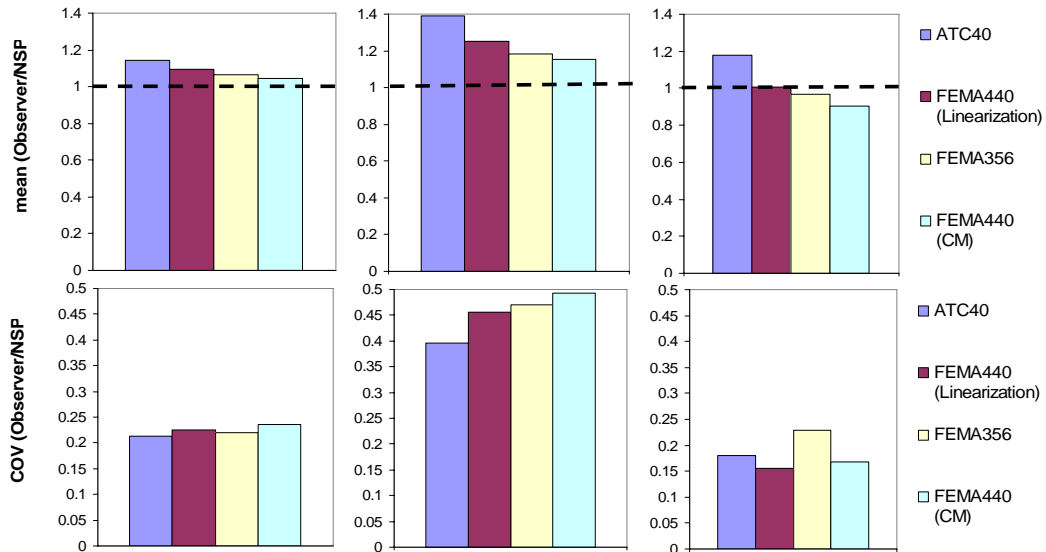


Fig.21 Ratio of observer to NSP predictions – mean on the top and cv on bottom – shears on left column, drift indices on center and total displacements on right.

### Concluding Comments

The results obtained in this project support the contention that the accuracy of current NSP is significantly higher in the lower floors than in the upper floors of buildings. For example, the coefficients of variation for shears and drift indices were found to be {0.45 and 0.22} when computed over all levels and {0.2 and 0.14} when only the data on the lower half of the buildings is considered. Since the lower levels are often critical this is a good sign yet it appears that there is room for improvement in upper floor performance. Although NSP are necessarily approximate (since the true complexity of the nonlinear dynamic response does not fit within the framework) the results obtained in this project suggest that they can be “sufficiently accurate” to identify important deficiencies and thus point to appropriate retrofit strategies. In closing it is opportune to emphasize that a necessary condition for any NSP to succeed is that the model used to represent the building be accurate (enough) and, in particular, that it be able to capture all the important sources of strength and stiffness degradation. An excellent example pointing to this fact is the Imperial County Services Building, where all NSP predict failure when the poorly confined concrete in the columns of the first story is properly modeled but neither can reproduce the observed behavior if this is not the case. Several other examples of this same point, not included in this paper due to space constraints, can be found in the final report [3].

### Acknowledgement

The research reported in this paper was supported by the California Strong Motion Instrumentation Program (CSMIP) through Standard Agreement NO. 1005-834, this support is gratefully acknowledged.

### References

- [1] ATC-55 (2005). *Applied Technology Council*, Redwood City, CA
- [2] Hernandez E., and Bernal D. "State estimation in systems with uncertain damping and stiffness properties", *Journal of Engineering Mechanics*, ASCE (in press).
- [3] Bernal D. (2007). Predictive capability of nonlinear static analysis procedures for seismic evaluation of buildings, CSMIP report on data interpretation project.
- [4] Husid, R. (1967). Gravity effects on the earthquake response of yielding structures, *Earthquake Engineering Research Laboratory*, California Institute of Technology, Pasadena.
- [5] Jennings P.C. and Husid, R. (1968). "Collapse of yielding structures under earthquakes", *Journal of Engineering Mechanics*, ASCE, Vol. 94, No.5, pp.1045-1065.
- [6] Bernal, D. (1992). "Instability of buildings subjected to earthquakes", *Journal of Structural Engineering*, ASCE, Vol. 18, No.8, pp. 2239-2260.

- [7] Bernal, D. (1998). "Instability of buildings during seismic response", *Engineering Structures*, Vol.20, No.4-6, pp.496-502.
- [8] FEMA 440 (2005), *Improvement of nonlinear static seismic analysis procedures*, prepared by Applied Technology Council for the Federal Emergency Management Agency, Washington, D.C.
- [9] FEMA 356 (2000), *Prestandard and Commentary for the Seismic Rehabilitation of Buildings*, prepared by the American Society of Civil Engineers for the Federal Emergency Management Agency, Washington, D.C.
- [10] Juang, J. (1994), *Applied system identification*, Prentice-Hall, Upper Saddle River, N.J.
- [11] Naeim, F. (1998), "Performance of 20 extensively-instrumented buildings during the 1994 Northridge earthquake", *Structural Design of Tall Buildings*, Vol. 7, No. 3, pp. 179-194
- [12] Van Overschee, P., and Moor, B.L. (1996). Subspace identification for linear systems: Theory, implementation and applications, Kluwer Academics, Boston MA.
- [13] Pappa R.S. and Elliott K.B., (1993). "Consistent-mode indicator for the eigensystem realization algorithm", *Journal of Guidance, Control and Dynamics*, Vol.16 No. 5, pp. 852-858.
- [14] ATC-9 (1984). An Evaluation of the Imperial County Services Building Earthquake response and Associated Damage, *Applied Technology Council*, Redwood City, CA.





**RECENT DEVELOPMENTS IN STRONG MOTION MEASUREMENTS IN JAPAN  
AND THE DAMAGING NIIGATA AREA EARTHQUAKES OF 2007**

**Kazuyoshi Kudo**

College of Industrial Technology, Nihon University, and  
Tokyo Electric Power Services Co. LTD

**Abstract**

The strong motion observation in Japan was initiated in 1953, 20 years behind from California. In 2004, celebrating 50th anniversary of strong motion observation in Japan was held sponsored by the Strong-Motion Earthquake Observation Council in the National Institute for Earth Science and Disaster Prevention (NIED), Japan Association for Earthquake Engineering, and Earthquake Research Institute, University of Tokyo. The first part of my presentation is a summary or review of the symposium and an introduction of the strong motion observation networks by the individual organizations.

The strong motion instrumentation program in Japan has drastically been changed after the 1995 Kobe earthquake from research oriented observations to quick information of shaking level or map for emergency responses associated with the rapid developments of data telecommunication.

**1. Strong Motion Observation Networks by the individual organizations**

a) Ground response observation networks

The representative or massive networks are K-NET consists of 1026 stations and KiK-net of 680 surface and down-hole pairs maintained by NIED and the seismic intensity networks operated by JMA (585 stations) and the 47 prefectural governments (about 2800 stations). Intensity data assembled by JMA are quickly broadcasted by TV and radio. The other ground response strong motion observations have been conducted by universities (mostly ERI) with 109 stations including 14 down-holes and the Ports and Airports Research Institute with 60 sites including down-hole measurements.

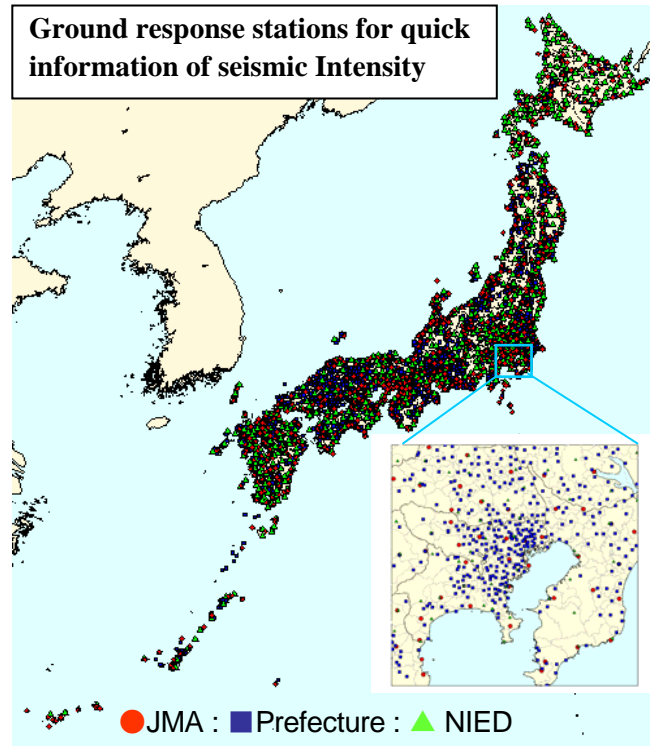
b) Structural responses and security for facilities.

The observations in buildings have been conducted at 77 sites by the Building Research Institute. The number of the site or building is very limited, but the majority of the observations (the number is uncertain) for building responses have been operated by big consulting companies jointly with the building owners.

For keeping security mainly roads and bridges, the National Institute of Land and Infrastructure Management (NILIM) have started on-line measurements at 700 sites in Japan

after the Kobe earthquake. The NILIM has conducted the observation of responses for civil engineering structures at 160 sites and dense array ground response observations at a few sites.

These observations have been operating by the governmental organizations. The large and dense strong motion observation networks have been established by private companies for emergency responses of individual facilities such as gas (Tokyo Gas: ground responses at about 3,800 sites in Tokyo Metropolitan region), electronic power companies (dams, nuclear power plants), railroad/subway, telecommunication companies and so on.



## 2. Results of the Symposium 2004 and some issues on strong motion instrumentation in Japan

The proceedings of the symposium is available on the URL (<http://www.k-net.bosai.go.jp/KYOUKAN/symp/symptop.htm>), unfortunately the papers are written in Japanese with English abstract and figure captions, except invited papers by Prof. W. D. Iwan and Prof. K-L. Wen.

The strong motion observation in Japan has been developed and improved after the Kobe earthquake, as K-NET, KiK-net, and intensity measurement network by JMA and Prefectures. Most remarkable improvements by K-NET are the homogenous installation of observation sites taking into account that the occurrence potential of moderately large earthquakes in and around Japan and the accessibility to the observed data within a very short time through the Internet. K-NET system has certainly accelerated and extended the studies on source inversion and on

variations of strong motion features. However, we summarized the requests to the government, researchers, and ourselves as a form of resolution as followings (these are not formal translation):

- i) Government should provide the budget to keep stable managements of fundamental networks such as K-NET, intensity network. Request to prefectures that waveform data are stored and opened to researchers.
- ii) Improvements of strong motion dense array observation aiming to solve each specific issue in the field of strong motion seismology and earthquake engineering are required.
- iii) Recommend the instrumentation to buildings and facilities, especially to public ones. The instrumentation should also be oriented for quick decisions on the security of facilities just after the earthquake.
- iv) Recommend the quick availability of strong motion data by all organizations as K-NET.
- v) Recommend the establishment of the database or databank. This is an urgent issue due to the rapid accumulation of strong as well as weak motion records.
- vi) Recommend the data use not only for research but also for security of society, including development of new generation of strong motion instruments.

### **3. Some topics on strong motion records recovered during a decade.**

During a decade after the Kobe earthquake, more than 10 damaging earthquakes occurred in Japan, e.g., Kagoshima (1997), Yamaguchi (1998), Tottori (2000), Geiyo (2001), Miyagi (2003), Tokachi-oki (2003), Niigata Chuetsu (2004), Fukuoka (2005), Miyagi-oki (2005), Noto (2007), Niigata Chuetsu-oki (2007). Most earthquakes occurred in land, so that near source records were retrieved by the K-NET, KiK-net, the intensity measurement networks and other networks.

- i) Very high level accelerations were recorded. The reasons of this are confidentially near source and site amplification due to shallow soft soils. In the same time, we should note that the soft soil effects showed some nonlinear behaviors.
- ii) It was our first experience that strong motion records were obtained densely in a wide area from the M8 class and then long period (3-15 sec.) strong motion were systematically investigated. The issues of long-period ground motion are urgent and important because of rapid increase of high rise buildings with base isolation even at lowland Tokyo and vicinity. Acceleration based strong motion observations have sometimes missed to retrieve the very late arrivals that the acceleration level is low but the velocity or displacement level is high. Therefore, some research groups tend to use strong velocity meter instead of accelerometers.

### **4. Revision of K-NET**

The K-NET renewed the instrument so as to link the seismic intensity network, to cover a high acceleration up to 4 G, to improve the resolution or quality of digitization, and to acquire

waveform data with quasi-real time. I believe that the resolution 2004 might somewhat assist the renewal of K-NET.

### **5. Niigata Chuetsu-oki earthquake (Mw6.7) of 2007**

The earthquake of July 16 was surprising for us in two reasons. The first one is that the very near source strong shaking struck the nuclear power station. The second one is that the large earthquake occurred at only 30 km apart from the Niigata Chuetsu earthquake of 2004 and with very short interval.

Prominent issues of the Niigata Chuetsu-oki earthquake of July 16 were:

- Four nuclear power plants among 7 ones were operating at the earthquake, but they have stopped safely without serious accidents or problems as the IAEA report.
- Nevertheless high acceleration of 1g at the basement that exceeded roughly twice of the design level, no damage was observed at least on buildings except some non-priority facilities. This issue is discussed in the field of structural engineering.
- The fault plane has not yet determined, that is, there is no room to doubt the mechanism solution of thrust, but a dip direction has not yet determined.

Relatively dense strong motion records near source region were obtained. They are from the K-NET, JMA, Niigata Prefecture, and Tokyo Electric Power Company (TEPCO). Strong motion records at the TEPCO Kashiwazaki-Kariwa Nuclear Power Station were released recently and the English version is now preparing. It is the first case that the strong motion data at a nuclear power station are released.

A few comments on the records are that strong nonlinear behaviors are found in the vertical array records obtained near the power station. K-NET records at Kashiwazaki shows strong spike-like pulse. The data analyses and interpretation of phenomenon are still in the beginning stage and wide as well as deep discussions will be required.

**RESULTS AND IMPLICATIONS OF THE NEXT GENERATION  
ATTENUATION (NGA) GROUND MOTION PROJECT**

Norman Abrahamson

Pacific Gas & Electric Company  
San Francisco, California

**Abstract**

The NGA project has developed give new ground motion attenuation models for application to California. The models are applicable to all relevant shallow crustal earthquakes in California: M5-8.5 for strike-slip earthquakes and M5-8.0 for reverse earthquakes; distance of 0-200 km; strike-slip, reverse, and normal mechanisms. The models are also defined for spectral periods up to 10 seconds. As a result, the user of the models does not need to extrapolate them for most applications.

Key changes from the previous models include the use of VS30 for the site condition, inclusion of a depth of rupture factor, inclusion of hanging wall factors, and inclusion of depth of soil factors. All of the models include non-linear site response effects. Three of the models include the effects of the soil non-linearity on the standard deviation.

Comparisons of the differences between the five NGA models and between the NGA models the previous models that they are replacing are shown. The new models show a reduction in the median ground motion close to large earthquakes and an increase in the standard deviation for large earthquakes. There is an increase in the short period median ground motion for sites over the hanging wall of thrust earthquakes. Overall, the NGA models lead to reduced design ground motions based on IBC procedures. About half of the reduction is due to use of VS30, consistent with the building code, rather than using generic rock models.



**DESIGN GROUND MOTION LIBRARY (DGML) –  
TOOL FOR SELECTING TIME HISTORY RECORDS FOR SPECIFIC  
ENGINEERING APPLICATIONS**

Robert Youngs, M. Power, G. Wang, F. Makdisi, and C.-C. Chin

Geomatrix Consultants, Oakland, California

**Abstract**

The Design Ground Motion Library (DGML) is a software package for searching for ground motion time histories suitable for use by engineering practitioners for the time history dynamic analysis of various facility types in California and other parts of the western United States. The DGML was developed in a project funded jointly by the California Geological Survey-Strong Motion Instrumentation Program (CGS-SMIP) and the Pacific Earthquake Engineering Research Center-Lifelines Program (PEER-LL). The project was carried out by a multidisciplinary project team of practitioners and researchers in structural engineering, geotechnical engineering, and seismology. Currently, the DGML is limited to recorded time histories from shallow crustal earthquakes of the type that occur in California and other parts of the western United States. The software package includes a database of ground motion records and a software tool for selecting, scaling, and evaluating time histories for applications. The DGML is currently on a DVD, and consideration is being given to converting the DGML to internet web-based usage. The ground motion database used in the DGML consists of the PEER-NGA data base created for the Next Generation of Attenuation (NGA) relationships project. The database includes time histories from CGS-SMIP, U.S. Geological Survey (USGS), and other reliable sources including selected record sets from international sources. The DGML is documented and supported by a Users Manual and a report.

The DGML has the broad capability to search for ground motion time history records on the basis of (1) the response spectral shape of the records in comparison to design or target response spectra and (2) other characteristics of the records. Ground motion response spectral shape over a period range significant to structural response has been found to be closely correlated to inelastic structural response in a number of research studies. The period range of significance may include periods shorter than the fundamental structure period because of higher mode effects and periods longer than the fundamental structure period because of structure softening during inelastic response. Accordingly, a key capability of the DGML software tool is searching for and ranking time history records on the basis of the degree of match of the response spectral shapes of the time histories with design or target spectra over a user-specified period range. To support this capability, the software tool can construct design or target spectra using different approaches.

Other criteria are also specified by the user in constraining searches for ground motion time history records. These search criteria include: parameters for earthquakes that produced the ground motion records (ranges of earthquake magnitude, type of faulting); ranges of earthquake

source-to-site distance for records; recording station site conditions (characterized by ranges of site shear wave velocity in the upper 30 meters,  $V_{s30}$ ); ranges of significant duration for records; presence of pulses in near-fault records; direction of horizontal component of records (fault-strike-normal (FN) direction, fault-strike-parallel (FP) direction, either FN or FP direction, or two-component pairs in FN and FP directions); maximum number of records to search for; and ranges of acceptable scaling factors for scaling records to the level of the target spectrum.

The software tool includes a graphic interface for data input, processing, and plotting of target response spectra, spectra of individual or multiple time histories, and average spectra for selected time histories. In addition, acceleration, velocity, and displacement time histories can be plotted for the selected time histories.



**DIRECTIVITY IN NGA EARTHQUAKE GROUND MOTIONS: ANALYSIS USING  
ISOCHRONE THEORY**

Paul Spudich<sup>1</sup> and Brian S.J. Chiou<sup>2</sup>

<sup>1</sup> US Geological Survey  
Menlo Park, California

<sup>2</sup> California Department of Transportation  
Sacramento, California

**Abstract**

We present correction factors that may be applied to the NGA models of Abrahamson and Silva, Boore and Atkinson, Campbell and Bozorgnia, and Chiou and Youngs to model the azimuthally varying distribution of the GMROTI50 component of ground motion (commonly called 'directivity') around earthquakes. Our correction factors are non-zero for  $M > 6.0$  and rupture distance less than 70 km. They may be used for planar or nonplanar faults having any dip or slip rake. The correction factors are a product of an approximation, based on isochrone theory, of true directivity, a term simulating the earthquake's slip distribution, and a point-source approximation of the earthquake's radiation pattern.



**DEVELOPMENT OF CRITERIA FOR THE SEISMIC DESIGN AND ANALYSIS OF  
TALL BUILDINGS IN CALIFORNIA**

Jack Moehle and Yousef Bozorgnia

Pacific Earthquake Engineering Research Center  
UC Berkeley  
Berkeley, CA

**Abstract**

Several west coast cities are seeing an upsurge in the construction of high-rise buildings. Many of these buildings feature framing systems, materials, heights, and dynamic properties not envisioned by our current building code prescriptive provisions. Rather than force these buildings to conform, many jurisdictions are allowing these new designs to proceed under the alternative procedures provision of the building code, which allows alternative lateral-force procedures using rational analyses based on well-established principles of mechanics in lieu of the prescriptive provisions. Most designs are opting for a performance-based approach in which a rational analysis demonstrates serviceability and safety equivalent to that intended by the code prescriptive provisions. Several questions arise in a performance-based design. What is equivalent performance? How should it be demonstrated? If dynamic analysis is conducted for a range of anticipated earthquake ground motions, how should the ground motions be selected and how should the design value determined? How should performance designs be reviewed?

The *Tall Buildings Initiative* is funding a range of short to intermediate-term projects in 2006-2009. The final product will be a set of written guidelines containing principles and specific criteria for tall building seismic design. The document is intended to support ongoing guidelines and code-writing activities of collaborating organizations, as well as being a stand-alone reference for designers of high-rise buildings. The main points relevant to the CSMIP program include: Selection of earthquake ground motions; Modification of earthquake ground motions to represent the design shaking level, including scaling and spectrum matching methods including considerations of epsilon and conditional mean spectra; Interactions between incoming ground motions and building foundations; and Interpretation of the results of multiple response history analyses for determination of design values.

This project is under way at the time of this presentation, including new funding from the CSMIP program. The presentation reviews the salient issues and current progress in addressing them.



**THE INTERSECTION OF EARTHQUAKE STRUCTURAL RESPONSE MONITORING  
AND STRUCTURAL HEALTH MONITORING**

Robert L. Nigbor

UCLA, Los Angeles, California

**Abstract**

As stated in the recent Guideline for ANSS Seismic Monitoring of Engineered Civil Systems, the mission of response monitoring within the ANSS program is to provide data and information products that will (1) contribute to earthquake safety through improved understanding and predictive modeling of the earthquake response of engineered civil systems and (2) aid in post-earthquake response and recovery. The second mission component intersects with the distinct field of Structural Health Monitoring (SHM). SHM is a broad field encompassing research and applications in Mechanical, Aerospace, and Civil Engineering. It is a very active area, with dedicated conferences such as the annual International Workshop on Structural Health Monitoring and several journals dedicated to SHM research.

The goal of SHM is the timely detection, location, and quantification of structural damage. At the present time there are successful SHM applications in other fields where the structures are well-defined and standardized (such as aircraft or rotating machinery). In these fields, the benefit is clear and the benefit/cost ratio is favorable. In civil engineering, research and development abounds and instrumentation technology exists for providing the data needed for SHM of buildings, bridges, and other large structures. However, uncertainty in the assessment of damage clouds the benefit, and costs are high. That said, there is now opportunity for overlap between earthquake monitoring of structures and SHM. Multi-disciplinary advances in the technologies of sensor networks, data acquisition, communication, real-time computation and system identification techniques have the potential to provide a useful and reliable post-earthquake damage assessment for instrumented structures. Testbeds such as the CSMIP-instrumented Vincent Thomas Bridge and the ANSS-instrumented UCLA Factor Building demonstrate the future potential of this overlap, combining earthquake monitoring with continuous monitoring and recording of data for SHM applications.



**NEW BUILDING CODE PROVISIONS AND THEIR IMPLICATIONS FOR DESIGN  
AND CONSTRUCTION IN CALIFORNIA**

David R. Bonneville

Senior Principal  
Degenkolb Engineers  
San Francisco, California

**Abstract**

The recently published 2007 *California Building Code* (CBC) represents the most significant change in seismic design and construction in California in a decade. The 2007 CBC requirements are adopted from the 2006 *International Building Code* (IBC), which in turn adopts seismic provisions essentially by reference from ASCE 7-05 - *Minimum Design Loads for Buildings and Other Structures*. The ASCE 7-05 requirements are presented in an entirely new format, which is more logical and which places the more commonly used sections in earlier chapters and the more specialized or advanced topics (e.g., response history procedures, and requirements for isolated or damped systems) in later chapters. Following are some of the more significant changes affecting practice:

- Ground Motion is defined by a design spectrum based on spectral values maps adopted from the 2003 NEHRP Provisions. The updated maps reflect recent USGS research, resulting in refinements in spectral values in many locations, compared to the 2000 NEHRP, and more importantly for California, significant changes in ground motion compared to the UBC zone maps with accompanying near fault adjustments. The design spectrum also introduces a new long-period branch, following the constant velocity branch, which will affect very long period structures.
- A *Seismic Design Category* (SDC) is assigned to each structure as a means of capturing both the seismic hazard, in terms of Mapped Acceleration Parameters (spectral values), Site Class (defining the soil profile), and the Occupancy Category, which is based on its importance or hazardous material contents. The SDC affects analysis, design and detailing requirements as well as the structural system that is allowed to be used and its height. The traditional UBC approach was to capture such requirements strictly based on zone.
- Requirements for Nonstructural Components and for Nonbuilding Structures are substantially modified and expanded. Nonstructural Components are assigned the same SDC as the building to which they are attached; however, a given building, and therefore its components, may contain more than one occupancy category, and thus more than one SDC. Components are also assigned their own Importance Factor, based on either importance or hazardous materials content. There are also special Certification requirements for equipment that must remain operable after an earthquake or that contains hazardous materials. Nonbuilding Structures are addressed in a separate chapter, covering those that are similar to

buildings and those that are not. The former are addressed in a manner similar to buildings, with factors for response modification, overstrength and displacement amplification. The later contains expanded requirements for tanks and vessels.